Ministry of Higher Education and Scientific Research
University of Baghdad
Institute of Laser for Postgraduate Studies

Investigation of Mechanical Effects on the Performance of Mach-Zehnder Interferometer Filters

A Thesis Submitted to the Institute of Laser for Postgraduate Studies, University of Baghdad in Partial Fulfillment of the Requirements for the degree of Master of Science in Laser/ Electronic and Communication Engineering

By
Ayah Thabit Yahiya
B.Sc. Electronics and Communication Engineering – 2012

Supervisor
Asst. Prof. Dr. Tahreer Safa'a Mansour

2018 AD **1439AH**

Certification

I certify that this thesis was prepared under my supervision at the Institute of Laser for Postgraduate Studies, University of Baghdad, as a partial fulfillment of requirements for the degree of "Master of Science in Laser/ Electronic and Communication Engineering".

Signature:

Name: **Dr.Tahreer Safa'a Mansour**

Title: **Asst. Professor**

Address: Institute of Laser for Postgraduate studies,

University of Baghdad.

Date: / / 2018

(Supervisor)

In view of the available recommendation, I forward this thesis for debate by Examining Committee.

Signature:

Name: **Asst. Prof. Dr. Shelan Khasro Tawfeeq**

Title: Head of the Scientific Committee.

Address: Institute of Laser for Postgraduate studies,

University of Baghdad.

Date: / / 2018

Examination Committee Certification

We certify that we have read this thesis “Investigation of Mechanical Effects on the Performance of Mach-Zehnder Interferometer Filters" and as Examination Committee, we examined the student in its content and in our opinion, it is adequate with standards as a thesis for a degree of Master in science in Laser /Electronic and Communication Engineering.

Signature:
Name: **Dr.Hussein Ali Jawad**
Title: Assistant Professor.
Address: Institute of Laser for Postgraduate Studies/ University of Baghdad
Date: / / 2018
(Chairman)

Signature:
Name: **Dr. Shelan Kh. Tawfeeq**
Title: Assistant Professor.
Address: Institute of Laser for Postgraduate Studies/ University of Baghdad
Date: / / 2018
(Member)

Signature:
Name: **Dr. Alaa Jasim Mousa**
Title: Lecturer.
Address: Islamic University
Date: / / 2018
(Member)

Signature:
Name: **Dr. Tahreer Safa’a Mansour**
Title: Assistant Professor.
Address: Institute of Laser for Postgraduate Studies, University of Baghdad.
Date: / / 2018
(Supervisor)

Approval by the Deanship of Institute of Laser for Postgradgate Studies, University of Baghdad.

Signature:
Name: **Prof. Dr. Abdual Hadi M. Al-Janabi**
Title: Dean.
Address: Institute of Laser for Postgraduate Studies, University of Baghdad.
Date: / / 2018

بسم الله الرحمن الرحيم

اللَّهُ نُورُ السَّمَاوَاتِ وَالْأَرْضِ مَثَلُ نُورِهِ
كَمِشْكَاةٍ فِيهَا مِصْبَاحٌ الْمِصْبَاحُ فِي زُجَاجَةٍ
الزُّجَاجَةُ كَأَنَّهَا كَوْكَبٌ دُرِّيٌّ يُوقَدُ مِنْ
شَجَرَةٍ مُبَارَكَةٍ زَيْتُونَةٍ لَا شَرْقِيَّةٍ وَلَا غَرْبِيَّةٍ
يَكَادُ زَيْتُهَا يُضِيءُ وَلَوْ لَمْ تَمْسَسْهُ نَارٌ
نُورٌ عَلَى نُورٍ يَهْدِي اللَّهُ لِنُورِهِ مَنْ يَشَاءُ
وَيَضْرِبُ اللَّهُ الْأَمْثَالَ لِلنَّاسِ وَاللَّهُ بِكُلِّ
شَيْءٍ عَلِيمٌ

صدق الله العظيم

(النور 35)

Dedication

To express my gratitude to those who supported and encouraged me, I dedicate this dissertation
To

The one who sucked me love and tenderness

.... My Mother

The big heart

.....My Father

The lovely heart
.....My Husband

And my lovely daughter lolo and my sister toshy

The souls which residue underneath the soil of our beloved Iraq

…..The great Martyrs

Ayah

Acknowledgement

Firstly, I thank **"ALLAH"** for guiding and retaining me during my whole life. I would like to thank my supervisor, **Ass.Prof.Dr Tahreer Safa'a Mansor,** for his guidance in every aspect of this thesis. She has allowed me to choose and direct my own project. She has given me a wealth of experience and professional confidence, which is arguably the most valuable inheritance from a graduate degree.

I would like to thank **Prof. Dr. Abdul Hadi M. Al-Janabi**,**,** the Dean of Institute of Laser for Postgraduate Studies and all the staff of the Institute for their effort during this research work. Special thanks are to **Asst. Prof. Dr. Mohammed K. Dhaher**, Asst. Dean of the Institute of Laser for Postgraduate Studies and **Dr. ZiyadAyad Taha**, head of the Engineering and Industrial Applications Department, for his continuous advice and support. Many thanks go to all the faculty members and staff of Institute of Laser for Postgraduate Studies, University of Baghdad, especially to **Asst. Prof. Dr. Hussein A. Jawad** for his valuable suggestions and advice. Great appreciation to **Asst. Prof. Dr. Shelan Khasro Tawfeeq**, for her encouragement. Special gratitude to, **Eng. Yuosif Ibrahim**, **Ibrahim Luay, Hassan Falah and Saif Aqeel** whose gave me great assistances to complete this work.

Finally, my words are unable to express my real happiness to my family especially my father and my husband for their patience and assistance.

Ayah

Abstract

Optical filters are very important component in optical systems. They are used to control the magnitude and phase of incoming signals. Different tunable optical filters were designed in this work (in-line and two arms all fiber Mach-Zehnder interferometers). These optical filters were investigated by experimental and simulation by optiwave system software Version (7.0).

The designed Mach-Zehnder interferometers (MZIs) can be used as tunable filter and phase shift by controlling their dimensions after applying two mechanical effects (the force and the strain).

The experimental results of in-line MZI with single mode -multimode -single mode Mach-Zehnder interferometer (SMS-MZI) setup the tunability range was (1554.721-1554.953) nm and phase shift range was (2.48-9.91) $m\,rad$,When the similar setup was used but with two arms MZI the tunability range was (1545.737-1547.862) nm and phase shift was (2.42-9.85) $m\,rad$.

The second configuration that is in-line single mode –fiber Bragg grating-single mode Mach-Zehnder interferometer (SFBGS-MZI) the tunability range was (1545.602-1545.631) nm, and phase shift was (0.1245-2.26)$m\,rad$, when the similar configuration was used but with two arms MZI, the tunability range was (1545.501-1545.562) nm, and phase shift range was (0.274-1.58)$m\,rad$.

Finally for two arms multimode Mach-Zehnder interferometer the tunability range was (1548.509-1548.516) nm and phase shift range was (4.45-16.9) $m\,rad$.

While The simulation results of in-line MZI with single mode .multimode .single mode Mach-Zehnder interferometer (SMS-MZI) the tunability range was (1554.730-1554.900) nm and phase shift was

(2.46-9.84) $m\,rad$, When the same setup was repeated but with two arms MZI the tunability range was (1545.737-1547.862) nm and phase shift was (2.42-9.85) $m\,rad$.

The second configuration that is two arms single mode –fiber Bragg grating-single mode Mach-Zehnder interferometer (SFBGS-MZI) the tunability range was (1545-1545.06) nm, and phase shift was (4.735-16.311)$m\,rad$.

Finally for two arms multimode Mach-Zehnder interferometer the tunaility range was (1548.509-1548.516) nm and phase shift range was (4.45-16.9) m rad.

From these results it was concluded that the Maximum tunability was obtained with two arms single mode –multimode –single mode Mach-Zehnder interferometer (SMS-MZI) equal to(2.131 nm) and acceptable Phase shift was obtained with two arms multimode- Mach-Zehnder interferometer (MM-MZI)configuration in the experimental and simulation work respectively.

List of Abbreviations	
LEDs	Light-emitting diodes
OPD	Optical path difference
WDM	Wavelength-division multiplexing
BER	Bit error rate
FPI	Fabry-perot interferometer
FBG	Fiber Bragg grating
SIs	Sagnac interferometers
dB	Decibel
PC	Polarization controller
MIs	Michelson interferometers
MZIs	Mach-Zehnder interferometers
LPGs	Long period fiber grating
MFDs	Mode fiber diameters
MMF	Multimode fiber
SMF	Single mode fiber
PCF	Photonic crystal fiber
LC	Liquid crystal
PBG	Photonic band gap
TOFs	Tunable optical filters
ASE	Amplified spontaneous emission
DWDM	Dense wavelength division multiplexing
OFD	Optical frequency discriminator
RI	Refractive index
CW LASER	Continues wave laser
SLD	Super luminescent diode
BBS	Broad band source
OSA	Optical spectrum analyzer

List of Symbols	
δ_{FPI}	The phase different of the fabry-perot interferometer
λ	Wavelength of the incident light
n	Refractive index of cavity material or cavity mode
L	Physical length of the cavity
B	Birefringent coefficient of the sensing fiber
n_f	Effective index of the fast mode
n_s	amplitude of the electric field
I_r	The intensity of reference arm
I_s	The intensity of sensing arm
$\Delta\varphi$	Phase difference between the sensing and reference arm
ΔL	Change in optical path length
n_{eff}	Effective refractive index of the mode
$I_\circ$	The intensity of the incident light
B	The visibility of the interference signal
$\emptyset(t)$	The thermally induced phase drift in the scanning interferometer
$\Delta\varphi_B$	Optical phase
$\Delta\lambda$	Phase shift
λ_B	Bragg wavelength
$\int_g$	The normalized fiber Bragg grating sensitivity for strain
ΔY	The variation in strain
$(\frac{\Delta\varphi_B}{\Delta Y})$	The phase sensitivity in response to strain
n_{eff}^{co}	Refractive index of the core
n_{eff}^{cl}	Refractive index of the clade
$L + \Delta L$	Optical path
ε_m	Elongation measurement

Contents

Chapter One

Introduction and Basic Concepts

1.1 Introdction

In optical communication systems, the three main components are optical transmitters, optical fibers, and optical receivers. The main component in the optical transmitter is optical modulator that has function of converting an input electrical signal into an optical signal and then launch it into an optical fiber. The major component of optical transmitters is an optical source, which is generally divided into two types; that is, light-emitting diodes (LEDs) and lasers.

The second component in optical communication system is optical fibers which transmit the optical signal to the third part of communication system that is a photo detector. The function of photo detector is to convert the received optical signal into a photocurrent.

Along these components, many types of impairments are added to the signal. These impairments result in a fluctuation to the signal; thus, the statistical properties of the signal are changed. The impairments are categorized into four types; that is, thermal noise, shot noise, signal-dependent noise, and intersymbol interference [1]. In-line fiber Mach-Zehnder interferometers have been one of the most important optical interferometers that may be constructed using many types of optical fiber like conventional fibers (single mode, multimode fibers), fiber Bragg grating , and photonic crystal fiber[2-5].

A typical conventional fiber Mach-Zehnder interferometer consists of two fiber arms which are split and combined by two optical couplers. The first coupler splits the incident light into two fiber beams. Usually the lengths of the two fiber beams are controlled to be different to introduce an optical path difference (OPD) between the two light paths. At the second coupler an interference spectrum is obtained as the two beams combine together with a certain OPD. The conventional two-beam fiber MZIs have been widely employed as optical filters, fiber modulators, environmental sensors.

However, these two beam fiber MZIs have their own limitations, such as complicated structure, big size and high cost. To overcome the above drawbacks, an in-line fiber MZI based on core-cladding-mode coupling has been proposed recently. Two light arms are both inside the same fiber in terms of core mode and cladding modes.

The cladding modes which have energy distributed in both core and cladding regions are excited by particular light steering elements, i.e. taper, core-offset, mode-mismatch, etc. Using only one piece of fiber, the in-line structure provides several advantages over conventional one such as compactness, high integrity, light weight, low cost and high stability [2].

Optical filters, and in particular all-fiber optical filters, are key components used extensively in fiber optic communications for wavelength-division multiplexing (WDM) and also in spectroscopy and fiber optic sensing [3- 5].

1.2 The Aim of the Work

The main of this work is to design different type of optical tunable filters using In-line and N-path Mach-Zehnder interferometer for enhancing the performance of optical communication system.

1.3 Interferometers

There exist representative four types of fiber optic interferometers, called Fabry-Perot, Sagnac, Michelson, and Mach-Zehnder. For each type of interferometer, the operating principles and the fabrication processes is presented.

1.3.1 Fabry-Perot Interferometer

Fabry-Perot interferometer (FPI) is generally composed of two parallel reflecting surfaces separated by a certain distance [6, 7]. Sometimes it is called an etalon [8]. Interference occurs due to the multiple superpositions of both reflected and transmitted beams at two parallel surfaces [9]. The fiber optic cases, the FPI can be simply formed by intentionally building up reflectors inside or outside the fibers. FPI sensors can be largely classified into two categories: one is extrinsic and the other is intrinsic [10, 11]. The extrinsic FPI sensor uses the reflections from an external cavity formed out of the interesting fiber [6]. Figure (1.1) a shows an extrinsic FPI sensor, in which the air cavity is formed by a supporting structure. Since it can utilize high reflecting mirrors, the extrinsic structure is useful to obtain a high finesse interference signal [12]. Furthermore, the fabrication is relatively simple and does not need any high cost equipment. However, extrinsic FPI sensors have disadvantages of low coupling efficiency, careful alignment, and packaging problem [8]. On the other hands, the intrinsic FPI fiber sensors have reflecting components within the fiber itself. For example, when the Reflectors are formed within a fiber by any means, as in Figure (1.1-b), it can have the intrinsic FP interference. The local cavity of the intrinsic FPI can be formed by a lot of methods such as micro machining [13–16], fiber Bragg gratings (FBGs) [17, 18], chemical etching [19, 20], and thin film deposition [21,22]. However, they still have a problem of using high cost fabrication equipment for the cavity formation. In other sense, when the cavity material is not the fiber itself, it is called extrinsic. However, the definition becomes vague due to the advent of specialty fibers and fiber devices [12].

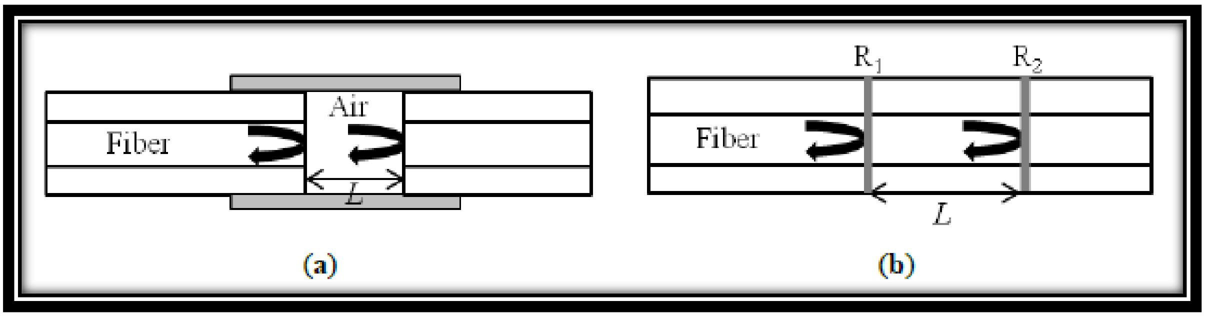

Figure (1.1*):* *a)* Extrinsic FPI sensor made by forming an external air cavity, b intrinsic FPI sensor formed by two reflecting components, R1 and R2, along a fiber [12].

The reflection or transmission spectrum of an FPI can be described as the wavelength dependent intensity modulation of the input light spectrum, which is mainly caused by the optical phase difference between two reflected or transmitted beams. The maximum and the minimum peaks of the modulated spectrum mean that both beams, at that particular wavelength, are in phase and out-of-phase, respectively, in the modulus of 2π. The phase difference of the FPI is simply given as [12].

$$\delta_{FPI} = \frac{2\pi}{\lambda} n2L \qquad (1.1)$$

Where λ is the wavelength of incident light, n is the RI of cavity material or cavity mode, and L is the physical length of the cavity. When perturbation is introduced to the sensor, the phase difference is influenced with the variation in the optical path length difference (OPD) of the interferometer.

1.3.2 Sagnac Interferometer

Sagnac interferometers (SIs) are recently in great interest in various sensing applications owing to their advantages of simple structure, easy fabrication, and environmental robustness [23]. SI consists of an optical fiber loop, along which two beams are propagating in counter directions with different polarization states. As schematically illustrated in Figure (1. 2), the input light is split into two directions by a 3 dB fiber coupler and the two counter-propagating beams are combined again at the same coupler. Unlike other fiber optic interferometers, the OPD is determined by the polarization dependent propagating speed of the mode guided along the loop. To maximize the polarization-dependent feature of SIs, birefringent fibers are typically utilized in sensing parts. The polarizations are adjusted by a polarization controller (PC) attached at the beginning of the sensing fiber. The signal at the output port of the fiber coupler is governed by the interference between the beams polarized along the slow axis and the fast axis. The phase of the interference is simply given as [23].

$$\delta_{SI} = \frac{2\pi}{\lambda} BL \qquad , \qquad B = |n_f - n_s| \tag{1.2}$$

Where B is the Birefringent coefficient of the sensing fiber, L is the length of the sensing fiber, and n_f and n_s are the effective indices of the fast and slow modes, respectively [23].

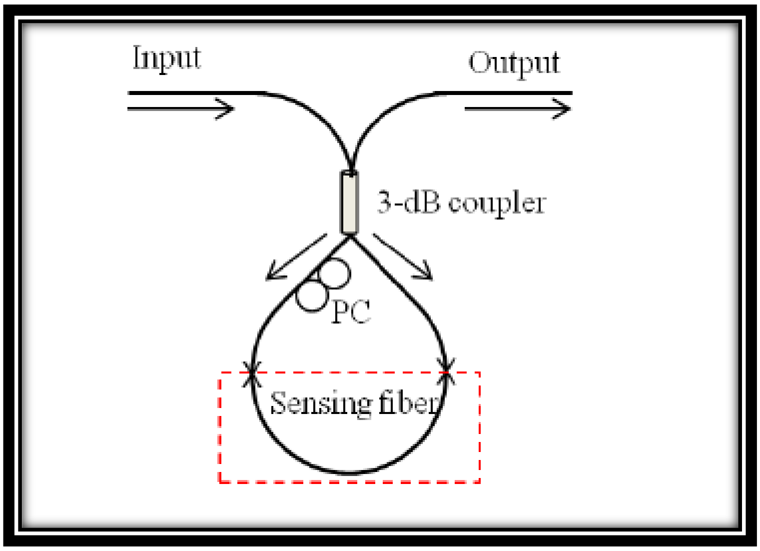

Figure (1.2): Schematic of the sensor based on a Sagnac interferometer [23].

1.3.3 Michelson Interferometer

Fiber-optic sensors based on Michelson interferometers (MIs) are quite similar to MZIs. The basic concept is the interference between the beams in two arms, but each beam is reflected at the end of each arm in an MI as shown in Figure (1.3-a) [24–27]. In fact, an MI is like a half of an MZI in configuration. Thus, the fabrication method and the operation principle of MIs are almost the same as MZIs. The main difference is the existence of a reflector(s). Since MIs use reflection modes, they are compact and handy in practical uses and installation. Multiplexing capability with parallel connection of several sensors is another beneficial point of MIs. However, it is essential to adjust the fiber length difference between the reference arm and the sensing arm of an MI within the coherence length of the light source. An in-line configuration of MI is also possible as shown with Figure (1.3-b). A part of the core mode beam is coupled to the cladding mode(s), which is reflected along with the uncoupled core mode beam by the common reflector at the end of the fiber [24-26].

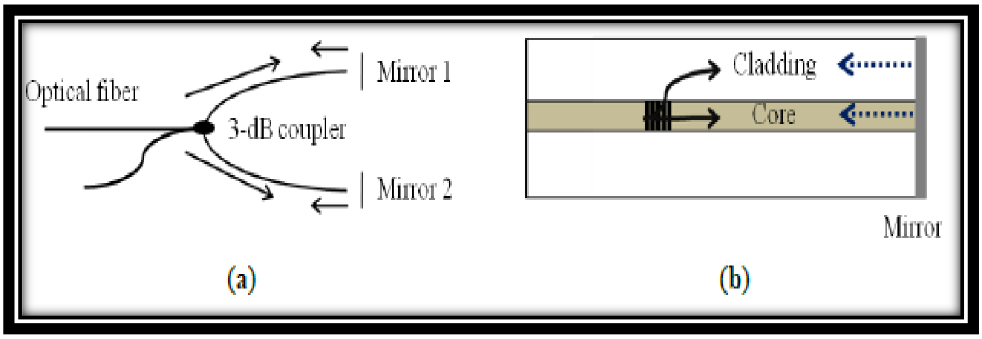

Figure (1.3): a) Basic configuration of a Michelson interferometer and b) Schematic of a compact in-line Michelson interferometer [27]].

1.3.4 Mach-Zehnder Interferometer

Mach-Zehnder interferometers (MZIs) have been commonly used in diverse sensing applications because of their flexible configurations. Early MZIs had two independent arms, which are the reference arm and the sensing arm, as illustrated in Figure (1.4). An incident light is split into two arms by a fiber coupler and then recombined by another fiber coupler. The recombined light has the interference component according to the OPD between the two arms. For sensing applications, the reference arm is kept isolated from external variation and only the sensing arm is exposed to the variation. Then, the variation in the sensing arm induced by such as temperature, strain, force and RI changes the OPD of the MZI, which can be easily detected by analyzing the variation in the interference signal [28].

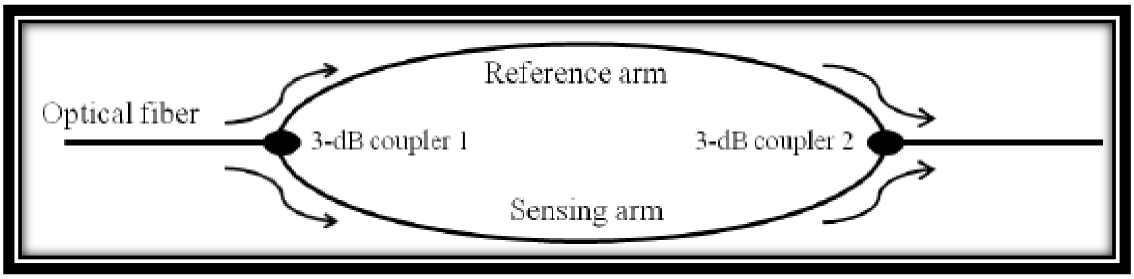

Figure (1.4): The scheme of using two separated arms in the MZIs has been rapidly replaced with the scheme of in-line waveguide interferometer since the advent of long period fiber gratings (LPGs) [28].

$$I = I_r + I_s + 2\sqrt{I_r I_s}\,\cos(\Delta\varphi) \tag{1.3}$$

Where I_r and I_s are the intensities of reference and sensing arm.
The phase difference between the sensing arm and reference arm is Described by [29]:

$$\Delta\varphi = \frac{2\pi \Delta L n_{eff}}{\lambda} \tag{1.4}$$

Where ΔL is the change in optical path length , λ is the wavelength in the vacuum, and n_{eff} is the effective refractive index of the mode.
In order to apply the force effect in optiwave software by these Equations [30]:

$$F = \varepsilon\, \Upsilon\, A \tag{1.5}$$

Where ε the strain, Υ the young modulus is constant (72.5), A is a surface of the stripping area of the fibers.

$$A = \pi\, D\, L \tag{1.6}$$

D: diameter of the fibers , L: length of the stripping area of the fibers.

$$\varepsilon = \frac{L}{\Delta L} \tag{1.7}$$

Where (ΔL) is the OPD between the two arms of MZIs, L: the length of the fiber

1.3.4.1 In-line Fiber Mach-Zehnder Interferometers

This sub section focuses on reviewing several typical kinds of in-line fiber Mach-Zehnder interferometers from the recent literature. These include: tapered fiber Mach-Zehnder interferometer, core-offset fiber Mach-Zehnder interferometer, grating based Mach- Zehnder interferometer, and Mode-mismatch based Mach-Zehnder interferometer [2].

1.3.5 Types of In-line Fiber Mach-Zehnder Interferometers

There are five types of In-line MZIs summarize in the sub sections below.

1.3.5.1 Tapered Fiber Mach-Zehnder Interferometer

Tapering is an effective way to convert a relative large ratio of energy in the fundamental mode to the high-order cladding modes in optical fiber. As light travels along the tapered fiber region where the diameter of the tapered fiber can be only a few microns over a length of a few centimeters, the original fiber core becomes so small that it has no significant influence any more. Thus, the energy loss from the fundamental mode would be coupled to the high order cladding modes. An effective in-line tapered MZI can be constructed by tapering a fiber at two point along the fiber as shown in Figure (1.5) [31]. This technique is cost effective and simple but weak mechanically essentially at the tapering region. This type of interferometer is widely used in sensing applications, especially in temperature and refractive index sensors since it is very sensitive to external disturbance [31].

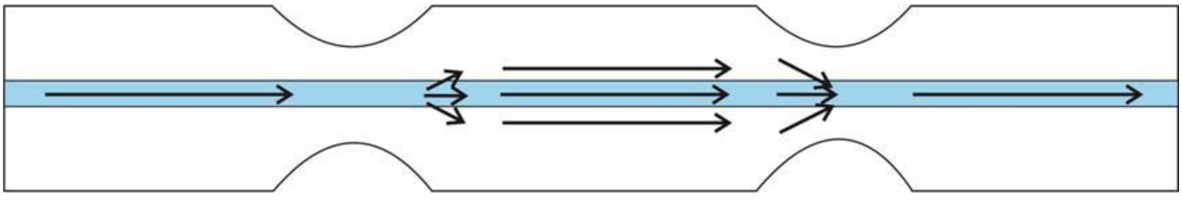

Figure (1.5): Profile of tapered fiber Mach-Zehnder interferometer [31, 32].

1.3.5.2 Core-Offset Fiber Mach-Zehnder Interferometer

Core-offset structure is formed by fusion splicing two segments of fibers with a pre-set offset value i.e. usually several micrometers. As shown in Figure (1.6), a part of the beam guided into the lead-in fiber the in form of core mode will be split into two parts. The first part represents the modes still guided within the core and the core mode give-up some of its energy to excite the cladding modes. Core-offset MZI has been used as an optical attenuator in optical communication systems [33].

Figure (1.6): a schematic profile of core-offset fiber Mach-Zehnder interferometer [33].

1.3.5.3 Grating Based Mach-Zehnder Interferometer

This type of in-line fiber MZI have a pair of FBGs in which a part of the light beam guided as a fundamental mode within the core of optical fiber is converted to cladding modes by the first FBG, now the core and the cladding modes are excited, and then the core and cladding modes are recoupled again to the fundamental mode (core modes) by the second FBG [31]. In general, there are two categories of this interferometer, short period FBG with submicron period and long period grating (LPG) with period ranging 100 μm-1 mm. The structure of a LPGMZI is depicted in Figure (1.7) This interferometer is preferred in refractive index sensing applications. The main challenge of this interferometer, it is working in limited bands of wavelength because of the phase matching phenomenon of fiber gratings and the LPG should be identical to have maximum performance.

Figure (1.7): LPG based Mach-Zehnder interferometer (LPGMZI) [31].

1.3.5.4 Mode-Mismatch Based Mach-Zehnder Interferometer

Another technique for splitting the beam in optical fiber is to employ fibers having different core sizes or actually different mode field diameters (MFDs) as illustrated in Figure (1.8). In this figure, a short length of MMF is fusion spliced between two standard SMFs to form single mode-Multi-mode-single mode (SMS) structure. The MMF has a larger core size compared with standard SMFs. However, the difference in MFDs between the fundamental core mode of the SMF and MMF leads to the decomposition of the fundamental core mode from SMF and excitation of the first few modes supported in MMF. These modes will be combined again in the second spliced region [30]. Among the other types of in-line fiber MZIs, mode-mismatching MZIs may have notable advantages such as ease of fabrication at relatively low cost and can be formed using different types of fibers. Core-mode mismatching can be widely utilized as optical filter, a strain sensor, and displacement sensor [34].

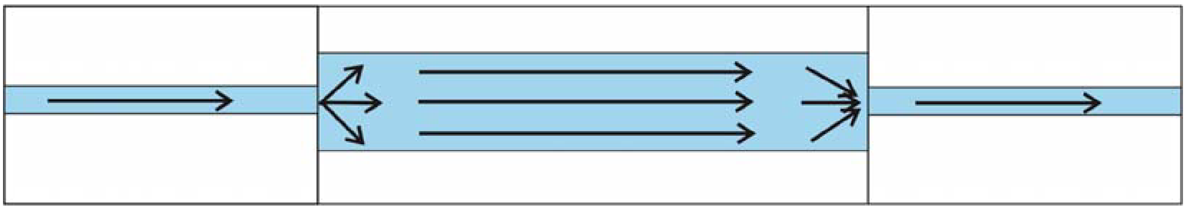

Figure (1.8): a typical structure of Mode-mismatch based MZI [30].

1.3.5.5 Fiber Bragg Grating Mach-Zehnder Interferometer

Fiber Bragg grating (FBG) embedded in a fiber Mach-Zehnder interferometer (MZI) is presented for sensing multi-parameters such as temperature, force, and strain. Various configurations of MZI combined with fiber Bragg grating have also been explored to measure ambient force and strain respectively. The formation the MZI has been illustrated using only one fiber Bragg gratings [34-36]. Figure (1.9) presented Mach-Zehnder interferometer with 50 mm long fiber Bragg grating with 6m interferometer arm. This interferometer was used for measurement the optical path deference duo to two Mechanical effects that are force and strain which applied of the central part of in-line fiber interferometer. This structure of interferometer is denoted as SFBGS-MZI [35].

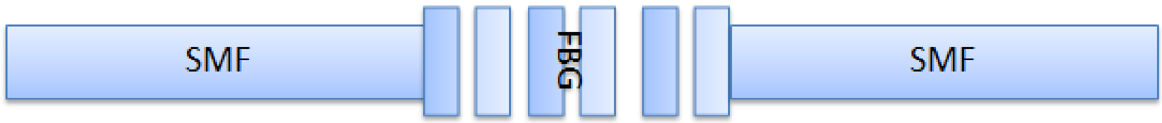

Figure (1.9): a typical structure of fiber Bragg grating MZI.

1.3.6 Two-Path Fiber Mach-Zehnder Interferometers

This type of interferometer can be employing with commercial two (1×2) couplers and two identical lossless optical fibers [36].The two lossless fiber can be two single mode fibers, two multimode fibers, two photonic crystal fibers and two fiber Bragg gratings. Figure (1.10) shows the schematic diagram of two path MZI interferometer.

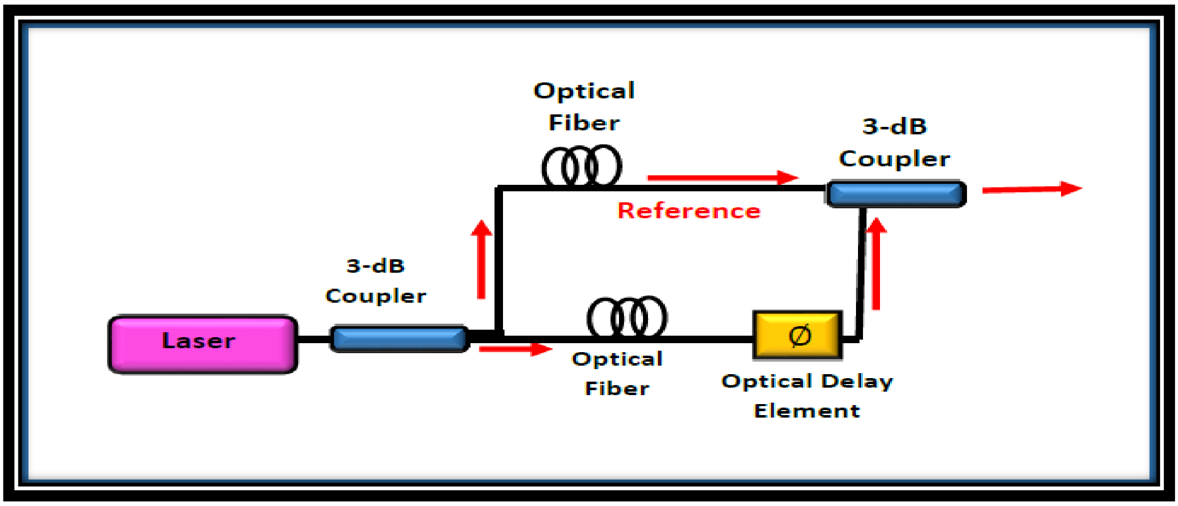

Figure (1.10): The schematic of two-path fiber MZI [36].

1.3.6.1 Single Mode Multimode Single Mode Machzehnder Interferometer

This type of interferometer based on coupled mode theory describe the interference pattern between single mode and multimode fibers. In This case a mode mismatch was occurred duo to different fiber core size [37].

1.3.6.2 Fiber Bragg Grating Machzehnder Interferometer

The simplest method to measure the signals of FBG is using a spectrometer. This method is very popular and widely used in the laboratory for a preliminary experiment or analysis. But the spectrometers are very expensive, in particular in the case where a wavelength resolution of ~1 pm is required to resolve a temperature change of ~0.1°C, or a strain change of 1 μstrain. In addition, conventional spectrometers are very large, which limits its application in practical fields.

A wide variety of techniques have been demonstrated for monitoring Bragg wavelength shifts, only certain techniques appear to have the potential for being reduced to a practical, cost-effective instrumentation system for use in ‘‘real-world’’ applications.

The most frequently utilized method for the interrogation of FBG sensors is based on passive broadband illumination of the device: light with a broad spectrum which covers that of the FBG sensors is input to the system; either the narrowband component reflected by the FBG is directed to a wavelength detection system, or the spectral ‘‘notches’’ in the transmitted are analyzed Demodulation techniques are mainly based on the edge filter, tunable filter, or interferometric scanning methods.

The edge filter method is based on the use of an edge filter which has a linear relationship between wavelength shifts and the output intensity changes of the filter, as shown in Figure (1.11-a) [38]. By measuring the intensity change, the wavelength shift induced by the measuring is obtained.

The measurement range is inversely proportional to the detection resolution. Tunable filter can be used to measure the wavelength shift of the FBG and the output is a convolution of both the spectrum of the tunable filter and that of the FBG, as shown in Figure (1.11-b). When the spectrum of the tunable filter matches that of the FBG, the convolution equals one, i.e. a maximum output occurs. By measuring this maximum point and the corresponding wavelength change of the tunable filter, the wavelength shift of the FBG is obtained.

The resolution is mainly determined by the signal-to-noise ratio of the return FBG signal and both the line widths of the tunable filter and the FBG. Normally, such an approach has a relatively high resolution plus a large working range. The FBG wavelength shift induced by strain and/or temperature can be detected with a scanned interferometer, which has been demonstrated for high-resolution dynamic and quasi-static strain measurements, termed the interferometric scanning method [39]. The normalized interference signal from a scanned interferometer (SI), as shown in Fig. (1.10-c), can be expressed as:

$$I/I_{\circ} = 1 + \mathrm{B}\cos[\Delta\varphi_B + \emptyset(t)] \qquad (1.6)$$

Where $I_\circ$ is the intensity of the incident light and B is the visibility of the interference signal. $\emptyset(t)$ is the thermally induced phase drift in the SI. The SI acts as a wavelength scanner for FBGs when the optical path of the SI is modulated. The strain- or temperature-induced change in the reflected wavelength from a FBG produces a change in the optical phase $\Delta\emptyset_B$:

$$\Delta\varphi_B = 2\pi\Delta L\,\Delta\lambda_B / \lambda_B{}^2 = 2\pi\,\Delta L\,\int_g \Delta Y/\lambda_B \qquad (1.7)$$

Where ΔY is the variation in strain applied to the FBG and ΔL_{SI} is the optical path difference (OPD) of SI. $\int g$ is the normalized FBG sensitivity for strain or temperature, given by:

$$\int g = (1/\lambda_B)\left(\frac{\Delta\lambda_B}{\Delta Y}\right) \qquad (1.8)$$

Hence, the phase sensitivity in response to strain $\left(\frac{\Delta\varphi_B}{\Delta Y}\right)$ is directly proportional to the OPD in the SI [40].

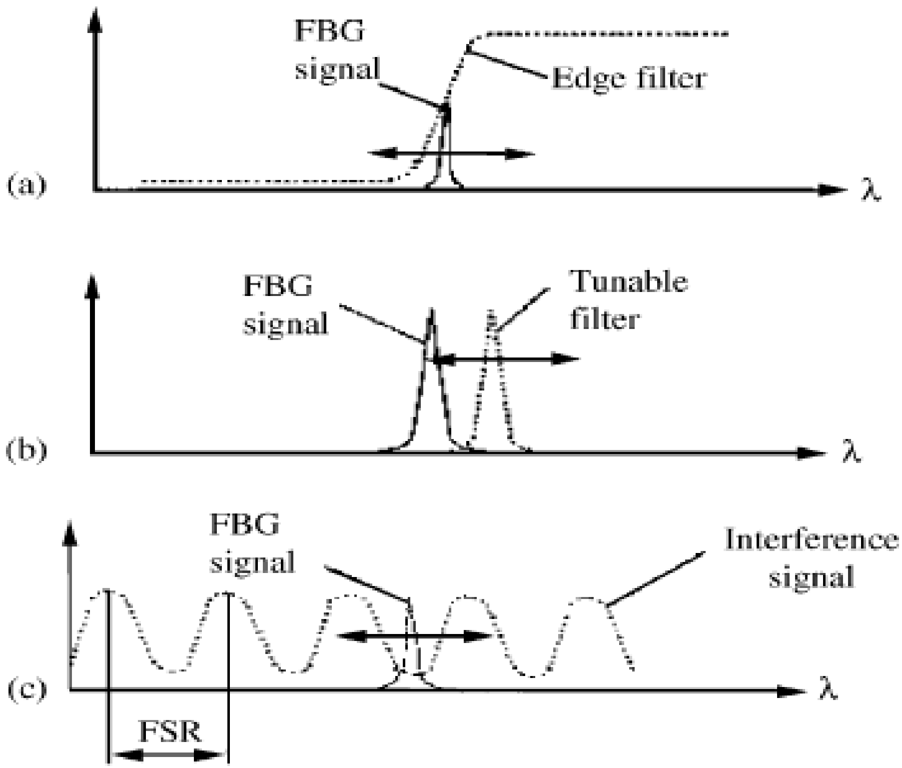

Figure (1.11): a) Principle of the edge filter method; b) principle of the tunable filter method; c) principle of the interferometric scanning method [38].

1.3.6.3 Multi-mode Mach-Zehnder Interferometer

Finally in these subsections the two arm of Mach-Zehnder interferometer consist of multimode fiber. A new method was presented with tunable all-fiber compact multimode fiber (MMF)-based filter and its applications in fiber sensors. The expression of the transmission of the optical filter is the same as that of a regular Mach–Zehnder interferometer (MZI) but with an additional optical phase shift in the sinusoidal function, which makes the MMF-based filter tunable. The phase shift could be changed by properly adjusting of a mechanical effect i.e. (force and strain). The proposed tunable filter has been employed for intensity interrogation of a fiber Bragg grating (FBG)-based temperature sensor where the MMF-based filter serves as an band pass filter. With the tuning technique [41].

1.4 Optical Filters

In the receiver side the basic component that must be used to rejection the optical noise in the received signal is optical filters which can be designed using different types of interferometers [42,43].

1.4.1 Types of Optical Filter

There are three type of optical filter will be explained in this sub section

1.4.1.2 Tunable Fabry-Perot Etalon Filter

The tunable Fabry-Perot etalon filter is made of two highly reflective mirrors separated by a distance of (λ/2), the distance causes the filter output spectral characteristic to peak sharply over a narrow band of wavelengths that are multiples of the (λ/2) distance, thus, the Fabry-Perot filter is used as a band-pass filter. This optical transmission system stores light energy at the selected frequencies by incorporating the feedback light with the light that was repeatedly or reflected within the system and thus circulates the light without escaping from the system. The tuning can be done by changing the distance between R1 and R2 (mirrors) corresponding to the desired wavelengths shown in Figure (1.12) [44,45].

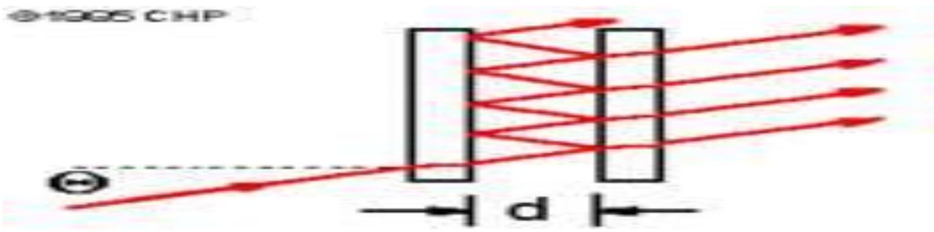

Figure (1.12): Basic concept of Fabry-Perot Etalon Filter [45].

1.4.1.2 All Optical Photonic Crystal Fiber Filters

Photonic crystal fiber (PCF) has been widely used in many applications like amplifiers, switching and tunable filters , all optical PCF filter can be achieved due to the optical properties of a PCF, which provides an opportunity to create tunable fiber-based devices by infiltrating high-index materials such as polymer, oil , and liquid crystal (LC) into the air holes. By filling the Hollow core-PCFs (PBG) with a liquid having a specific refractive index, the transmitted light will occur only over a certain wavelength ranges corresponding to the band gap of the cladding for the HC-PCF, these range of band gap can be tuned or shifted depending on the refractive index in the holes of the PCF so that, the optical properties of PBG can be changed by changing the liquids that are filled inside the PCF [46]

1.4.1.3 Tunable Optical Filter

Tunable optical filters (TOFs) may be constructed with passive or active optical components. The main characteristic of TOFs is their ability to select the range of filtered wavelengths. To be useful in optical communication systems, however, they must satisfy certain requirements [47].

i. Wide tuning range
ii. Constant gain

iii. Narrow bandwidth
iv. Fast tuning
v. Insensitivity to temperature (no frequency drift with temperature variations)

In telecommunication networks, TOFs can be used for amplified spontaneous emission (ASE) suppression of optical signals, for single channel demultiplexing from a multichannel WDM optical signal stream, and in flexible and dynamic wavelength add/drop applications.

Tuning speed directly determines the switching speed between different circuits, and therefore, high speed is a fundamental requirement for tunable filters. For circuit-switched networks, tuning time of no more than few milliseconds is essential very high-speed tunable filters, in the microsecond and nanosecond range, are a must in packet- and cell-switched networks [6].

Bandwidth and tuning range become more and more critical with the increased deployment of DWDM systems. Using filters of a very narrow bandwidth and a large tuning range is, so far, the most effective way to increase the channel capacity and to reduce the crosstalk in DWDM networks.

TOFs are occasionally used in fiber optic sensing applications for wavelength demultiplexing of fiber Bragg grating sensors for wavelength shift and spectral scanning in interferometric sensors.

Bandwidth is from sub-nanometer up to above ten nanometers, and tuning range from tens of nanometers to above 100 nm, varying from system to system.

Tuning speed also varies, but generally slow. For example, a scanning time of a few second may be enough for the measurement of static and very slow signals, such as temperature, strain, and chemical or biomedical concentration. However, in most application areas, fiber-optic sensors have to face fierce competition from their electronic counterparts available extremely cheap in the market.

Repeatability and stability are equally important parameters as those mentioned above in all applications. Highly repeatable and stable TOFs mean high resolution and accuracy in measurement instruments, and high reliability or low bit-error-rate (BER) in communications, and high quality in video distribution networks. Any survivable tunable filter technology must be highly repeatable and stable in long terms [47].

1.5 The Mach-Zehnder Interferometer Filter

The Mach-Zehnder filter is based on the interference of two coherent monochromatic sources that are based on the length difference, and thus the phase difference, of two paths, thus contributing positively or negatively. In fiber-optic systems, a phase difference between two optical paths may be artificially induced. Consider an input fiber with two wavelengths λ_1 and λ_2' the optical power of both wavelengths is equally split (directional coupler 1), and each half is coupled into a waveguide, one of which is longer than the other Land *(ΔL)*. The two halves arrive at a second directional coupler or combiner at different phases and, based on the phase variation and the position of the output fiber, each wavelength interferes constructively on one of the two output fibers and destructively on the other. That is, wavelength λ_1 interferes constructively on the first fiber and wavelength λ_2 on the second Figure (1.13) [47].

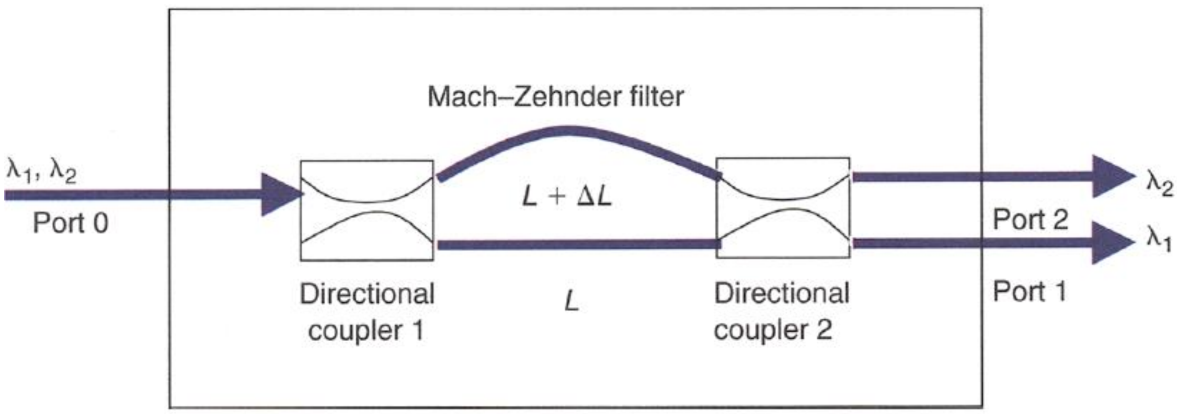

Figure (1.13): The principle of a Mach-Zehnder filter [47].

This arrangement is used to construct an integrated device that functions as a filter or as a wavelength separator, known as a *Mach-Zehnder filter*, according to which two frequencies at its input port are separated and appear at two output ports. A more detailed description of the Mach-Zehnder filter follows [47].

1.6 Tunability of the Mach-Zehnder Filter

If the quantity of optical path different between two arms (ΔL*)* can be adjusted at will, it is clear that the Mach-Zehnder filter can be tuned. The purpose of the quantity ΔL is to introduce the desired phase shift at the entry point of directional coupler 2. Thus, the phase shift is controlled by controlling the propagation delay of the path $L + \Delta L$ with respect to path L. This is accomplished either by altering the refractive index of the path (and thus the effective optical path), by altering its physical length, or by both means [47].

The phase may be controlled by one of several methods

i. Mechanical compression, by means of a piezoelectric crystal, alters the physical length of the waveguide segment and its refractive index.

ii. Certain optical materials alter their refractive index when exposed to heat; a thin-film thermoelectric heater placed on the longer path would control the refractive index of the path. A polymer material known to change its refractive index when exposed to heat is per-fluoro-cyclo-butane (PFCB).

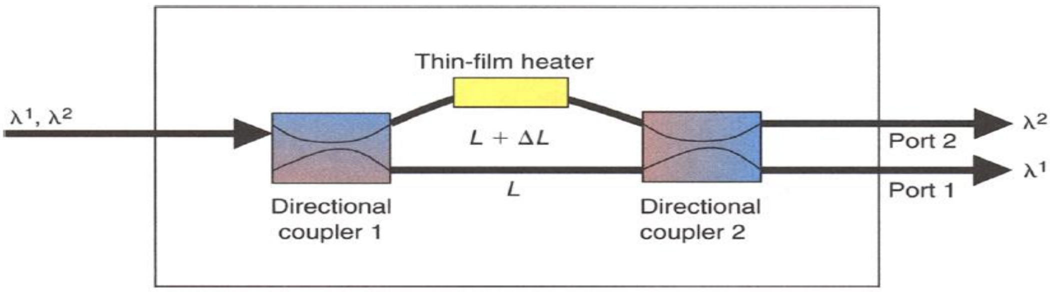

Figure (1.14): A Mach-Zehnder filter can be tuned by controlling the temperature of the $L+\Delta L$ path [47].

Thus, by controlling the refractive index of the path, the phase on the effective optical path $L + \Delta L$ is controlled and the wavelength selectability of the device is accomplished, making the Mach-Zehnder filter a tunable *optical* frequency discriminator (OFD) [47].

1.7 Literature Survey

In the following, a literature survey is given for some important research works in the field of all optical filters that are most related to this work.

2004 D. Gauden, E. Goyat, C. Vaudry, P. Yvernault and D. Pureur [48].

Tunable Mach-Zehnder-based add-drop multiplexer

Fiber type	twin core fiber
Effect type	heating
Tunability	1.7 nm

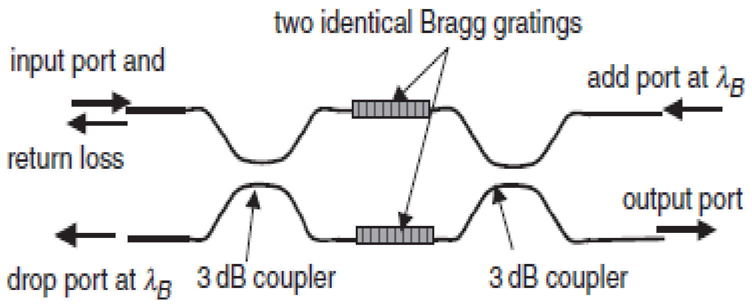

Twin core fiber based MZI

2007 ZHANG Zhi-guo, ZHANG Min, and YE Pei-da [49].** MZI-based wavelength interrogation system with tunable-FBG Fiber type FBG Effective type Temperature Tunability 0.02 nm 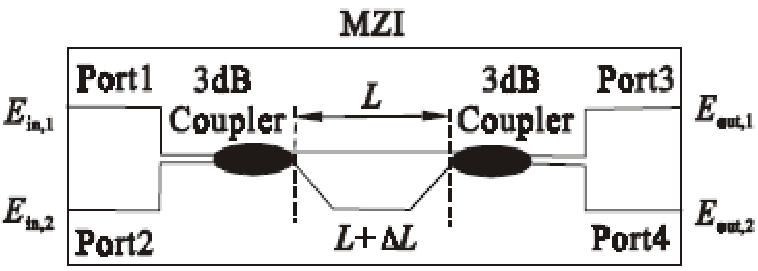 Fig.2 Schematic diagram of Mach-Zehnder interferometer
2010 Ai-Ping Luo1, Zhi-Chao Luo,1,2 Wen-Cheng Xu,1,* and Hu Cui1[50]. Wavelength switchable flat-top all-fiber comb filter based on a double-loop Mach-Zehnder interferometer Tunability 0.98 nm 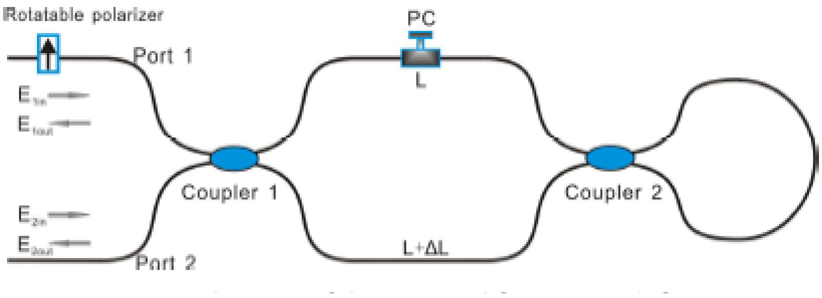 **Schematic of the proposed flat-top comb filter**.

2010 J. E. Antonio-Lopez,1 A. Castillo-Guzman,2 D. A. May-Arrioja,3,* R. Selvas-Aguilar,2 and P. LiKamWa4[51].

Tunable multimode-interference band pass fiber filter

Fiber type MMF

A capillary tube filled with refractive-index-matching liquid is used to effectively increase the length of the MMF

Tunability 30 nm

(Color online) Schematic of the tuning mechanism for the tunable MMI fiber filter.

2015 Y. Li, B. Zhou, L. Zhang, and S. He[52].

Tunable Fabry–Perot filter in cobalt doped fiber formed by optically heated fiber Bragg gratings pair

Fiber type FBG

Effective type Heating

Tunability 0.6 nm

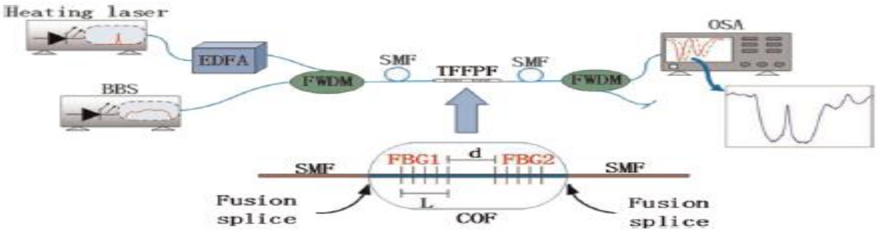

Wavelength division multiplexer (two channels: transmission channel, 1550710nm; reflection channel, 1260_1610nm except1550 10 ±nm);

2016 Long Huang, Peng Xiang, Dalei Chen, Peng Wang, Tao Pu, and Xiangfei Chen[53].

A Linearized Tunable Single Band pass Microwave Photonic Filter

Fiber type phase-shifted fiber Bragg grating (PS-FBG)

Effective type Pc

the frequency-tunable range of the single band pass MPF are 80 MHz and 5.5 GHz

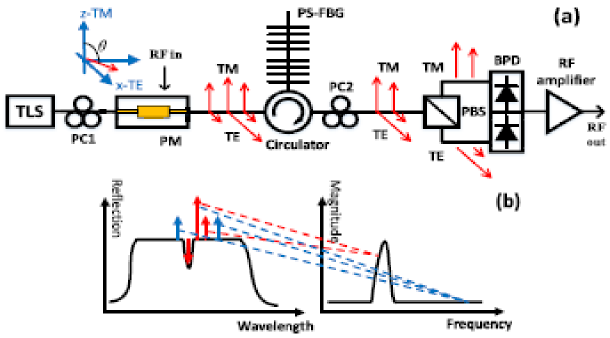

Experimental setup of the proposed MPF. (b) Principle to achieve

An MPF with a single pass band. TLS, tunable laser source; PC,

PM. PS-FBG. PBS: BPD.

2016 Farid Ahmed, Vahid Ahsani, Akram Saad, and Martin B.G. Jun.[54].

Bragg Grating Embedded in Mach-Zehnder Interferometer for Refractive Index and Temperature Sensing.

Fiber type FBG

Sensing type RI &Temperature

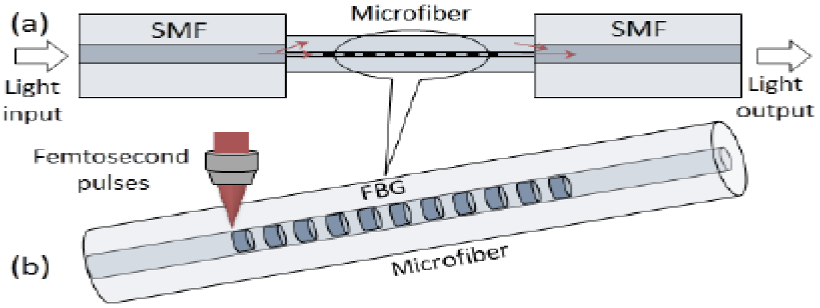

Schematic of integrated MZI and FBG sensor: Structural configuration of the sensor (a) and schematic of point-by-point fabrication of FBG in microfiber spliced between SMFs (b)

2017 Samar Kareem Ibrahim [30].

BUILDING TUNABLE SPECTRAL FILTER USING FIBER BRAGG GRATING

The tunability is about 0.519 nm for thermal technique

The tunability for strain technique is about 0.561 nm

Type fiber uniform FBG

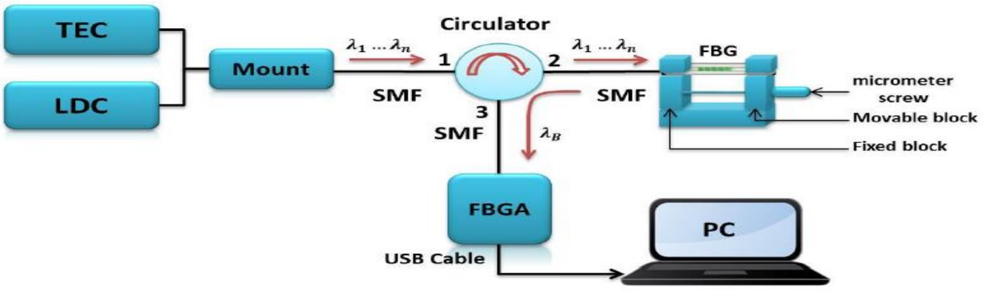

Experimental setup of FBG-TF utilizing strain technique.

Zhou[55].

Tunable Multimode Fiber Based Filter and Its Application in Cost-Effective Interrogation of Fiber-Optic Temperature Sensors.

Fiber type MMF

Sensing effect PC

Tunability =1.275

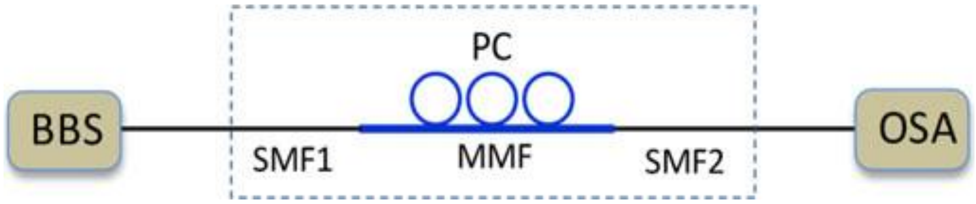

Experimental setup of all-fiber MZI. SMF1 and SMF2: single mode fiber; MMF: multimode fiber; PC: polarization controller; BBS: broadband source; OSA: optical spectrum analyzer.

2017 Anwaar A.AL-Dergazly,Farah S.Al-Thahaby[56].

Tunable Fiber Bragg Grating for Magnetic Field Sensor

Fiber type Pcf

Sensing effect PC

Tunability 0.042

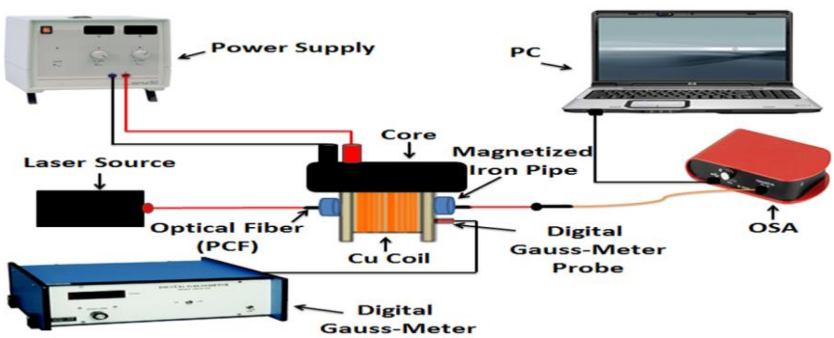

The experimental arrangement diagram of magnetic field sensor.

1.8 Thesis outline

This thesis is divided into three chapters.

Chapter One: Is an introduction into the topic. After the theoretical background on the tunable optical filter and interferometers. Brief literature survey related to this work is provided.

Chapter two: Covers Procedures of this Work. Then, the simulation and experimental setups are given. The simulation results in this chapter considers as the theoretical framework required designing TOFs with MZI.

Chapter three: Contains deep investigation and discussion of the simulated and practical results.

2.1 Introduction

In this chapter, the simulation and experimental work for optical tunable filters are demonstrated and constructed respectively using MZIs. The simulation work was carried out by optisystem software (version 7.0).The details of the research work is illustrated in Figure (2.1).

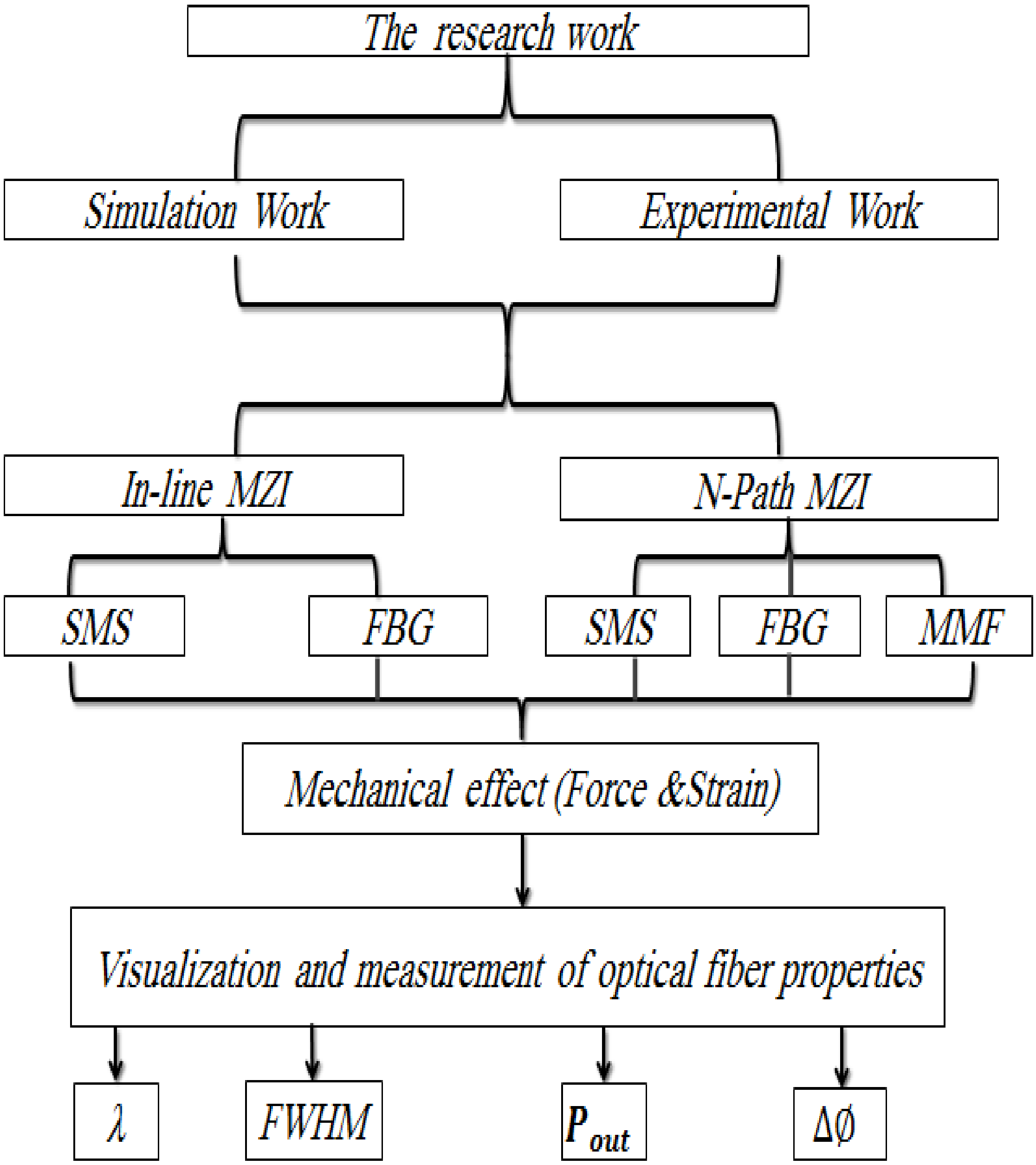

Figure (2.1): Block diagram for the work

2.2 The Simulation Work Components Specifications

The specifications of the components used by optiwave simulation software are presented in the following sections.

2.2.1 The Optical Sources

The Continuous Wave Laser Source

The specifications of this source are shown Table (2.1):

Table (2.1) the specification of Continuous laser source

Parameters	Values	Units
The operating wavelength (λ)	1554.730	nm
Power	1.85	mW

The spectrum of the CW Laser Source shown in Figure (2.2)

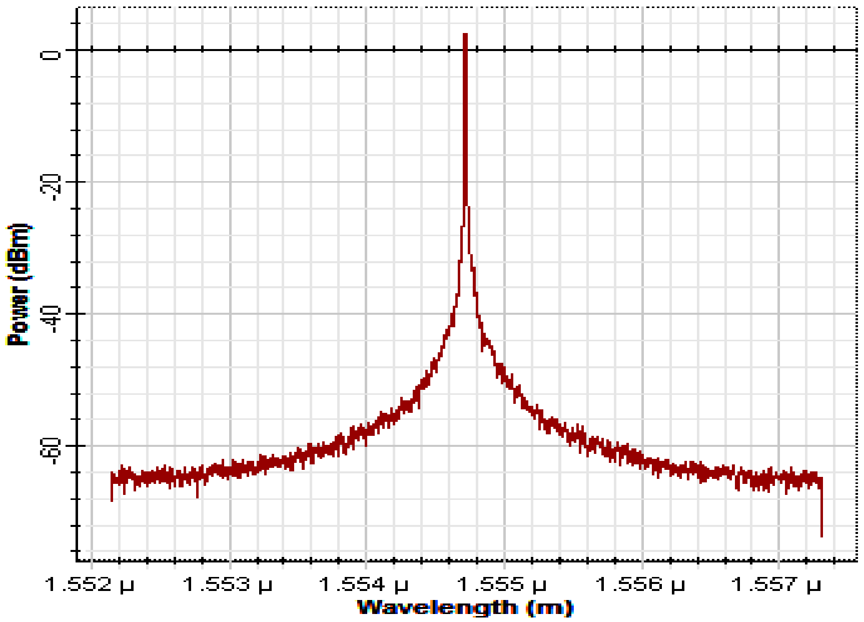

Figure: (2.2): The optical spectrum of CW Laser Source

The Broad Band Optical Source

Specifications of the broad band source are shown in Table (2.2)

Table (2.2) The specifications of the broad band source		
Parameters	**Values**	**Units**
The operating wavelength (λ)	1545	nm
Power	31.2	mW

The spectrum of the broad band source shown in Figure (2.3)

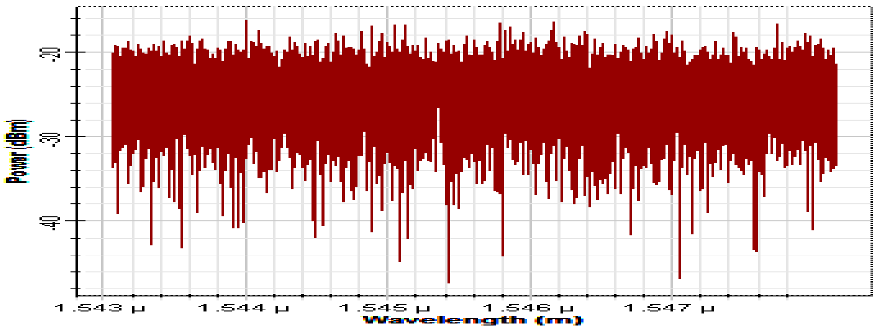

Figure: (2.3): The optical spectrum of the broad band source

2.2.2. The Optical Fibers

Single Mode Fibers

Table (2.3) shows the specifications of a single mode fiber (SMF).

Table (2.3): Specification of SMF		
Parameters	**Value**	**Units**
Operating wavelength	1550	nm
Fiber length	50	cm
Core diameter	8.3	μm
Cladding diameter	125	μm

Multimode Fibers

Table (2.4) shows the specifications of a multimode fiber (MMF).

Table (2.4): Specification of MMF		
Parameters	**Value**	**Units**
Operating wavelength	1550	nm
Fiber length	20	cm
Core diameter	62.5	μm
Cladding diameter	125	μm

2.2.3 Fiber Bragg Gratings

Table (2.5) shows the specifications of fiber Bragg gratings.

Table (2.5) shows the specification of fiber Bragg gratings				
Bragg wavelength [nm]	**Frequency [THz]**	**Band width [nm]**	**Grating length [mm]**	**Reflectivity %**
1545.559	193.958	0.206	10	94.37
1545.670	193.956	0.212	10	95.26

2.3 The Experimental Work Components and Equipment

The specifications of the components and equipment used in the experimental work are presented in the following sections.

2.3.1 The Optical Sources

The Continuous Wave Laser source

The spectrum of the CW Laser source is shown in Figure (2.4)

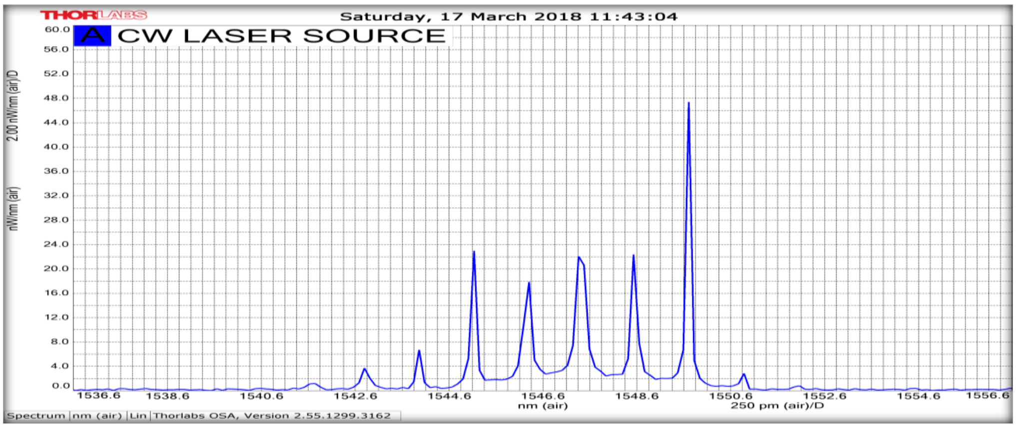

Figure (2.4): the spectrum of the continuous laser source

The spectrum of the continuous laser source must have a wavelength (1550 nm) as specified in the data sheet in Appendix (I) but when measured by optical spectrum analyzer (OSA), the wavelength was (1549.688) nm, because the room temperature was about $45C^{\circ}$ and the optical fibers connected between the laser source and the OSA for spectral measurement are very sensitive to high temperature, accordingly there was a difference in the wavelength . The optical output power at (1549.688) nm was equal to (1.85) mW.

Broad Band Source (BBS)

The spectrum of the BBS is shown in Figure (2.5). The optical spectrum of BBS extends from (1450) nm to (1650) nm. The maximum optical power of the BBS is (31.2) mW.

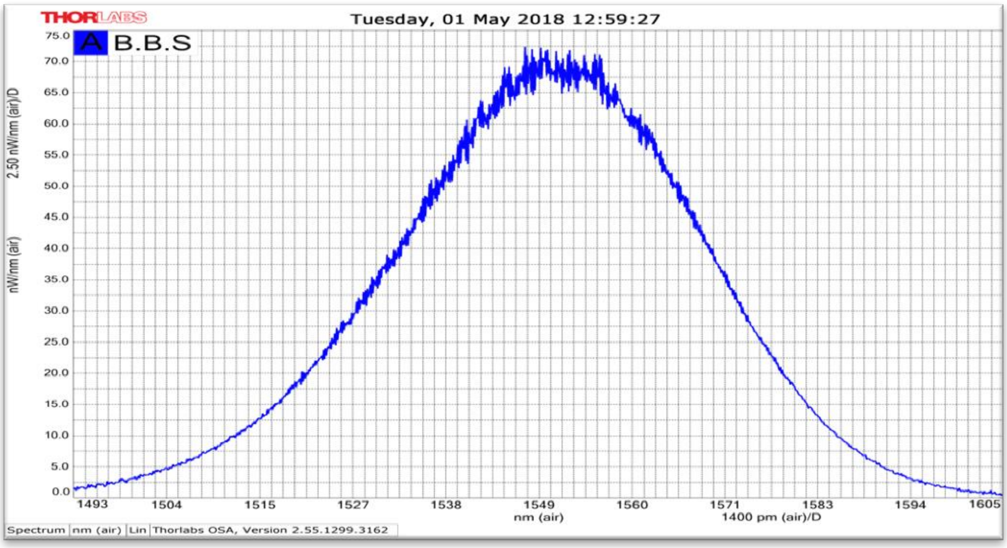

Figure (2.5): The optical spectrum of the BBS

The BBS consists of Ic chipset which is the basic element that generates the optical signal. Laser diode controller (LDC) gives the required power for the emitted optical signal. Temperature electric control (TEC) controls the emitted wavelengths and the optical output power.

2.3.2 The Optical Fibers

The optical fibers used in the experimental work have the same specifications as those used in the simulation work.

2.3.3 Fiber Bragg Gratings

Specifications of the fiber Bragg gratings used in the experimental work are listed in Appendix (H).

2.3.4 Mechanical Effects

Two mechanical effects were used in the experimental works which are force and strain. The details of these two mechanical effects are listed below.

Force Effect

The force effect was achieved by applying different weights. The structure that was used to apply these weights consists of different dimensions of bases made from aluminum as shown in Figure(2.6). The ground base dimensions are (27*27*1.5) cm. The pieces over the ground base are considered as bracketed tool. It consisted of two pieces of polished carbon steel or aluminum with dimensions of (5.5*3*1.5) cm.

The dimensions of balanced base are (19*19*0.5) cm. This design involves reset process for parts of the system over a bracketed tool. The purpose of reset process is to ensure that the weights are zero on the MMF and that the structure used to apply the force effect is calibrated.

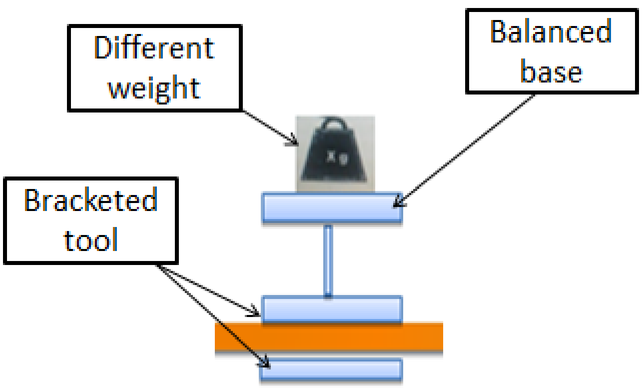

Figure (2.6): Schematic diagram of force effect structure

The Strain Effect

The micro strain is used to stretch the FBG to validate the strain technique for shifting the Bragg wavelength. The micrometer should be set to zero before using it in the experiment. The fiber Bragg grating is positioned between two blocks and fixed by screws. The movable block is used to apply the strain effect. Figure (2.7) shows the micrometer used in the experiment.

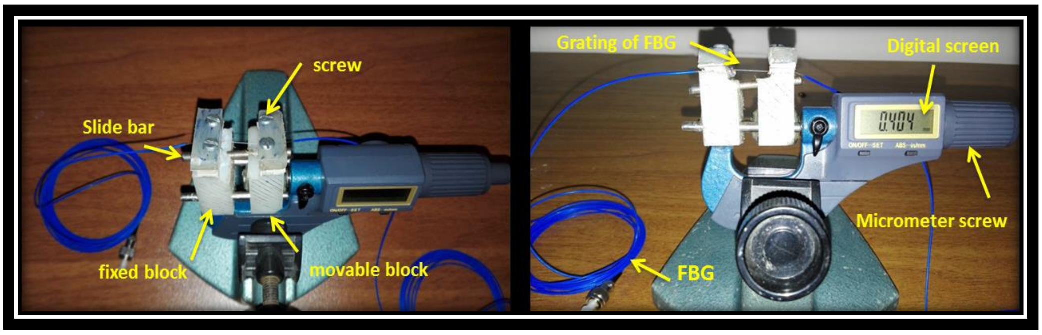

Figure (2.7): Micrometer used for strain effect.

2.3.5 The Optical Spectrum Analyzer (OSA)

The OSA, 202C, used in these experiments is from THORLABS. The specifications of the OSA are listed in Appendix (F).

2.4 Simulation and Experimental Works

As it was listed in Figure (2.1), a simulation study for each part in the block diagram was carried out followed by an experiment for that part. In the following sections the details of all the simulation studies and experiments are presented.

2.4.1 In-line Mach-Zehnder Interferometers

Two types of In-line MZI have been used in the simulation and experimental work to design tunable band pass and notch optical filters. The details will be presented below.

2.4.1.1 Single Mode –Multimode-Single Mode Mach-Zehnder Interferometer (SMS-MZI).

Simulation Work

The model of tunable optical band bass filter carried out by optisystem software is shown in Figure (2.8). The model is based on SMS-MZI.

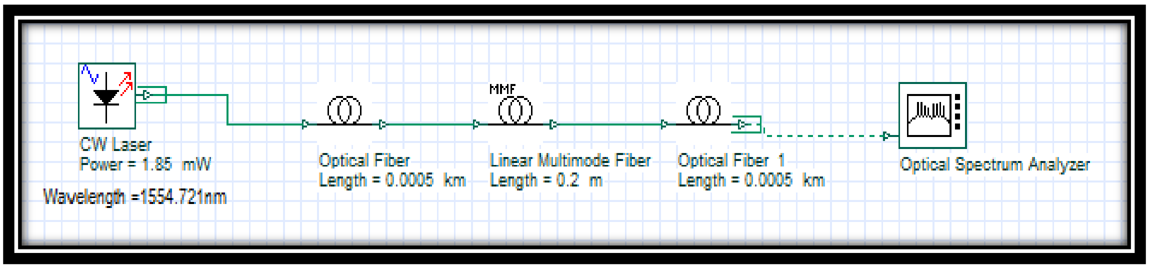

Figure (2.8): The model of in-line SMS-MZI band pass optical filter system.

In order to apply the force effect in optiwave software Equations (1.5), (1.6) and (1.7), were used to find the amount of the fiber length corresponding to the applied force.

The phase shift in the output optical signal for the simulation models and the experimental work was calculated by applying Equation (1.4).

Experimental Work

Figure (2.9) shows the schematic diagram for experimental setup for the tunable optical band pass filter.

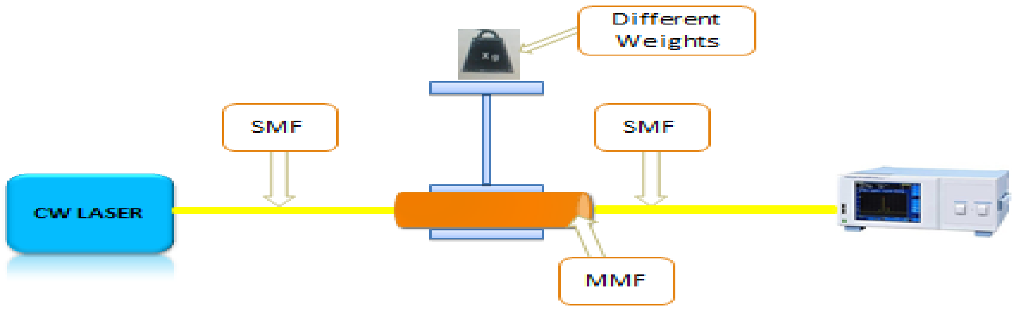

Figure (2.9): Schematic diagram of a tunable optical in-line SMS-MZI filter with weight effect system.

The CW LASER source was used in this setup. In this experiment a 20 cm MMF was spliced from its two ends with 50 cm SMF.

SM and MM fibers were spliced by fusion splicing machine (740) from (DVP), Appendix (J).

The parameters of splicing machine are shown Table (2.6):

Table (2.6) parameters of fusion splice SMF and MMF	
Fiber type	AOTO
Mode Title1	AUTO
Mode Title2	SM/NS/DS/MM
Cleave limit	4.4°
Loss limit	0.20dB
Arc Time	Auto
Cleaning Arc	150ms

The splicing regions gave minimum losses as shown Figure (2.10).

Figure (2.10): Fusion splicing of SMF and MMF.

With no weight applied the OSA gave a central wavelength of (1554.721) nm with an optical power of (1.85)mW.

In this experiment the weight was changed from (0-1) kg in steps of 0.250 kg.

The transmitted signal from SMS-MZI was transmitted to the OSA to check the transmission spectra. In the transmitted wavelength, more than one change will be obtained because of the MMF that has been influenced by the external effect (weight). These effects changed the transmitted wavelengths.

OSA measured the signal and then it displayed the results on a computer screen. The shift of a central wavelength in the transmitted signal can be observed.

A picture of this experiment shown in the Figure (2.11).

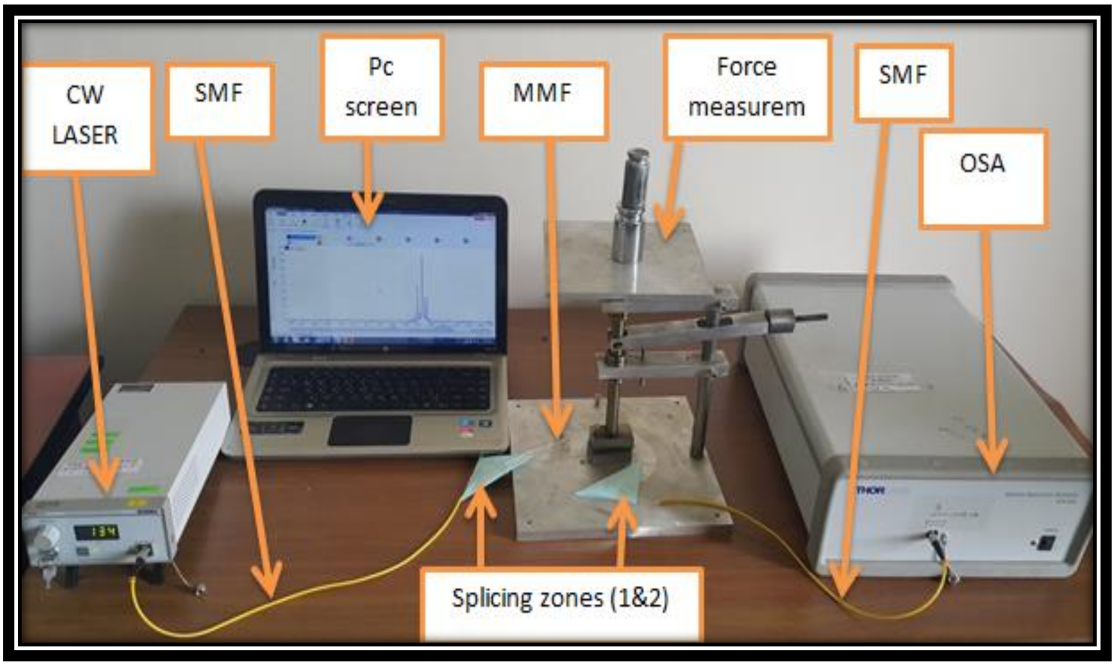

Figure (2.11): the experimental setup for In-line SMS-MZI.

2.4.1.2 Single mode –Bragg grating-Single mode Mach-Zehnder Interferometer (SFBGS-MZI)

The schematic diagram of in-line SFBGS -MZI setup is shown in Figure (2.12):

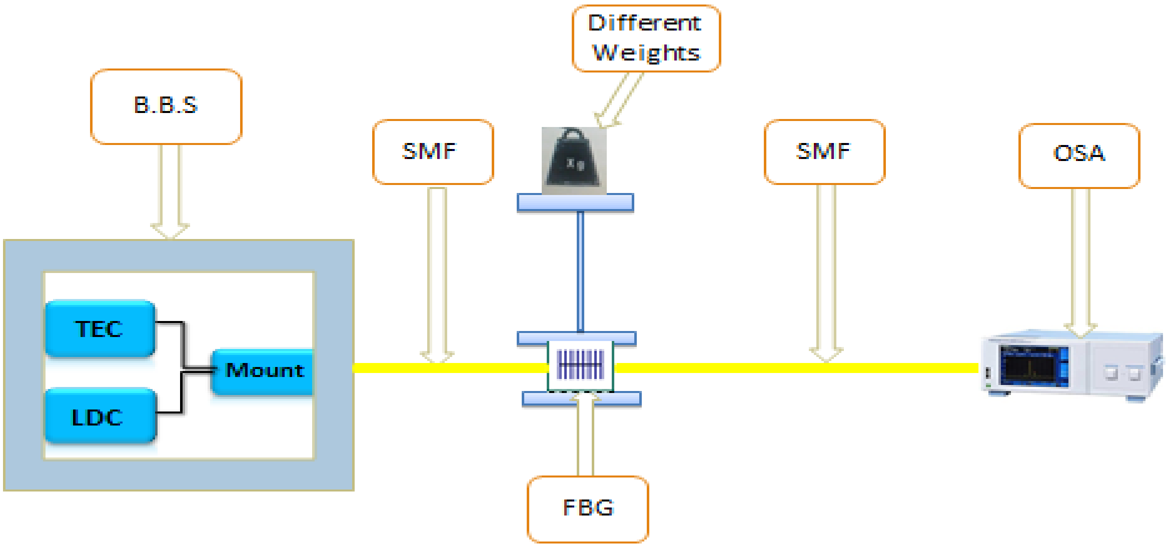

Figure (2.12): Schematic diagram of a tunable optical in-line SFBGS-MZI filter with weight effect.

It consist of a broad band source, SMF with a length of (3) m, FBG with grating length 10 mm, SMF with length (3) m connected to the optical spectral analyzer (OSA).

The phase shift in the output optical signal for the simulation models and the experimental work was calculated by applying Equation (1.4).

Figure (2.13) shows the picture of the experimental setup of In-line SFBGS-MZI.

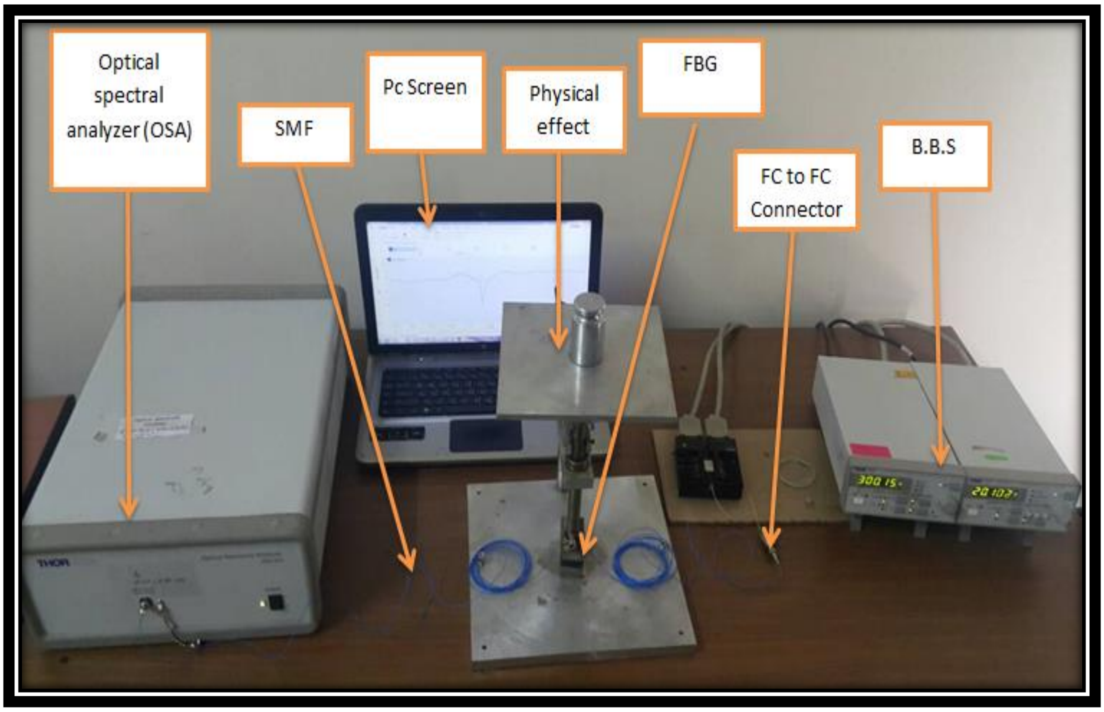

Figure (2.13): The experimental setup for SFBGS-MZI.

2.4.2 N-Path Mach-Zehnder interferometers

Three types of two-path MZI have been used in the simulation and experimental work to design tunable band pass and notch optical filters. The details will be presented below.

2.4.2.1 Single mode-Multimode-Single mode Mach-Zehnder Interferometer (SMS-MZI).

Simulation Work

The model of tunable optical band bass filter based on SMS-MZI is presented in Figurer (2.14). The model is based on SMS-MZI in the upper and the lower paths.

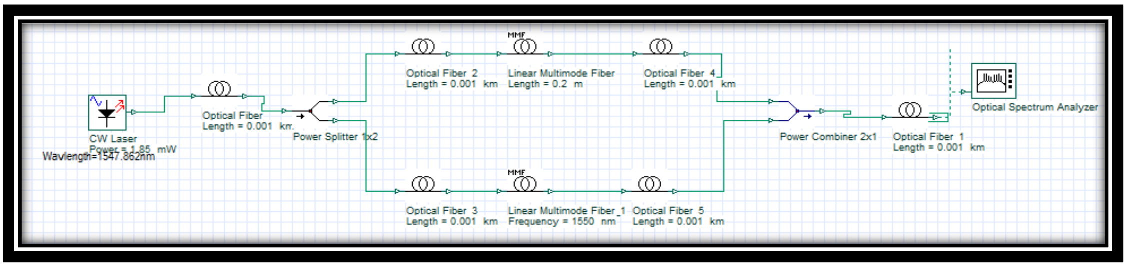

Figure (2.14): The model of simulated tunable optical two-path SMS-MZI band pass filter system.

Experimental work

The schematic diagrams of the experiments for the force effect and the strain effect are shown in Figures (2.15) and (2.16) respectively.

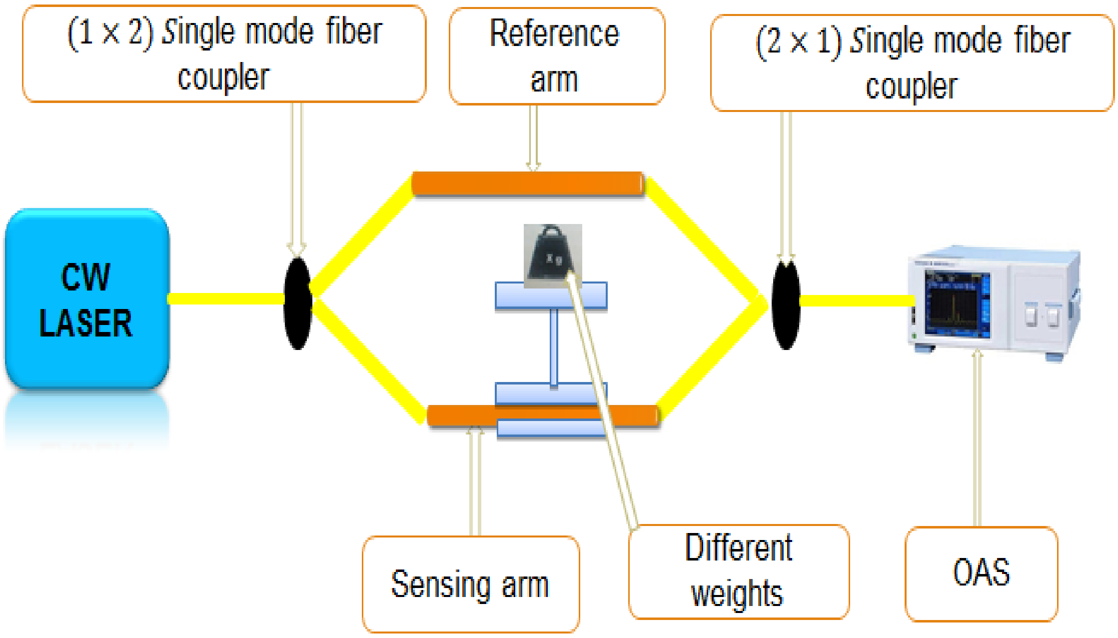

Figure: (2.15): Schematic diagram of a tunable optical filter based on two-path SMS-MZI with force effect.

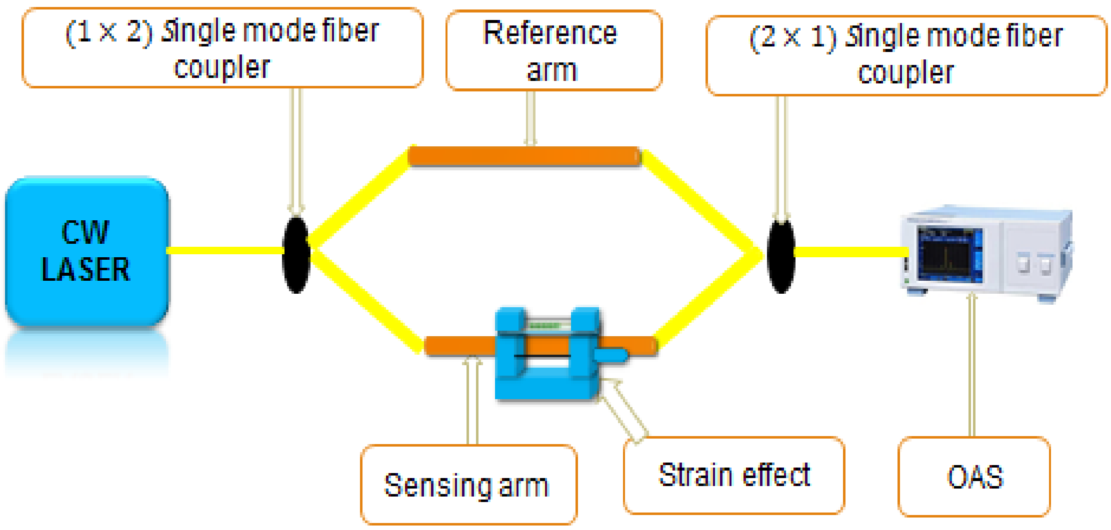

Figure: (2.16): Schematic diagram of a tunable optical filter based on two-path SMS-MZI with strain effect.

The setups consist of (1× 2) and (2×1) single mode couplers at the input and the output respectively two split and recombine at the input and the output of the device respectively. The upper arm consists of MMF as a reference arm and the lower arm consists of MMF with the strain effect. The lower arm is the sensing arm. When force or strain is applied on the lower arm of SMS- MZI, the optical path difference between the two arms will be obtained.

The pictures of these experiments are shown in Figures (2.17) and (2.18).

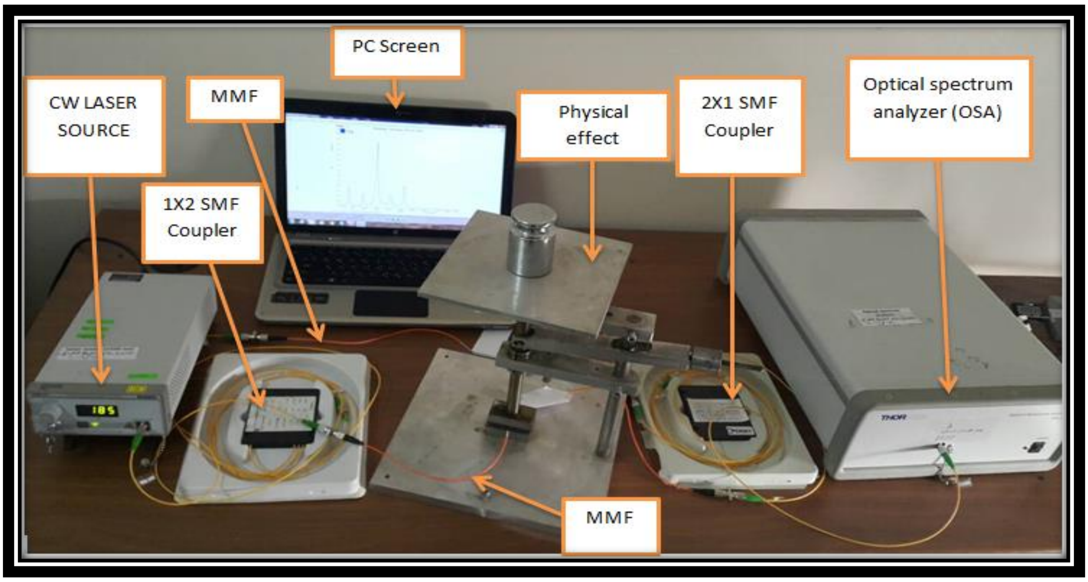

Figure (2.17): The experimental setup for two-paths SMS-MZI with force effect

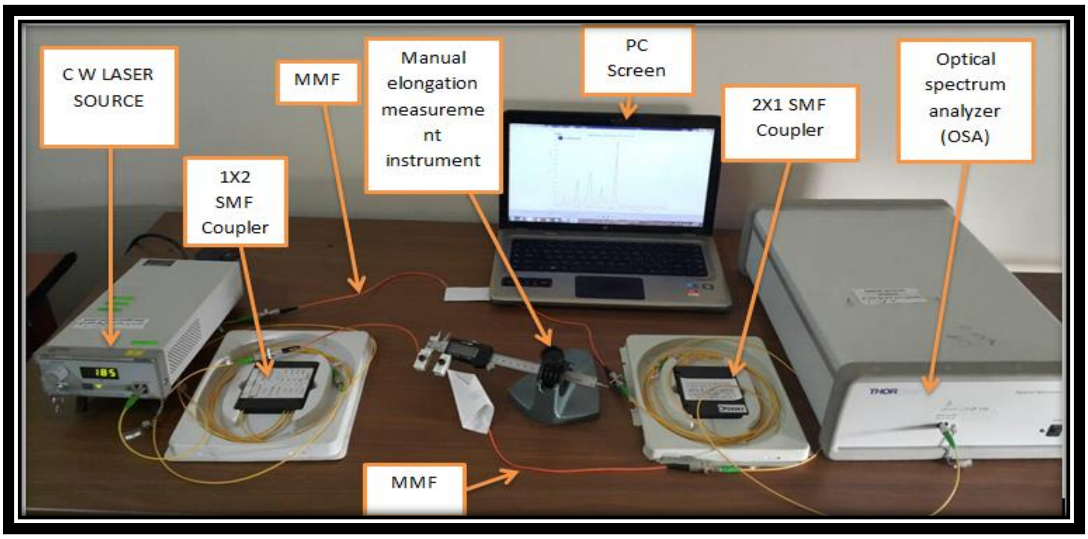

Figure (2.18): The experimental setup for two-paths SMS-MZI with strain effec*t*

2.4.2.2 Single mode-Fiber Bragg Grating-Single mode Mach-Zehnder interferometer (SFBGS-MZI).

Simulation Work

The model of tunable optical notch filter based on SFBGS-MZI is presented in Figurer (2.19). The model is based on SFBGS-MZI in the upper and the lower paths**.**

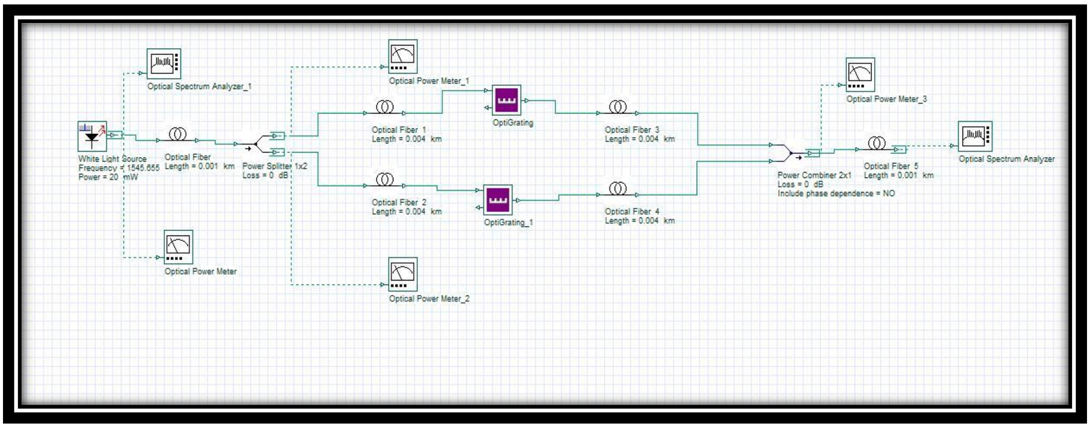

Figure (2.19): The model of simulated tunable optical two-path SFBGS-MZI notch filter system.

Experimental work

The schematic diagrams of a SFBGS-MZI are presented in Figures (2.20) and (2.21) with force and strain effects respectively.

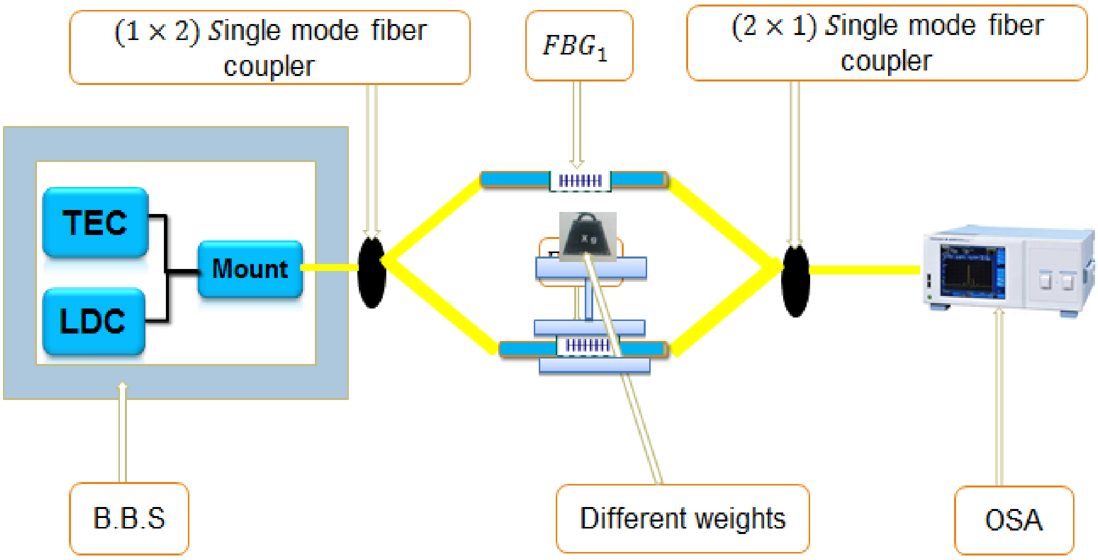

Figure (2.20): Schematic diagram of a tunable optical filter based on two-path SFBGS-MZI with force effect.

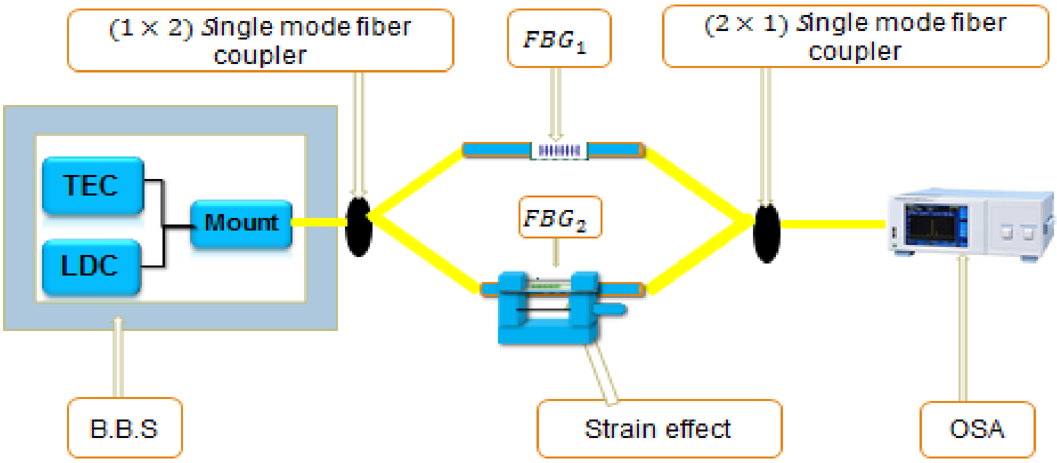

Figure (2.21): Schematic diagram of a tunable optical filter based on two-path SMS-MZI with strain effect.

These setups are the same as those of two-path SMS-MZI, but the MMF were replaced by FBGs in both arms of the two setups. In addition, the CW LASER source was replaced by BBS.

Pictures of these experiments are shown in Figures (2.22) and (2.23).

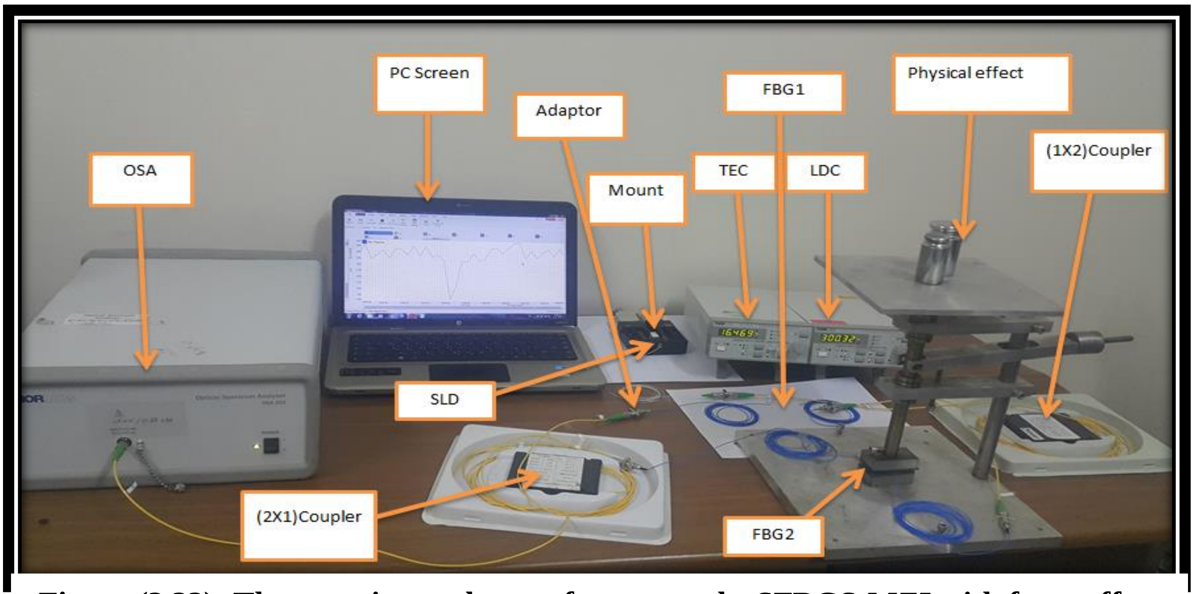

Figure (2.22): The experimental setup for two-paths SFBGS-MZI with force effect

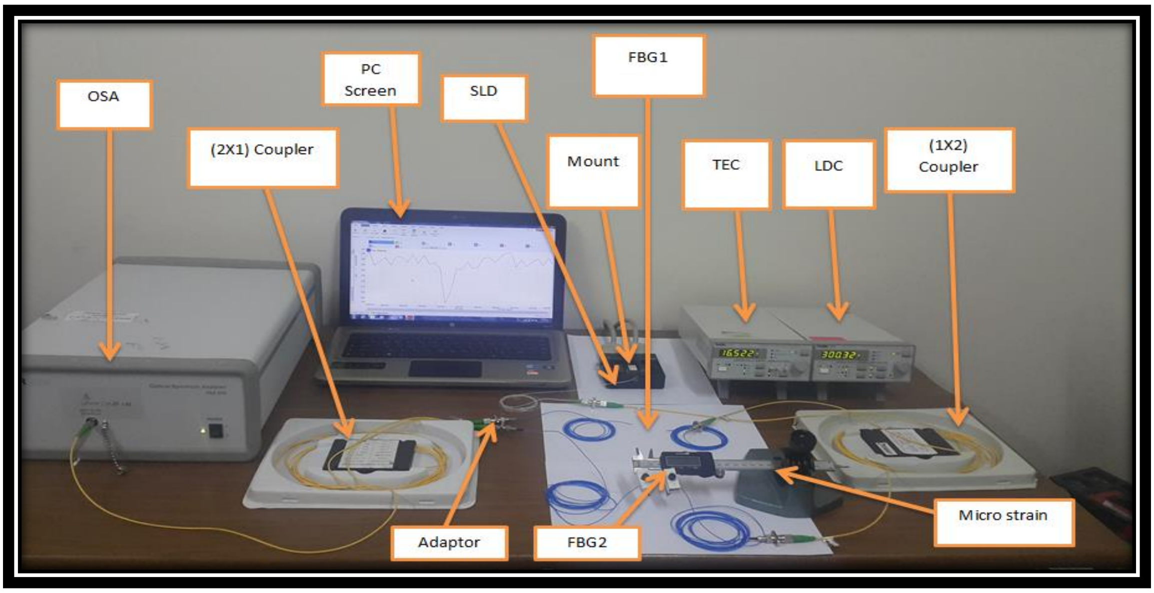

Figure (2.23): The experimental setup for two-paths SFBGS-MZI with strain effect

2.4.2.3 Multimode Mach-Zehnder interferometer

Simulation Work

The model of tunable optical band pass filter based on MM-MZI is presented in Figurer (2.24). The model is based on MM-MZI in the upper and the lower arms.

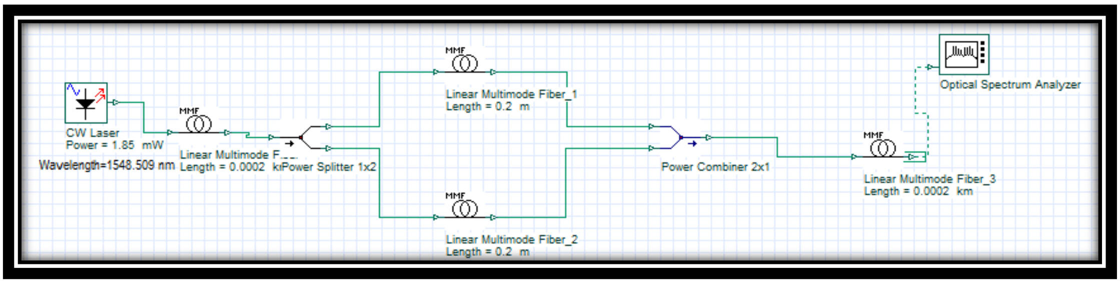

Figure (2.24): The model of simulated tunable optical two-path MM-MZI band pass filter system.

Experimental work

The schematic diagrams of the experiments for the force effect and the strain effect are shown in Figures (2.25) and (2.26) respectively.

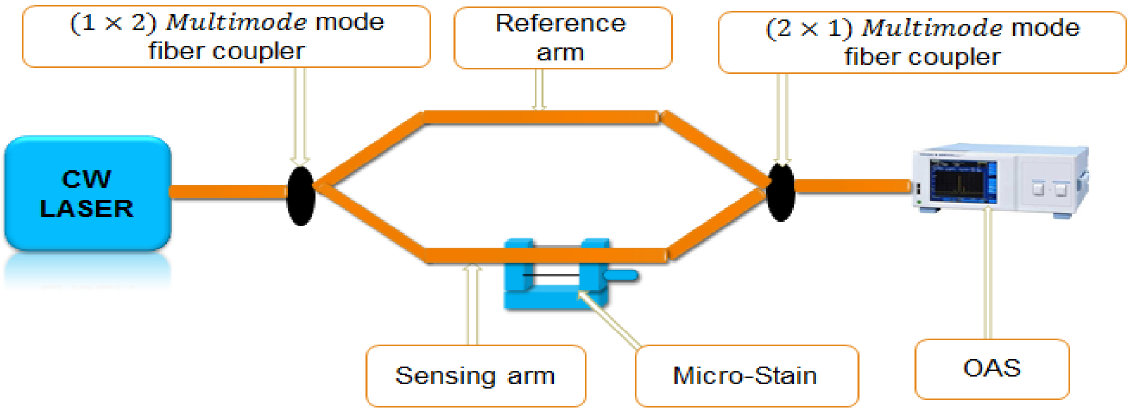

Figure (2.25): Schematic diagram of a tunable optical filter based on two-path MM-MZI with force effect.

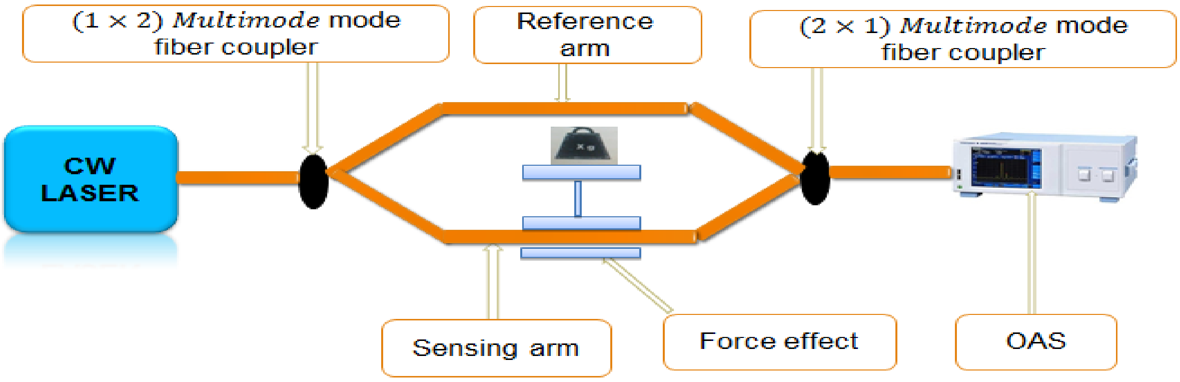

Figure (2.26): Schematic diagram of a tunable optical filter based on two-path MM-MZI with strain effect.

The setups consist of (1× 2) and (2×1) multi- mode couplers at the input and the output respectively two split and recombine at the input and the output of the device respectively. The upper arm consists of MMF as a reference arm and the lower arm consists of MMF with the force effect.

The setups of these experiments are shown in Figures (2.27) and (2.28).

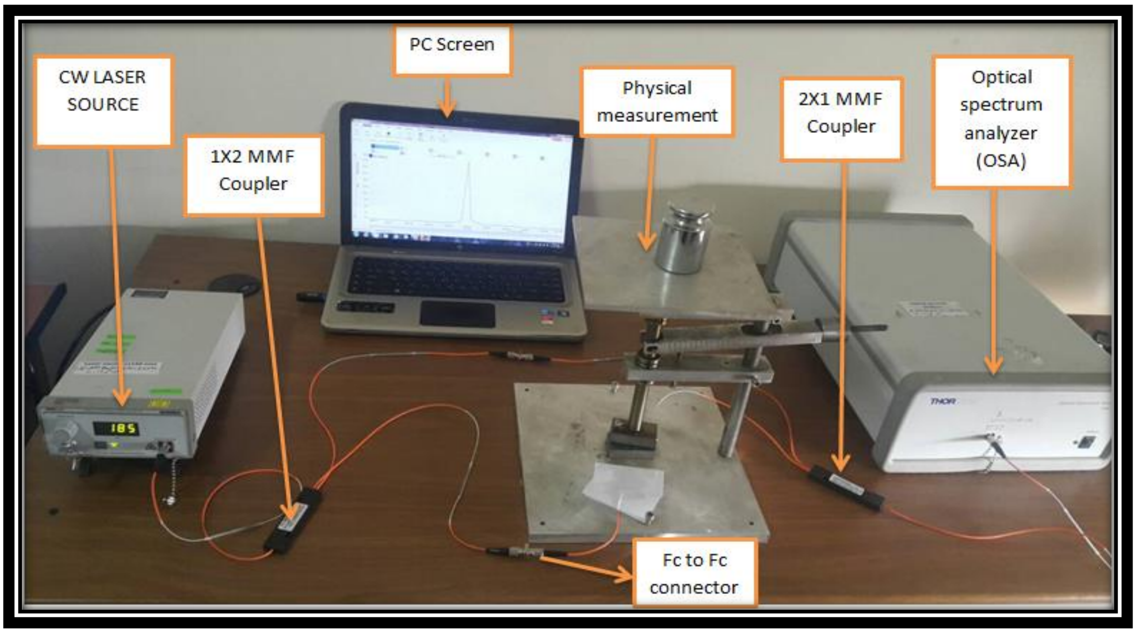

Figure (2.27): The experimental setup for two-paths MM-MZI with force effect

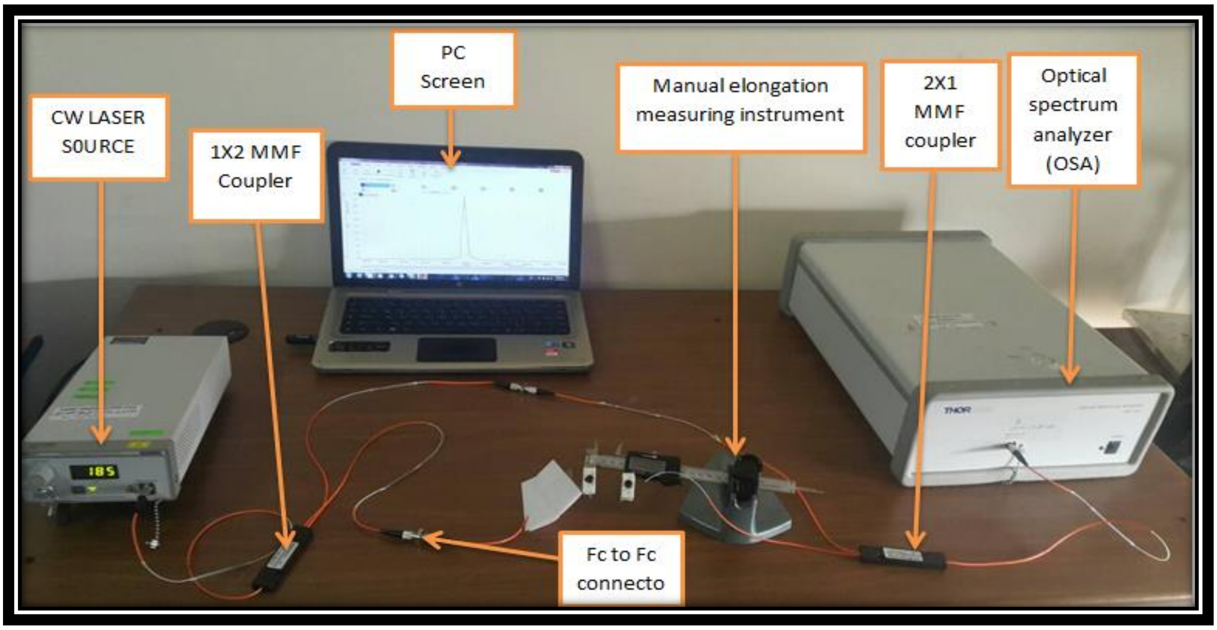

Figure (2.28): The experimental setup for two-paths MM-MZI with strain effect

3.1 Introduction

In this chapter, simulation and experimental results for the tunable filters designed in Chapter two are presented and discussed.

3.2 Simulation and Experimental Results

In the following sections the simulation results and experimental results are are illustrated for all types of the optical filters presented in Chapter two.

3.2.1 In-line Mach-Zehnder Interferometers

In-Line MZI filters, SMS and SFBGS -MZIs results are presented in the following sections.

3.2.1.1 Single Mode-Multimode-Single Mode Mach-Zehnder Interferometer with force effect

Simulation Results

The output spectra for In-line SMS-MZI due to force effect that was obtained by applying different values of weights on the MMF. From Figure (3.1), it is clear that there is a shift in the central wavelength for the output optical signal monitored by the OSA of the Optiwave system.

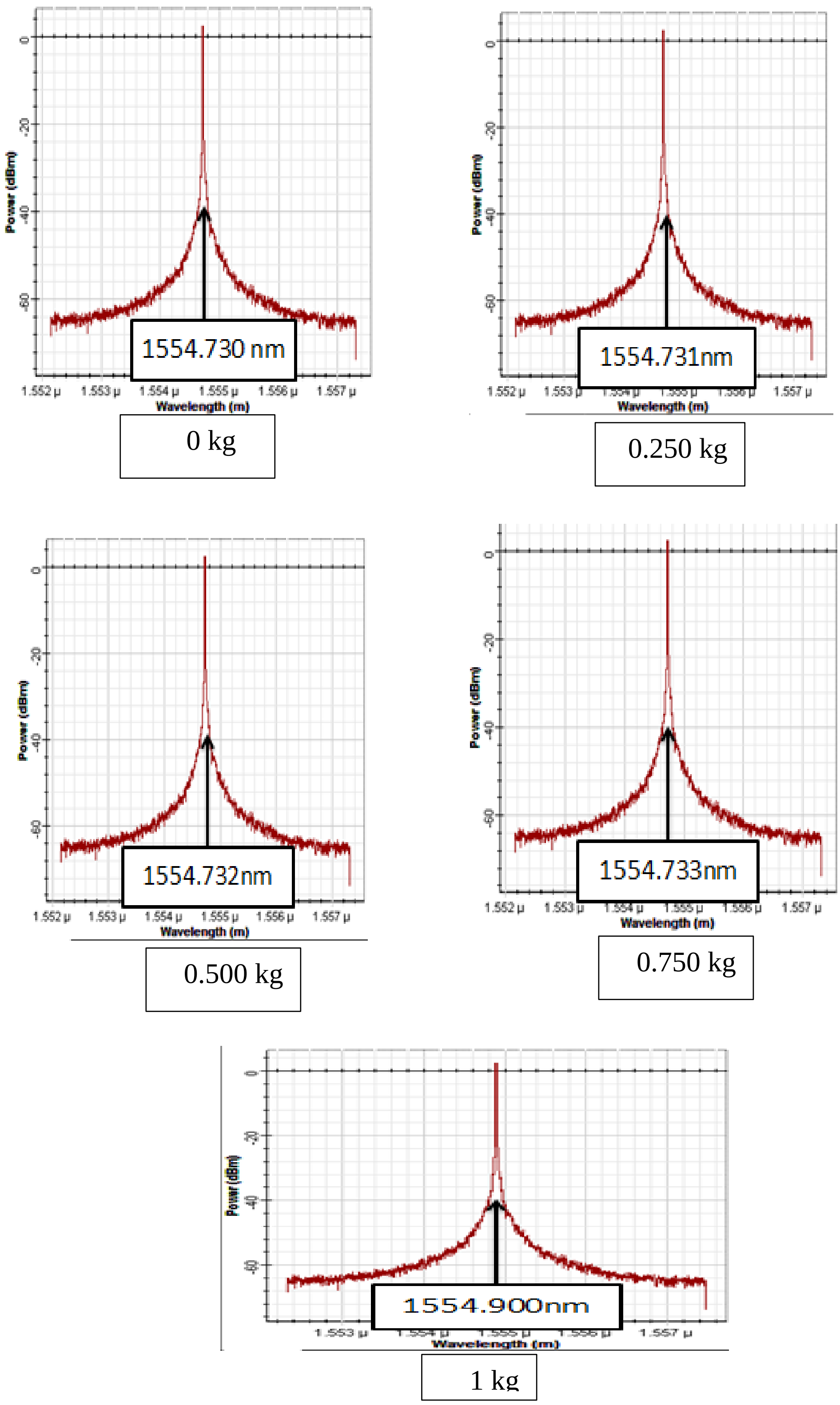

Figure (3.1) Wavelength shift for In-line SMS-MZI due to different values of applied force.

Experimental results

Figure (3.2) shows the output spectra for In-line SMS-MZI for different weights applied on the MMF are visualized by the OSA.

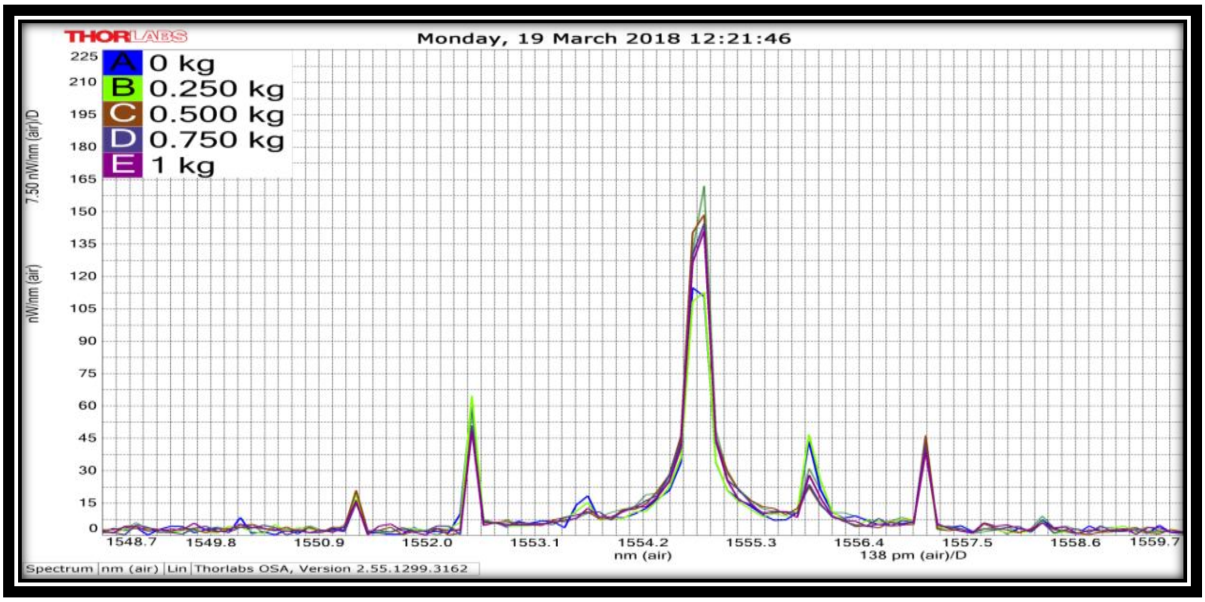

Figure (3.2) Tunable optical band pass filter when applying different sets of weights on the cross section area of MMF.

Table (3.1) lists the values of the shift in the central wavelength shifted, the FWHM, the output optical power and the phase shift in the output optical signal. From this table, the central wavelength shift and the output optical power are inversely proportional, while the phase shift of SMS-MZI are directly proportional to the applied weights. In addition, FWHM has a non-linear variation. The same behavior can be seen for both simulation and experimental results.

Table (3.1) shows that the simulated results are slightly different from experimental results due to the laboratory environments.

Table (3.1) the weight effect on the central wavelength, FWHM, output optical power and phase shift for in-line SMS-MZI								
Weight (kg)	**Central wavelength shift (nm)**		**FWHM (pm)**		P_{dBm}		$\Delta\varphi(m\ rad)$	
	Sim.	**Exp.**	**Sim.**	**Exp.**	**Sim.**	**Exp.**	**Sim.**	**Exp.**
0	1554.730	1554.721	200000	273.204	6.402	16.1	0	0
0.250	1554.731	1554.723	200000.04	275.681	6.40197	16.7	2.46	2.48
0.5	1554.732	1554.725	200000.05	272.301	6.40196	17	4.93	4.96
0.75	1554.733	1554.727	200000.055	271.078	6.40194	16.9	7.53	7.57
1	1554.900	1554.953	200000.06	269.737	6.40029	17.1	9.84	9.91
(Note: Sim stands for simulation , Exp stands for experimental)								

3.2.1.2 Single Mode-Bragg Grating-Single Mode MZI (SFBGS-MZI) Experimental Results with Force Effect

Figure (3.3), it is clear that there is a shift in the central wavelength for the output optical signal monitored by the OSA.

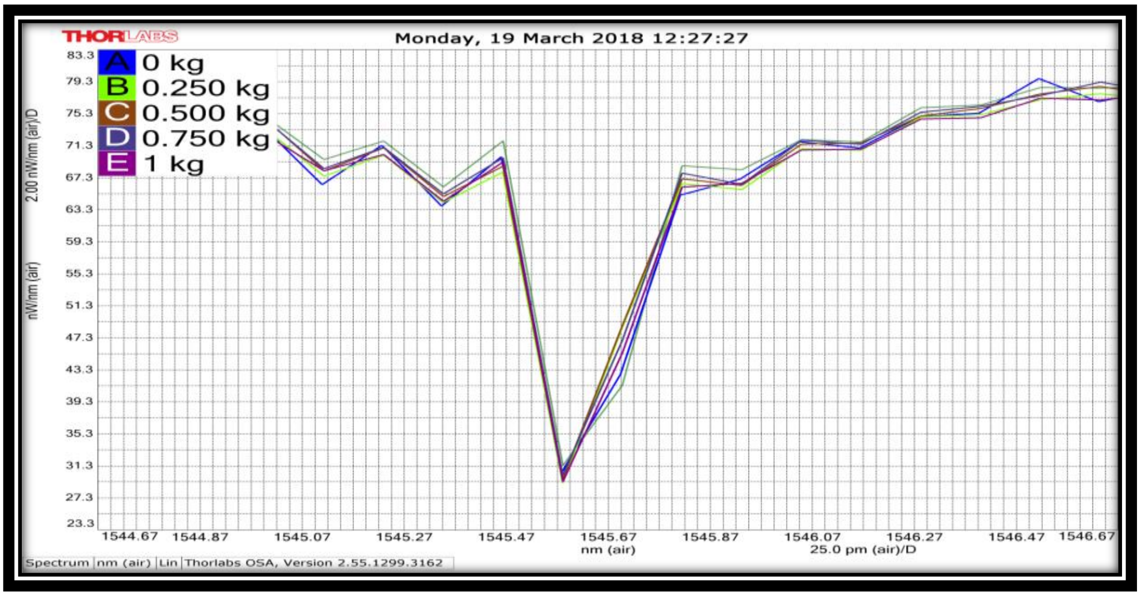

Figure (3.3) Tunable optical notch filter when applied different sets of weights on the cross section area of FBG for one arm SFBGS-MZI

Table (3.2) lists the effect of different values of weights (forces) on the central wavelength, FWHM, output optical power and phase shift of the output optical signal for in-line SFBGS-MZIs.These same behavior for central wavelength, FWHM, output optical power and the phase shift of the output optical signal with the change of the applied weight can be seen for in-line SFBGS-MZI as was obtained for in-line SMS-MZI.

Table (3.2) Effect of different values of weights on the central wavelength, FWHM, output optical power and phase shift for in-line SFBGS-MZI.

Weight(Kg)	Bragg wavelength (nm)	FWHM(pm)	P_{dBm}	$\Delta\varphi(m\,rad)$
0	1545.602	215.729	14.6	0
0.250	1545.603	172.908	14.5	0.1245
0.500	1545.604	175.123	14.5	0.182
0.750	1545.611	189.368	14.3	1.24
1	1545.631	201.312	14.4	2.26

3.2.2 Two-path Mach-Zehnder interferometers

Two-path MZI filters, SMS, SFBGS and MMF -MZIs results are presented in the following sections.

3.2.2.1 Single mode -Multi mode -Single mode Mach-Zehnder interferometer

Simulation results with force effect

Figure (3.4) shows the output spectra for two-path SMS-MZI due to force effect that was obtained by applying different values of weights on the MMF. It is clear that there is a shift in the central wavelength for the output optical signal monitored by the OSA of the Optiwave system.

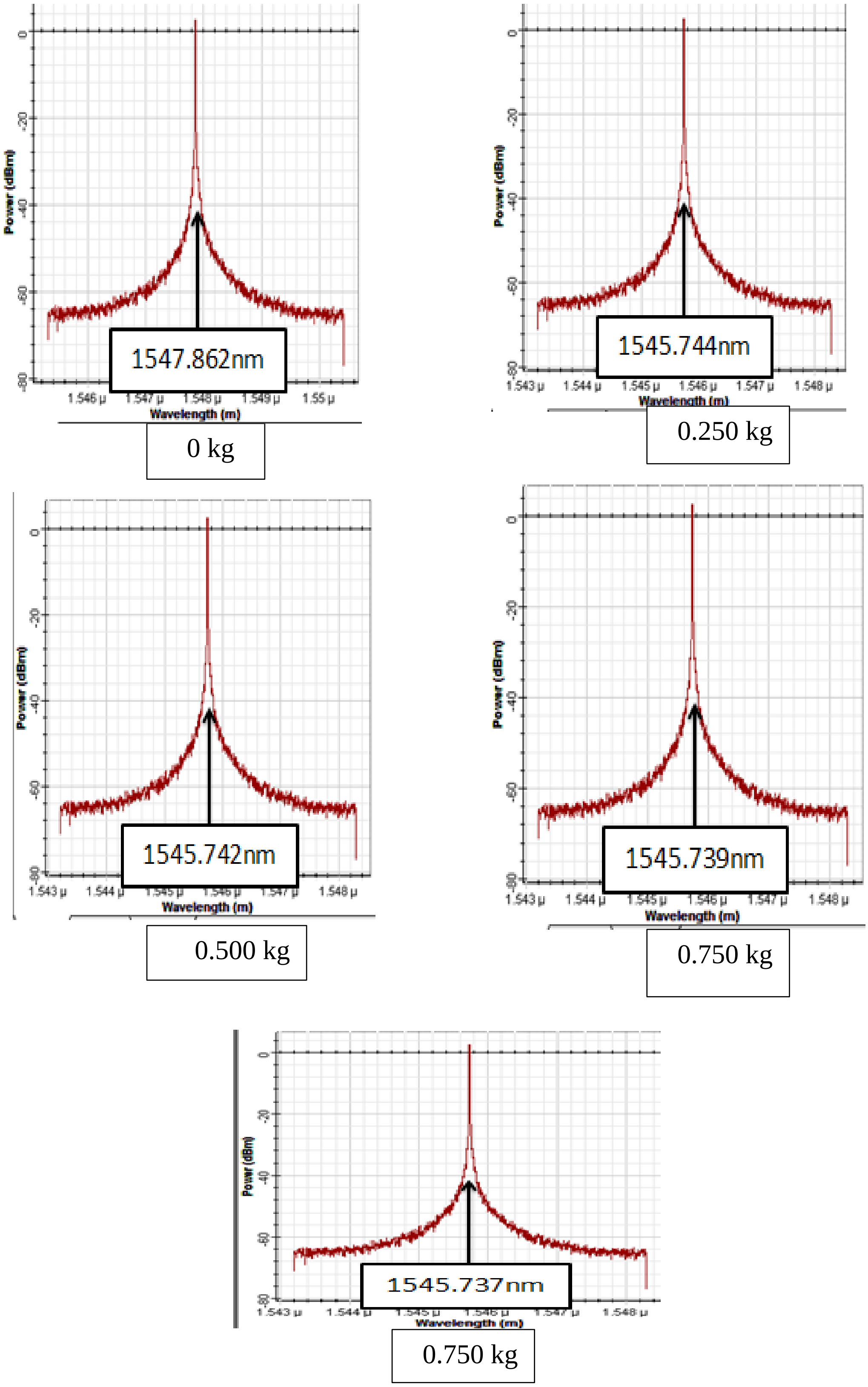

Figure (3.4) Wavelength shift for two-path SMS-MZI due to different values of applied force.

Experimental results with force effect

Figure (3.5), it is clear that there is a shift in the central wavelength for the output optical signal monitored by the OSA.

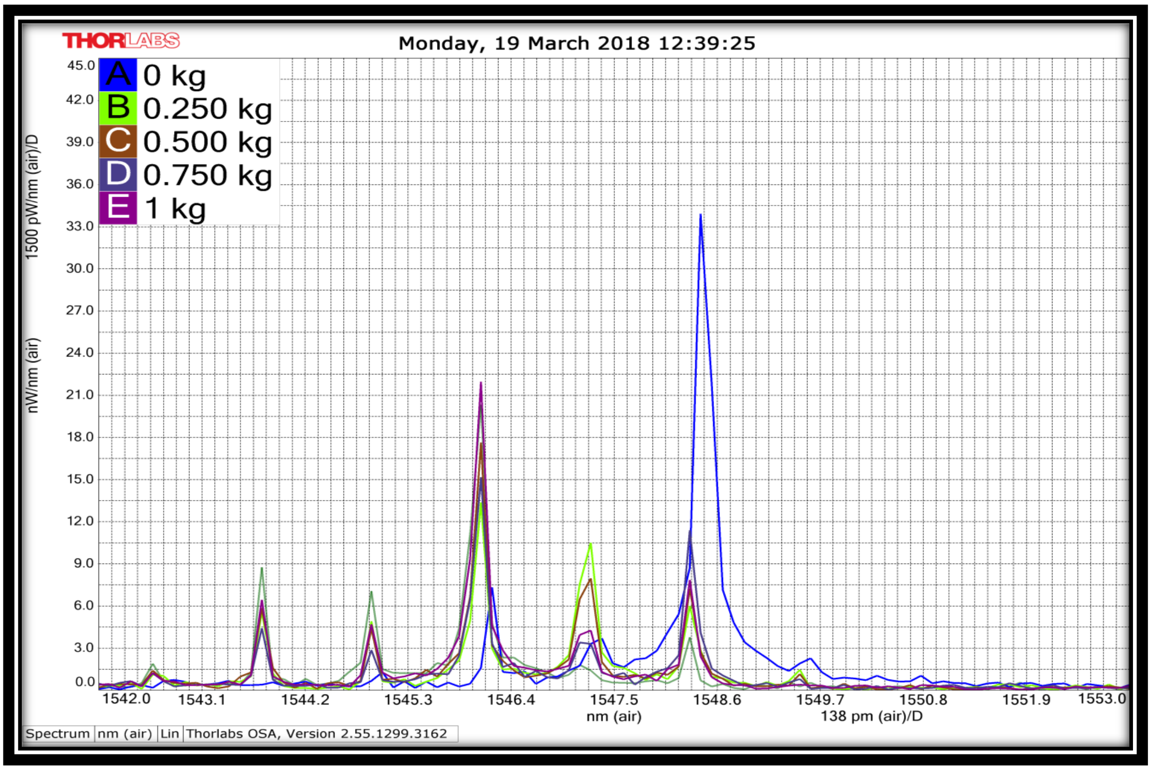

Figure (3.5) Tunable optical band pass filter when is applying different sets of weights on the cross section area of MMF.

The output spectra for two-path SMS-MZI due to force effect that was obtained by applying different values of weights on the MMF. From Figure (3.5), it is clear that there is a shift in the central wavelength for the output optical signal monitored by the OSA.

Table (3.3) lists the values of the shift in the central wavelength shifted, the FWHM, the output optical power and the phase shift in the output optical signal. From this table, the central wavelength shift and the output optical power are inversely proportional, while the phase shift between the two arms of SMS-MZI are directly proportional to the applied weights. In addition, FWHM has a non-linear variation. The same behavior can be seen for both simulation and experimental results.

Table (3.3) the weight effect on the central wavelength, FWHM, output optical power and phase shift for two-path SMS-MZI

Weight (kg)	Central wavelength shift (nm)		FWHM (pm)		P_{dBm}		$\Delta\varphi(m\,rad)$	
	Sim	Exp	Sim	Exp	Sim	Exp	Sim	Exp
0	1547.862	1547.862	200000.05	239.341	6.58231	13	0	0
0.250	1545.744	1545.737	200000.06	157.135	6.56714	11.2	2.42	2.47
0.5	1545.742	1545.743	200000.06	156.853	6.56713	11.5	4.91	4.95
0.75	1545.739	1545.733	200000.07	160.758	6.56710	11	78.05	7.58
1	1545.737	1545.731	200000.08	166.465	6.56709	11.7	9.85	9.89

Simulation results with strain effect

The output spectra for In-line SMS-MZI due to strain effect that was obtained by applying different values of strain on the MMF. From Figure (3.6), it is clear that there is a shift in the central wavelength for the output optical signal monitored by the OSA of the Optiwave system.

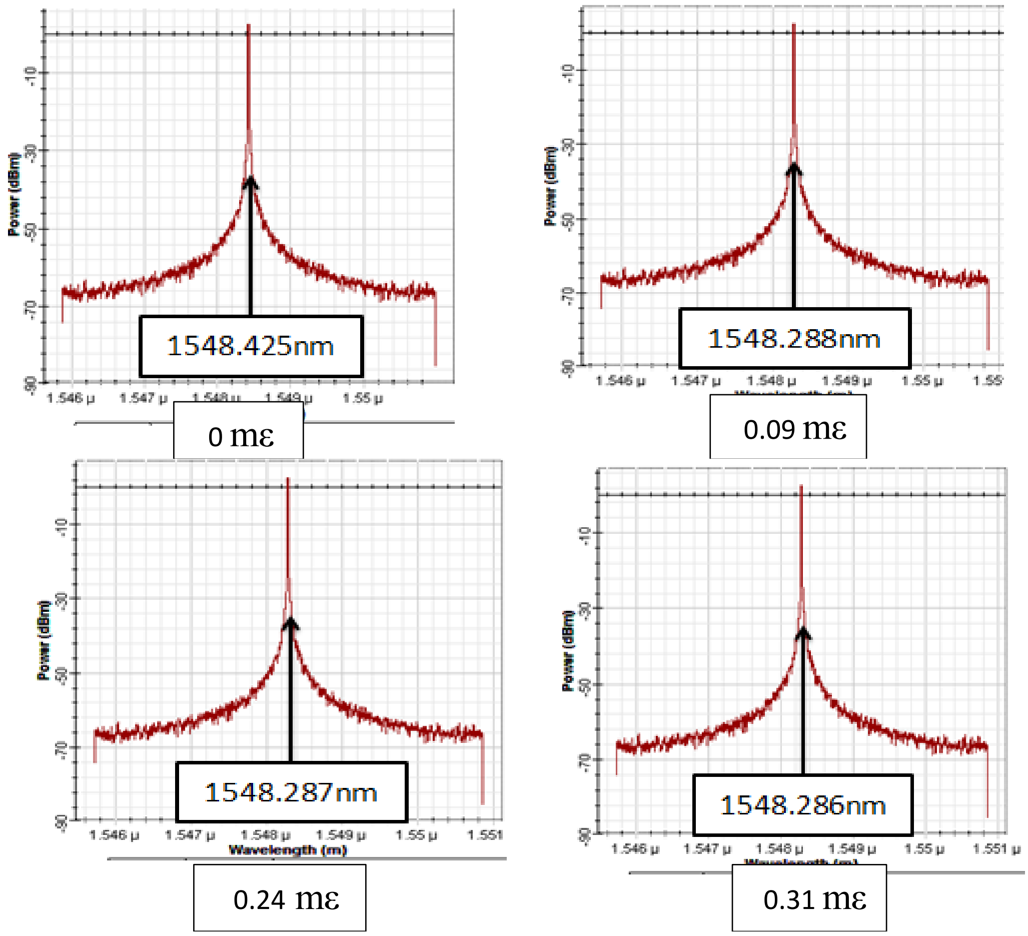

Figure (3.6) Wavelength shift for two-path SMS-MZI due to different values of applied strain.

Experimental results with strain effect

The output spectra for two-path SMS-MZI due to strain effect that was obtained by applying different values of strain on the MMF. From Figure (3.7), it is clear that there is a shift in the central wavelength for the output optical signal monitored by the OSA.

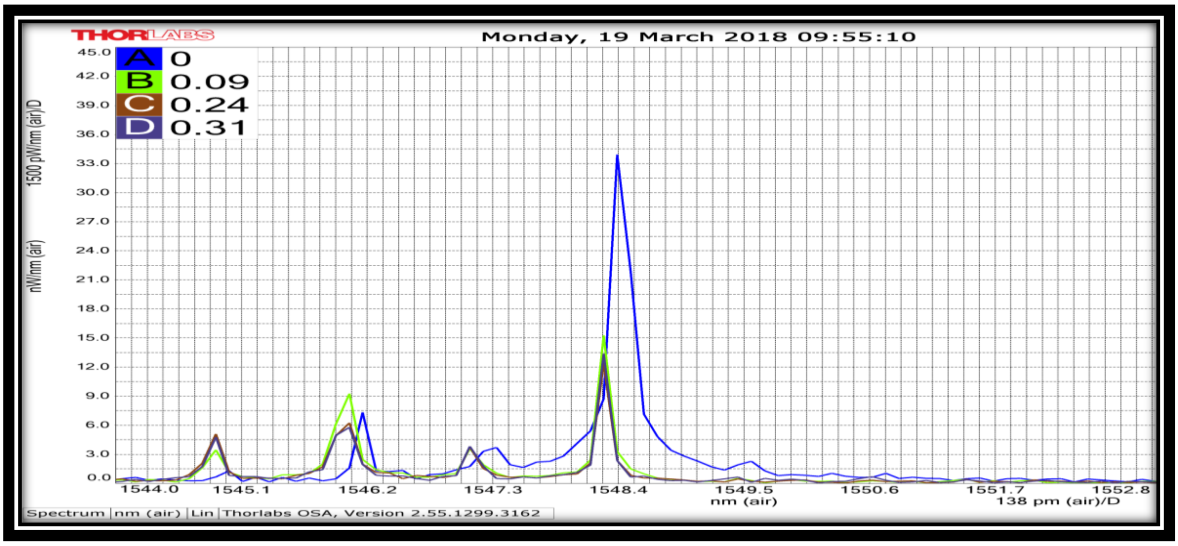

Figure (3.7) Tunable optical band pass filter when different sets of strain is applied on the cross section area of MMF.

Table (3.4) lists the values of the shift in the central wavelength shifted, the FWHM, the output optical power and the phase shift in the output optical signal. From this table, the central wavelength shift and the output optical power are inversely proportional, while the phase shift between the two arms of SMS-MZI are directly proportional to the applied strain. In addition, FWHM has a non-linear variation. The same behavior can be seen for both simulation and experimental results.

Table (3.4) the strain effect on the central wavelength, FWHM, output optical power and phase shift for two-path SMS-MZI

Strain (mε)	Central wavelength shift (nm)		FWHM (pm)		P_{dBm}		$\Delta\varphi(m\,rad)$	
	Sim	Exp	Sim	Exp	Sim	Exp	Sim	Exp
0	1548.425	1548.425	200000	321.070	7.00636	13	0	0
0.09	1548.288	1548.276	200000.03	140.132	7.00480	11.2	0.55	0.53
0.24	1548.287	1548.274	200000.05	133.269	7.00478	11.5	1.46	1.42
0.31	1548.286	1548.273	200000.06	133.271	7.00477	11	1.89	1.85

3.2.2.2 Single mode –Fiber Bragg Grating -Single mode Mach-Zehnder interferometer

Simulation results with strain effect

The output spectra for two-path SFBGS-MZI due to strain effect that was obtained by applying different values of strain on the FBG. From Figure (3.8), it is clear that there is a shift in the central wavelength for the output optical signal monitored by the OSA of the OptiGrating system.

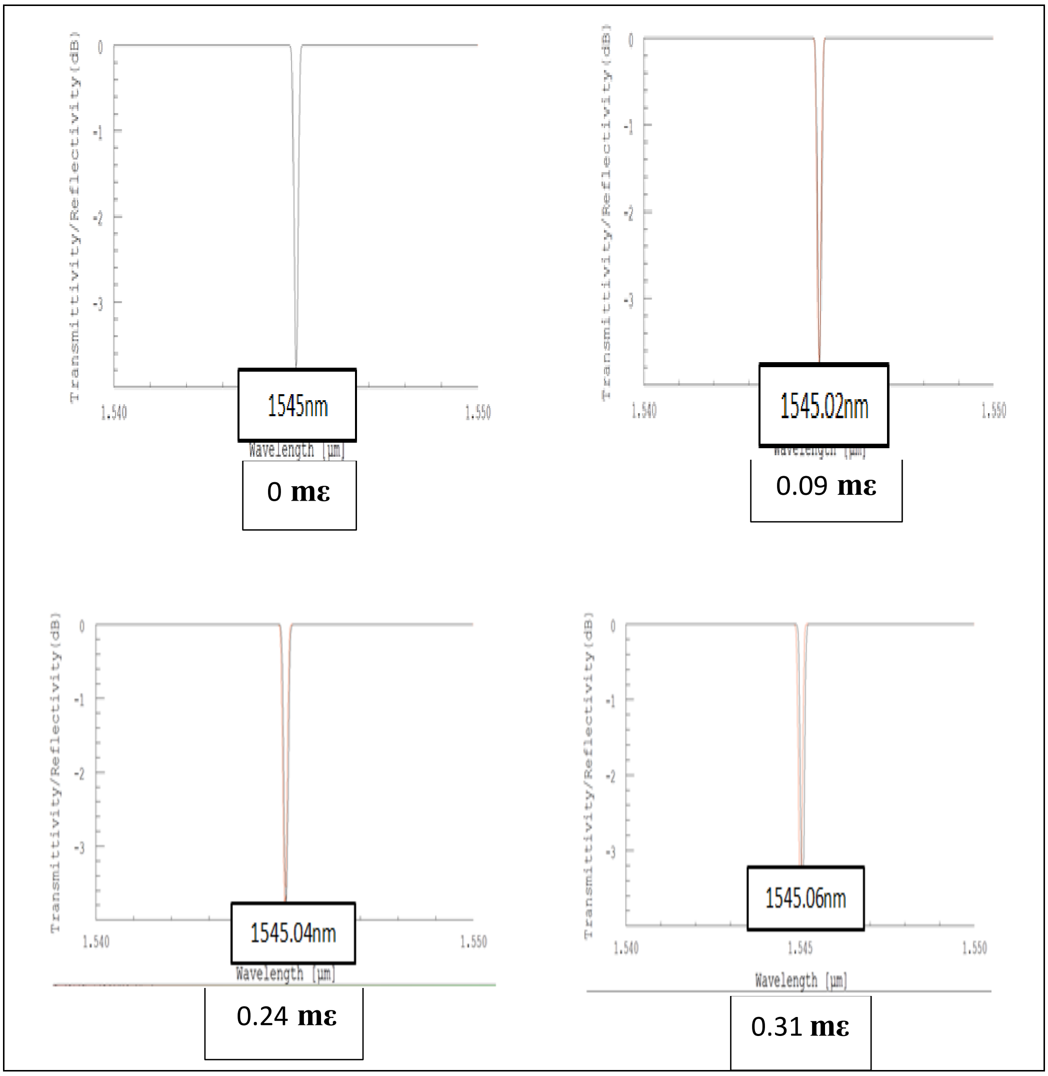

Figure (3.8) Wavelength shift for two-path SFBGS-MZI due to different values of applied strain.

Experimental results with strain effect

The output spectra for two-path SFBGS-MZI due to strain effect that was obtained by applying different values of strain on the effected arm of SFBGS-MZI. From Figure (3.9), it is clear that there is a shift in the central wavelength for the output optical signal monitored by the OSA.

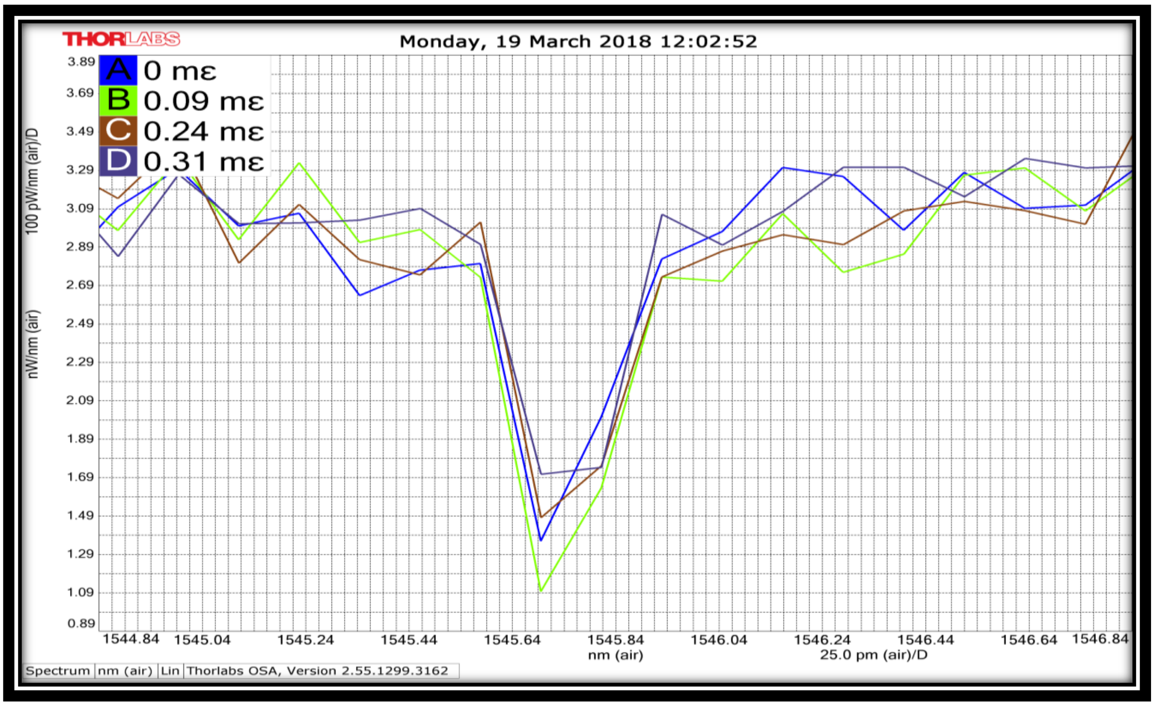

Figure (3.9) Tunable optical notch filter when a different set of strain is applied on the cross section area of FBG for two-path SFBGS-MZI

Table (3.5) lists the values of the shift in the central wavelength shifted, the FWHM, the output optical power and the phase shift in the output optical signal. From this table, the central wavelength shift and the output optical power are inversely proportional, while the phase shift between the two arms of SMS-MZI are directly proportional to the applied strain. In addition, FWHM has a non-linear variation. The same behavior can be seen for both simulation and experimental results.

Table (3.5) the strain effect on the central wavelength, FWHM, output optical power and phase shift for two-path SFBGS-MZI

strain (mε)	Central wavelength shift (nm)		FWHM (pm)		P_{dBm}		$\Delta\varphi(m\,rad)$	
	Sim	Exp	Sim	Exp	Sim	Exp	Sim	Exp
0	1545	1545.725	100000	197.529	20.8	22	0	0
0.09	1545.02	1545.736	120000	216.389	20.6	21.17	4.735	5.37
0.24	1545.04	1545.750	120000	233.607	18	20.6	12.628	9.47
0.31	1545.06	1545.765	120000	238.081	16.56	20.9	16.311	10.6

Experimental Results with force effect

The output spectra for two-path SFBGS-MZI due to force effect that was obtained by applying different values of weights on the FBG. From Figure (3.10), it is clear that there is a shift in the central wavelength for the output optical signal monitored by the OSA.

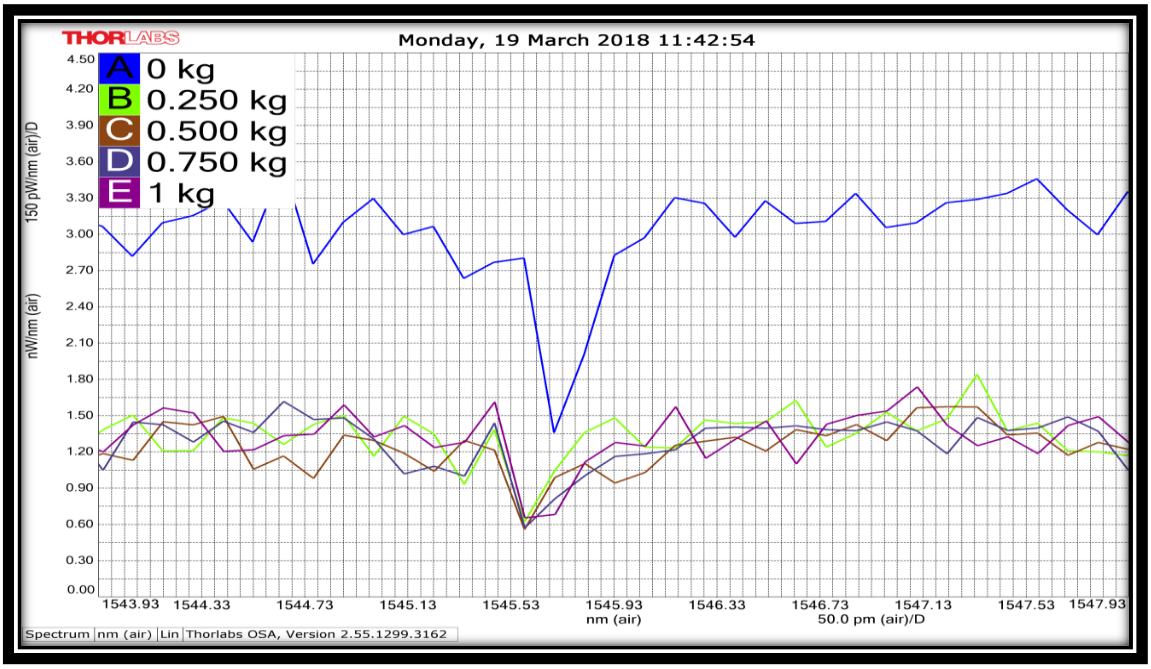

Figure (3.10) Tunable optical notch filter when is applying different sets of force on the cross section area of FBG.

In case of two-path SFBGS-MZI, different sets of forces are applied and the most important parameters of the optical filter are varied as shown in Table (3.6)

Table (3.6) Effect different sets of forces on the central wavelength, FWHM, and output optical power for two-path SFBGS-MZI.

Weight (kg)	Bragg wavelength (nm)	FWHM(pm)	P_{dBm}	$\Delta\varphi(m\,rad)$
0	1545.601	169.455	42.52	0
0.25	1545.501	185.234	27.5	0.274
0.5	1545.511	291.743	27.8	0.745
0.75	1545.556	280.418	26.4	1.51
1	1545.562	295.712	26.1	1.58

3.2.2.3 Multimode- Mach-Zehnder Interferometer

Simulation results with force effect

The output spectra for two-path MMF-MZI due to force effect that was obtained by applying different values of weights on the MMF. From Figure (3.11), it is clear that there is a shift in the central wavelength for the output optical signal monitored by the OSA of the Optiwave system.

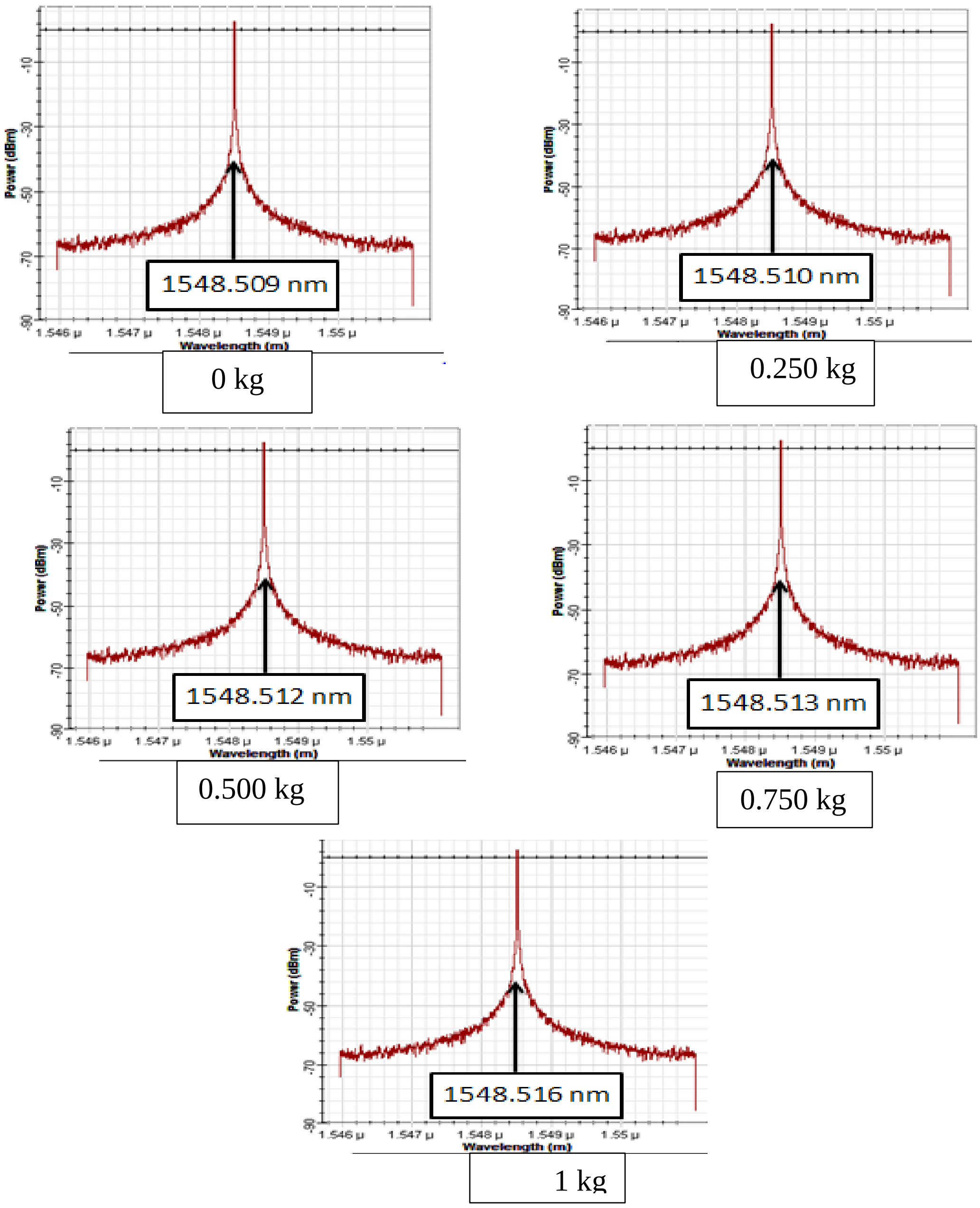

Figure (3.11) Wavelength shift for two-path MM-MZI due to different values of applied force.

Experimental results with force effect

The output spectra for In-line SFBGS-MZI due to force effect that was

(3.12), it is clear that there is a shift in the central wavelength for the output optical signal monitored by the OSA.

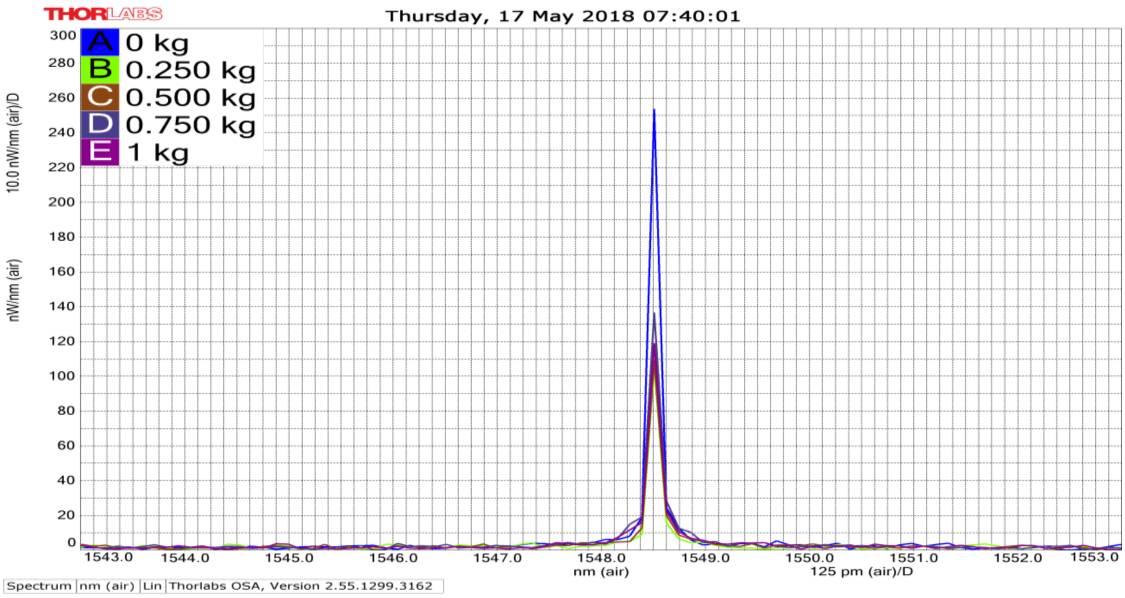

Figure (3.12) Tunable optical band pass filter when is applied different sets of weight on the cross section area of MMF for two-path MM-MZI

Table (3.7) lists the values of the shift in the central wavelength shifted, the FWHM, the output optical power and the phase shift in the output optical signal. From this table, the central wavelength shift and the output optical power are directly proportional, also the phase shift between the two arms of SMS-MZI are directly proportional to the applied weights. In addition, FWHM has a non-linear variation. The same behavior can be seen for both simulation and experimental results.

Table (3.7) the weight effect on the central wavelength, FWHM, output optical power and phase shift for two-path MM-MZI								
Weight (kg)	**Central wavelength shift (nm)**		**FWHM (pm)**		P_{dBm}		$\Delta\varphi(m\ rad)$	
	Sim	**Exp**	**Sim**	**Exp**	**Sim**	**Exp**	**Sim**	**Exp**
0	1548.509	1548.509	200000.02	145.216	7.00725	16.18	0	0
0.250	1548.510	1548.511	200000	143.276	7.00727	17.4	4.45	4.155
0.5	1548.512	1548.512	199999.96	129.653	7.00728	17.9	8.9	8.31
0.75	1548.513	1548.513	199999.93	138.227	7.00729	18.7	12.9	12.7
1	1548.516	1548.515	199999.91	135.233	7.00731	18.9	16.9	16.6

Simulation results with strain effect

The output spectra for two-path MMF-MZI due to strain effect that was obtained by applying different values of strain on the MMF. From Figure (3.13), it is clear that there is a shift in the central wavelength for the output optical signal monitored by the OSA of the Optiwave system

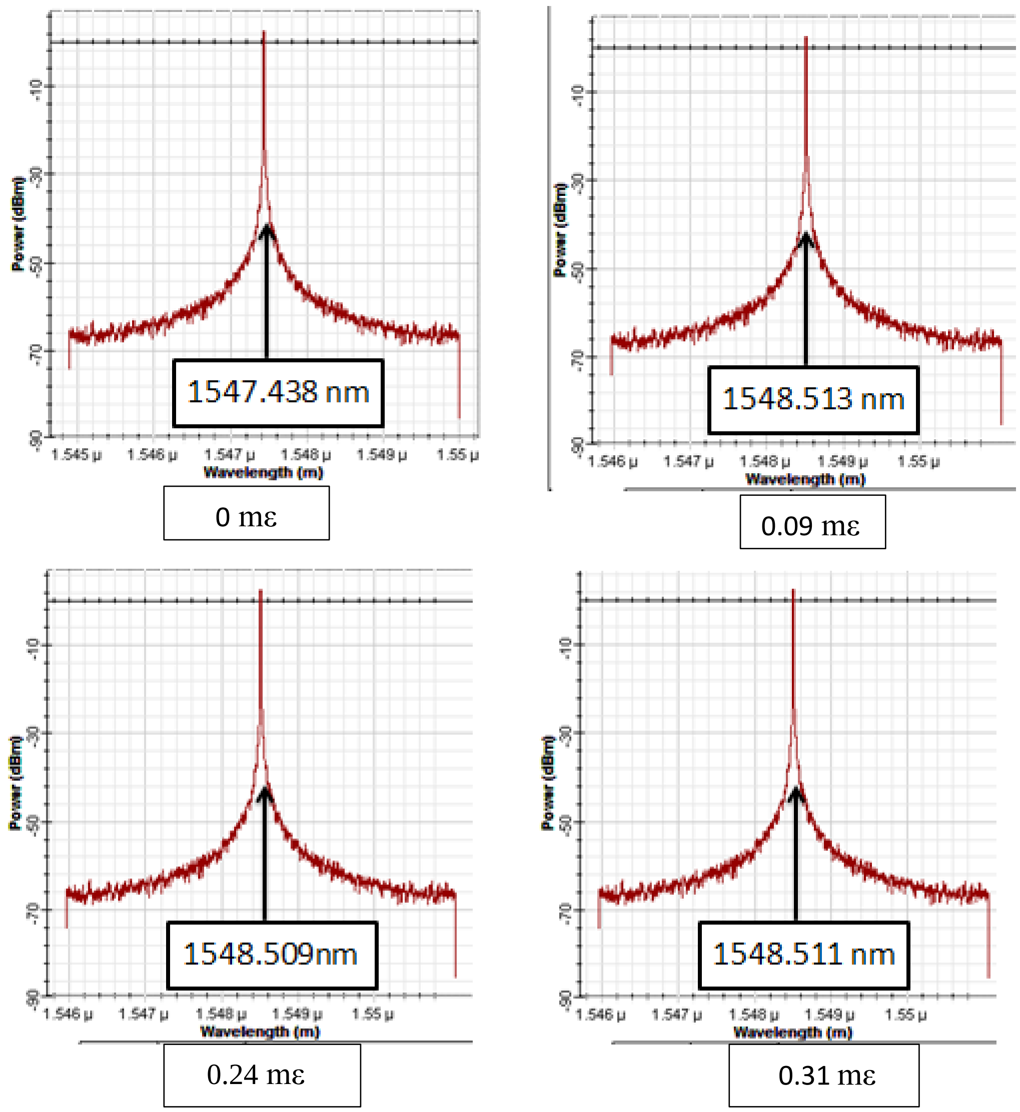

Figure (3.13) Wavelength shift for two-path MM-MZI due to different values of applied strain.

Experimental results with strain effect

The output spectra for two-path MM-MZI due to strain effect that was obtained by applying different values of strain on the MMF. From Figure (3.14), it is clear that there is a shift in the central wavelength for the output optical signal monitored by the OSA.

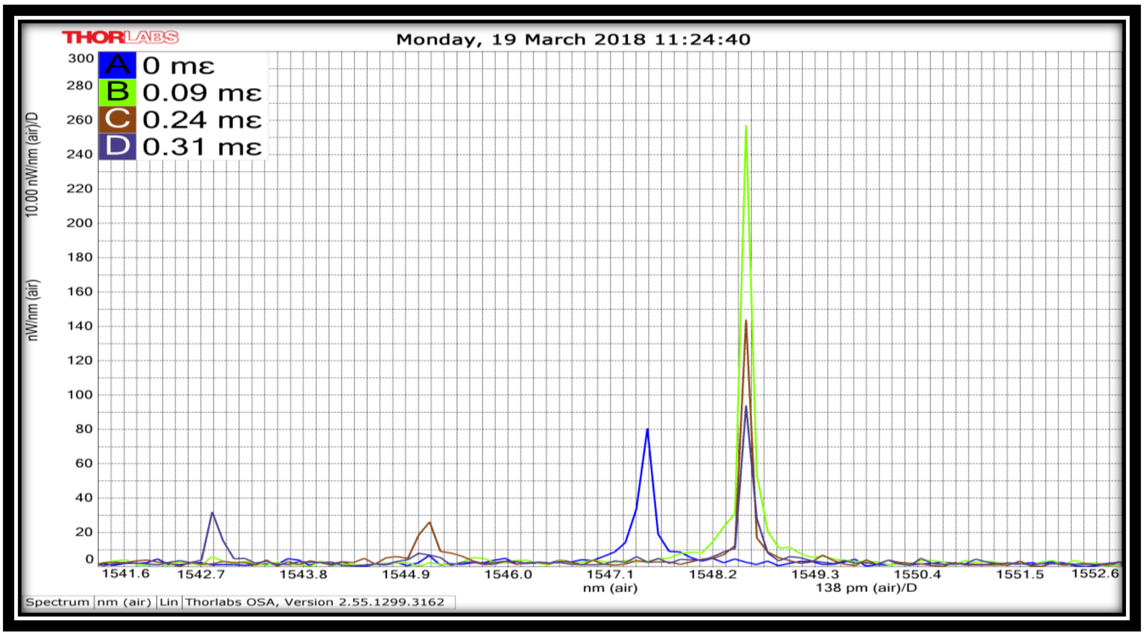

Figure (3.14) Tunable optical band pass filter when applied different sets of strain on the cross section area of MMF for two arms MM-MZI

Table (3.8) lists the values of the shift in the central wavelength shifted, the FWHM, the output optical power and the phase shift in the output optical signal. From this table, the central wavelength shift and the output optical power are inversely proportional, while the phase shift between the two arms of SMS-MZI are directly proportional to the applied weights. In addition, FWHM has a non-linear variation. The same behavior can be seen for both simulation and experimental results.

Table (3.8) the strain effect on the central wavelength, FWHM, output optical power and phase shift for two-path SFBGS-MZI									
strain (mε)	**Central wavelength shift (nm)**		**FWHM (pm)**		P_{dBm}		$\Delta\varphi(m\,rad)$		
	Sim	**Exp**	**Sim**	**Exp**	**Sim**	**Exp**	**Sim**	**Exp**
0	1547.438	1547.438	200000	169.616	6.99239	16.2	0	0
0.09	1548.513	1548.512	200000.01	135.830	7.00730	18.9	0.57	0.52
0.24	1548.511	1548.509	200000.03	129.199	7.00728	17.1	1.49	1.42
0.31	1548.509	1548.506	200000.05	144.145	7.00726	15.1	1.87	1.84

3.4 Comparison between simulation and experimental results for all MZIs systems.

A compression between simulation and experimental results for all MZIs systems is shown in Table (3.9).

Table (3.9) Compression between all types of MZIs with Tunability and Phase shift			
In-line MZI	**Type of Mechanical effect**	**Tunability (nm)**	$\Delta\emptyset(m\,rad)$
a. SMS-MZI			
Simulation work	Force	0.170	(0-9.84)
Experimental work	Force	0.232	(0-9.91)
b. SFBGS-MZI			

Experimental work	Force	0.029	(0-2.26)
Two-Path MZI **a. SMS-MZI** **Simulation work** **Experimental work**	 Force Force	 2.118 2.131	 (0-9.85) (0-9.89)
SMS-MZI **Simulation work** **Experimental work**	 Strain Strain	 0.139 0.152	 (0-1.89) (0-1.85)
b. SFBGS-MZI **Experimental work**	 Force	 0.1	 (0-1.58)
SFBGS-MZI **Simulation work** **Experimental work**	 Strain Strain	 0.06 0.04	 (0-16.311) (0-10.6)
c. MM-MZI **Simulation work** **Experimental work**	 Force Force	 0.007 0.006	 (0-16.9) (0-16.6)
MM-MZI **Simulation work** **Experimental work**	 Strain Strain	 1.075 1.074	 (0-1.87) (0-1.84)

3.5 Conclusion

Two types of photonic devices were constructed by using different fibers MZIs (in-line and two-path MZIs). These devices are optical tunable filters (notch and band pass filters).

During the experimental and simulation works, several points were concluded which are:

1- It is successfully building band pass and notch optical filters using all fiber Mach-Zehnder interferometer (MZIs).

2- Tunable notch filter was obtained only with single mode –fiber Bragg grating- single mode Mach-Zehnder interferometer (SFBGS-MZI) with one and two-path configurations.

3- Maximum tunability was obtained with two-path single mode –multimode –single mode Mach-Zehnder interferometer (SMS-MZI) equal to(2.131) nm in experimental work while the tunability in simulation work was obtained (2.118) nm with force effect.

4- A Phase shift was obtained with two-path multimode Mach-Zehnder interferometer (MM-MZI) configuration, it is equal (0-16.6)$m\ rad$ while the phase shift in simulation work was obtained (0-16.9) $m\ rad$ with force effect.

5- There are differences between the simulation and experimental results due to the simulation program was done in optiwave system version (7.0), the splicing losses between two fibers were not considered.

3.6 Future Work

1- Designing a Fabry-Perot micro cavity array fiber Bragg filters.

2-Using photonic crystal fiber instead of fiber Bragg grating and multimode fiber to design tunable optical filter and phase modulators.

3- Applying another physical effect (temperature) to obtain fine tunable optical filter for each type.

4- Using the designed notch fiber Bragg grating filter for WDM/OCDA systems.

5- Building two-path Mach-Zehnder interferometer using SSFBG and array FBG.

References

[1] G. P. Agrawal, *Fiber-Optic Communication Systems: Fourth Edition*. (2011).

[2]A. Yariv and P. Yeh, *Photonics: optical electronics in modern communications*, no. November. (2007)

[3] K. O. Hill, Y. Fujii, D. C. Johnson, and B. S. Kawasaki, Appl. Phys. Lett. **32**, 647 (1978).

[4] G. Meltz, W. W. Morey, and W. H. Glenn, Opt. Lett. **14**, 823 (1991).

[5] A. M. Vengsarkar, P. L. Lemaire, J. B. Judkins, V. Bhatia, T. Erdogan, and J. E. Sipe, J. Lightwave Technol. **14**, 58 (1996).

[6]Y. J. Rao, "Recent progress in fiber-optic extrinsic Fabry-Perot interferometric sensors," *Opt. Fiber Technol.*, vol. 12, no. 3, pp. 227–237, (2006).

[7] Tao Wei,1 Yukon Han,2 Yanjun Li, 1 Hai-Lung Tsai,2 and Hai Xiao1," Temperature-insensitive miniaturized fiber inline Fabry-Perot interferometer for highly sensitive refractive index measurement" Optical Society of America.,Vol. 16, no. 8, (2008).

[8] J. S. Sirkis, D. D. Brennan, M. A. Putman, T. A. Berkoff, A. D. Kersey, and E. J. Friebele, "In-Line Fiber Etalon for Strain-Measurement," *Opt. Lett.*, vol. 18, no. 22, pp. 1973–1975, (1993).

[9] Pedrotti, F.L.; Pedrotti, L.M.; Pedrotti, L.S. *Introduction to Optics*; Pearson International: Upper Saddle River, NJ, USA, (2007).

[10] W. H. Tsai and C. J. Lin, "A novel structure for the intrinsic Fabry-Perot fiber-optic temperature sensor," *J. Light. Technol.*, vol. 19, no. 5, pp. 682–686, (2001).

[11] S. H. Kim, J. J. Lee, D. C. Lee, and I. B. Kwon, "Study on the development of transmission-type extrinsic Fabry-Perot interferometric

optical fiber sensor," *J. Light. Technol.*, vol. 17, no. 10, pp. 1869–1874, (1999).

[12] D. Hunger, T. Steinmetz, Y. Colombe, C. Deutsch, T. W. Hänsch, and J. Reichel, "A fiber Fabry-Perot cavity with high finesse," *New J. Phys.*, vol. 12, (2010).

[13] Z. Ran, Y. Rao, J. Zhang, Z. Liu, and B. Xu, "A miniature fiber-optic refractive-index sensor based on laser-machined Fabry-Perot interferometer tip," *J. Light. Technol.*, vol. 27, no. 23, pp. 5426–5429, (2009).

[14] Y.-J. Rao, M. Deng, D.-W. Duan, X.-C. Yang, T. Zhu, and G.-H. Cheng, "Micro Fabry-Perot interferometers in silica fibers machined by femtosecond laser," *Opt. Express*, vol. 15, no. 21, p. 14123, (2007).

[15]Z. L. Ran, Y. J. Rao, W. J. Liu, X. Liao, and K. S. Chiang, "Laser-micromachined Fabry-Perot optical fiber tip sensor for high-resolution temperature-independent measurement of refractive index," *Opt. Express*, vol. 16, no. 3, p. 2252, (2008).

[16] T. Wei, Y. Han, H.-L. Tsai, and H. Xiao, "Miniaturized fiber inline Fabry-Perot interferometer fabricated with a femtosecond laser.," *Opt. Lett.*, vol. 33, no. 6, pp. 536–538, (2008).

[17] [X. Wan and H. F. Taylor, "Intrinsic fiber Fabry–Perot temperature sensor with fiber Bragg grating mirrors," *Opt. Lett.*, vol. 27, no. 16, p. 1388, (2002).

[18] Z. Wang, F. Shen, L. Song, X. Wang, and A. Wang, "Multiplexed fiber fabry-pérot interferometer sensors based on ultrashort bragg gratings," *IEEE Photonics Technol. Lett.*, vol. 19, no. 8, pp. 622–624, (2007).

[19] Y. Zhang, X. Chen, Y. Wang, K. L. Cooper, and A. Wang, "Microgap multicavity Fabry-Pérot biosensor," *J. Light. Technol.*, vol. 25, no. 7, pp. 1797–1804, (2007).

[20] V. R. Machavaram, R. A. Badcock, and G. F. Fernando, “Fabrication of intrinsic fibre Fabry-Perot sensors in silica fibres using hydrofluoric acid etching,” *Sensors Actuators, A Phys.*, vol. 138, no. 1, pp. 248–260, (2007).

[21] J. R. Zhao, X. G. Huang, W. X. He, and J. H. Chen, “High-resolution and temperature-insensitive fiber optic refractive index sensor based on fresnel reflection modulated by Fabry-Perot interference,” *J. Light. Technol.*, vol. 28, no. 19, pp. 2799–2803, (2010).

[22] P. Morris, A. Hurrell, A. Shaw, E. Zhang, and P. Beard, “A Fabry–Pérot fiber-optic ultrasonic hydrophone for the simultaneous measurement of temperature and acoustic pressure,” *J. Acoust. Soc. Am.*, vol. 125, no. 6, pp. 3611–3622, (2009).

[23] H. Y. Fu *et al.*, “Pressure sensor realized with polarization-maintaining photonic crystal fiber-based Sagnac interferometer,” *Appl. Opt.*, vol. 47, no. 15, p. 2835, (2008).

[24] L. Yuan, L. Zhou, and J. Wu, “Fiber optic temperature sensor with duplex Michleson interferometric technique,” *Sensors Actuators A Phys.*, vol. 86, no. 1–2, pp. 2–7, (2000).

[25] R. Kashyap and B. Nayar, “An all single-mode fiber Michelson interferometer sensor,” *J. Light. Technol.*, vol. 1, no. 4, (1983).

[26] K. T. O’Mahoney, R. P. O’Byrne, S. V. Sergeyev, L. Zhang, and I. Bennion, “Short-scan fiber interferometer for high-resolution bragg grating array interrogation,” *IEEE Sens. J.*, vol. 9, no. 10, pp. 1277–1281, (2009).

[27] Y. Zhao and F. Ansari, “Intrinsic single-mode fiber-optic pressure sensor,” *IEEE Photonics Technol. Lett.*, vol. 13, no. 11, pp. 1212–1214, (2001).

[28] J. H. Lim, H. S. Jang, K. S. Lee, J. C. Kim, and B. H. Lee, "Mach-Zehnder interferometer formed in a photonic crystal fiber based on a pair of long-period fiber gratings.," *Opt. Lett.*, vol. 29, no. 4, pp. 346–348, (2004).

[29] L. Yuan, Q. Wen, C. Liu, Y. Jie, and G. Li, "Twin multiplexing strain sensing array based on a low-coherence fiber optic Mach-Zehnder interferometer," *Sensors Actuators, A Phys.*, vol. 135, no. 1, pp. 152–155, (2007).

[30] *Samar Kareem Ibrahim,"* BUILDING TUNABLE SPECTRAL FILTER USING FIBER BRAGG GRATING', A Thesis Submitted to the Department of Laser and Optoelectronics Engineering / University of Technology in Partial Fulfillment of the Requirements for the Degree of Master Science In Optoelectronics Engineering,(2017).

[31] B. H. Lee *et al.*, "Interferometric fiber optic sensors," *Sensors*, vol. 12, no. 3. pp. 2467–2486, (2012).

[32] Q. Wang *et al.*, "High sensitivity refractive index sensor based on splicing points tapered SMF-PCF-SMF structure Mach-Zehnder mode interferometer," *Sensors Actuators, B Chem.*, vol. 225, pp. 213–220, (2016).

[33] E. Huerta-Mascotte *et al.*, "A core-offset mach zehnder interferometer based on a non-zero dispersion-shifted fiber and its torsion sensing application," *Sensors (Switzerland)*, vol. 16, no. 6, (2016).

[34] A. Guzman and R. Aguilar, "Tunable Rare-Earth Doped Fiber Laser", INTECH, ch. 5, (2013).

[35] Y. Wang, M. Yang, D. N. Wang, S. Liu, and P. Lu, "Fiber in-line Mach-Zehnder interferometer fabricated by femtosecond laser micromachining for refractive index measurement with high sensitivity," *J. Opt. Soc. Am. B*, vol. 27, no. 3, pp. 370–374, (2010).

[34] C. R. Liao, Y. Wang, D. N. Wang, and M. W. Yang, “Fiber in-line Mach-Zehnder interferometer embedded in FBG for simultaneous refractive index and temperature measurement,” *IEEE Photonics Technol. Lett.*, vol. 22, no. 22, pp. 1686–1688, (2010).

[35] Y. F. Lu, C. Y. Shen, C. Zhong, D. B. Chen, X. Y. Dong, and J. H. Cai, "Refractive Index and Temperature Sensor Based on Double-Pass M-Z Interferometer With an FBG," IEEE Photon. Technol. Lett., vol. 26, no. 11, pp. 1124-1127, Jun. (2014).

[36] A. Bahrampour, S. Tofighi, M.Bathaee and F.Farman, “Optical Fiber Interferometers and Their Applications”, INTECH, ch. 1, Sharif University of Technology, Iran

[37] Qi. Wang, L. Kong, Y. Dang, F. Xia, Y. Zhang, Y. Zhao, H. Hu, J. Li, “High Sensitivity Refractive Index Sensor Based on Splicing Points Tapered SMF-PCF-SMF Structure Mach-Zehnder Mode Interferometer”, Sensors and Actuators B: Chemical, Vol. 225, pp. 213-220, (2016).

[38] Y.-J. Rao, “In-fibre Bragg grating sensors,” *Meas. Sci. Technol.*, vol. 8, no. 4, pp. 355–375, (1997).

[39] A. D. Kersey, W. W. Morey, and T. A. Berkoff, “Fiber-optic Bragg grating strain sensor with drift-compensated high-resolution interferometric wavelength-shift detection,” *Opt. Lett.*, vol. 18, no. 1, p. 72, (1993).

[40] D. a. Jackson, a. D. Kersey, M. Corke, and J. D. C. Jones, “Pseudoheterodyne detection scheme for optical interferometers,” *Electron. Lett.*, vol. 18, no. 25–26, p. 1081, (1982).

[41] Li Wei, Anum Khattak, Connor Martz, Da-Peng Zhou **“**Tunable Multimode Fiber Based Filter and Its Application in Cost-Effective Interrogation of Fiber-Optic Temperature Sensors” Vol. 9, No. 2, April (2017).

[42] University of Cluj Napoca – Romania,”Optical spectral filters and gratins”,ftp.utcluj.ro/pub/users/cemil/dwdm/dwdm_Intro/**4**_5311739.pdf

[43] Institute of Astrophysics of Canarias (IAC),” Tunable Filters Basics”,.

www.iac.es/proyecto/OSIRIS/OSITOO/blascabrera/Fundamentals.pdf

[44]”chapter4: fabry-perot filters”, university of Johannesburg,(2000).

[45] T.S. Al-Falah, PhD. Thesis,”Effect of temperature variation on the performance of liquid-filled photonic bandgap fiber”,Iinstitude of Laser for Postgraduate Studies , Baghdad University,(2009).

[46] C.-R. Lee, J.-D. Lin, Y.-J. Huang, S.-C. Huang, S.-H. Lin, and C.-P. Yu, “All-optically controllable dye-doped liquid crystal infiltrated photonic crystal fiber,” *Opt. Express*, vol. 19, no. 10, p. 9676, (2011).

[47] S. V. Kartalopoulos, “Optical spectral filters and gratings,” *Introd. To Dwdm Technol.*, pp. 71–89, (2000).

[48] D. Gauden, E. Goyat, C. Vaudry, P. Yvernault and D. Pureur,” Tunable Mach-Zehnder-based add-drop multiplexer”,Vol.40, No.21, 14th October (2004).

[49] ZHANG Zhi-guo**, “ZHANG Min, and YE Pei-da, MZI-based wavelength interrogation system with tunable-FBG”**,** Vol.3 No.5, 15 September (2007).

[50] A.-P. Luo, Z.-C. Luo, W.-C. Xu, and H. Cui, “Wavelength switchable flat-top all-fiber comb filter based on a double-loop Mach-Zehnder interferometer.,” *Opt. Express*, vol. 18, no. 6, pp. 6056–6063, (2010).

[51] J. E. Antonio-Lopez, a Castillo-Guzman, D. a. May-Arrioja, R. Selvas-Aguilar, and P. Likamwa, “Tunable multimode-interference bandpass fiber filter,” *Opt. Lett.*, vol. 35, no. 3, pp. 324–326, (2010).

[52] L. Huang *et al.*, "A Linearized Tunable Single Bandpass Microwave Photonic Filter," *IEEE Microw. Wirel. Components Lett.*, vol. 26, no. 11, pp. 963–965, (2016).

[53] Y. Li, B. Zhou, L. Zhang, and S. He, "Tunable Fabry-Perot filter in cobalt doped fiber formed by optically heated fiber Bragg gratings pair," *Opt. Commun.*, vol. 344, pp. 156–160, (2015).

[54] F. Ahmed, V. Ahsani, A. Saad, and M. B. G. Jun, "Bragg grating embedded in Mach-Zehnder interferometer for refractive index and temperature sensing," *IEEE Photonics Technol. Lett.*, vol. 28, no. 18, pp. 1968–1971, (2016).

[55] L. Wei, A. Khattak, C. Martz, and D. P. Zhou, "Tunable Multimode Fiber Based Filter and Its Application in Cost-Effective Interrogation of Fiber-Optic Temperature Sensors," *IEEE Photonics J.*, vol. 9, no. 2, (2017).

[56] Anwaar A.AL-Dergazly,Farah S.Al-Thahaby," Tuneable Fiber Brag Grating for Magnetic Field Sensor" Vol.20 No.5, pp.1112-1123,(2017

APPENDIX (A)

Corning® SMF-28™ Optical Fiber

Product Information

PI1036
Issued: April 2002
Supersedes: December 2001
ISO 9001 Registered

Corning® Single-Mode Optical Fiber

The Standard For Performance

Corning® SMF-28™ single-mode optical fiber has set the standard for value and performance for telephony, cable television, submarine, and utility network applications. Widely used in the transmission of voice, data, and/or video services, SMF-28 fiber is manufactured to the most demanding specifications in the industry. SMF-28 fiber meets or exceeds ITU-T Recommendation G.652, TIA/EIA-492CAAA, IEC Publication 60793-2 and GR-20-CORE requirements.

Taking advantage of today's high-capacity, low-cost transmission components developed for the 1310 nm window, SMF-28 fiber features low dispersion and is optimized for use in the 1310 nm wavelength region. SMF-28 fiber also can be used effectively with TDM and WDM systems operating in the 1550 nm wavelength region.

Features And Benefits

- Versatility in 1310 nm and 1550 nm applications
- Enhanced optical properties that optimize transmission performance
- Outstanding geometrical properties for low splice loss and high splice yield
- OVD manufacturing reliability and product consistency
- Optimized for use in loose tube, ribbon, and other common cable design

The Sales Leader

Corning SMF-28 fiber is the world's best selling fiber. In 2001, SMF-28 fiber was deployed in over 45 countries around the world. All types of network providers count on this fiber to support network expansion into the 21st Century.

Protection And Versatility

SMF-28 fiber is protected for long-term performance and reliability by the CPC® coating system. Corning's enhanced, dual acrylate CPC coatings provide excellent fiber protection and are easy to work with. CPC coatings are designed to be mechanically stripped and have an outside diameter of 245 µm. They are optimized for use in many single- and multi-fiber cable designs including loose tube, ribbon, slotted core, and tight buffer cables.

Patented Quality Process

SMF-28 fiber is manufactured using the Outside Vapor Deposition (OVD) process, which produces a totally synthetic ultra-pure fiber. As a result, Corning SMF-28 fiber has consistent geometric properties, high strength, and low attenuation. Corning SMF-28 fiber can be counted on to deliver excellent performance and high reliability, reel after reel. Measurement methods comply with ITU recommendations G.650, IEC 60793-1, and Bellcore GR-20-CORE.

Optical Specifications

Attenuation

Wavelength (nm)	Attenuation* (dB/km)	
	Premium	Standard
1310	≤0.34	≤0.35
1550	≤0.20	≤0.22

*Alternate attenuation values available upon request

Point Discontinuity

No point discontinuity greater than 0.10 dB at either 1310 nm or 1550 nm.

Attenuation at the Water Peak

The attenuation at 1383 ± 3 nm shall not exceed 2.1 dB/km.

Attenuation vs. Wavelength

Range (nm)	Ref. λ (nm)	Max. α Difference (dB/km)
1285 - 1330	1310	0.05
1525 - 1575	1550	0.05

The attenuation in a given wavelength range does not exceed the attenuation of the reference wavelength (λ) by more than the value α.

Attenuation with Bending

Mandrel Diameter (mm)	Number of Turns	Wavelength (nm)	Induced Attenuation* (dB)
32	1	1550	≤0.50
50	100	1310	≤0.05
50	100	1550	≤0.10
60	100	1550	≤0.05

*The induced attenuation due to fiber wrapped around a mandrel of a specified diameter.

Cable Cutoff Wavelength (λ_{ccf})

$\lambda_{ccf} \leq 1260$ nm

Mode-Field Diameter

9.2 ± 0.4 µm at 1310 nm

10.4 ± 0.8 µm at 1550 nm

Dispersion

Zero Dispersion Wavelength (λ_0):

1302 nm $\leq \lambda_0 \leq$ 1322 nm

Zero Dispersion Slope (S_0):

≤ 0.092 ps/(nm²•km)

$$\text{Dispersion} = D(\lambda) :\approx \frac{S_0}{4}\left[\lambda - \frac{\lambda_0^4}{\lambda^3}\right] \text{ ps/(nm•km)},$$

for 1200 nm ≤ λ ≤ 1600 nm

λ = Operating Wavelength

Polarization Mode Dispersion

Fiber Polarization Mode Dispersion (PMD)

	Value (ps/$\sqrt{\text{km}}$)
PMD Link Value	≤ 0.1*
Maximum Individual Fiber	≤ 0.2

* Complies with IEC 60794-3:2001, section 5.5, Method 1, September 2001.

The PMD link value is a term used to describe the PMD of concatenated lengths of fiber (also known as the link quadrature average). This value is used to determine a statistical upper limit for system PMD performance.

Individual PMD values may change when cabled. Corning's fiber specification supports network design requirements for a 0.5 ps/$\sqrt{\text{km}}$ maximum PMD.

Environmental Specifications

Environmental Test Condition	Induced Attenuation 1310 nm/1550 nm (dB/km)
Temperature Dependence -60°C to +85°C*	≤0.05
Temperature-Humidity Cycling -10°C to +85°C*, up to 98% RH	≤0.05
Water Immersion, 23°± 2°C*	≤0.05
Heat Aging, 85° ± 2°C*	≤0.05

*Reference temperature = +23°C

Operating Temperature Range

-60°C to +85°C

Dimensional Specifications

Length (km/reel): fiber lengths available up to 50.4*

* Longer spliced lengths available at a premium.

Glass Geometry

Fiber Curl: ≥ 4.0 m radius of curvature
Cladding Diameter: 125.0 ± 0.7 µm
Core-Clad Concentricity: ≤ 0.5 µm
Cladding Non-Circularity: ≤ 1.0%

Defined as: $\left[1-\frac{\text{Min. Cladding Diameter}}{\text{Max. Cladding Diameter}}\right] \times 100$

Coating Geometry

Coating Diameter: 245 ± 5 µm
Coating-Cladding Concentricity: <12 µm

Mechanical Specifications

Proof Test

The entire fiber length is subjected to a tensile proof stress ≥ 100 kpsi (0.7 GN/m²)*.

* Higher proof test levels available at a premium.

Performance Characterizations

Characterized parameters are typical values.

Core Diameter: 8.2 µm

Numerical Aperture: 0.14

NA is measured at the one percent power level of a one-dimensional far-field scan at 1310 nm.

Zero Dispersion Wavelength (λ_0): 1313 nm

Zero Dispersion Slope (S_0): 0.086 ps /(nm²•km)

Refractive Index Difference: 0.36%

Effective Group Index of Refraction, (N_{eff} @ nominal MFD):

1.4677 at 1310 nm
1.4682 at 1550 nm

Fatigue Resistance Parameter (n_d): 20

Coating Strip Force:

Dry: 0.6 lbs. (3N)
Wet, 14-day room temperature: 0.6 lbs. (3N)

Rayleigh Backscatter Coefficient (for 1 ns pulse width):

1310 nm: -77 dB
1550 nm: -82 dB

Refractive Index Profile (typical fiber)

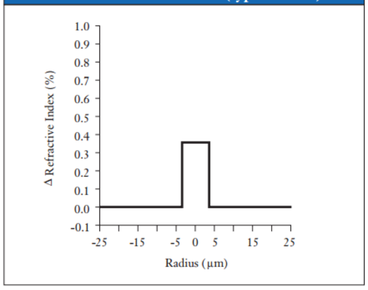

Spectral Attenuation (typical fiber)

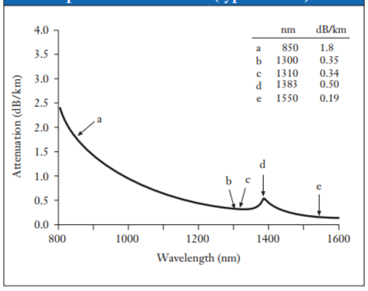

Ordering Information

To order Corning® SMF-28™ fiber, contact your sales representative, or call the Optical Fiber Customer Service Department at **607-248-2000** or **+44-1244-287-437** in Europe. Please specify the following parameters when ordering.

Fiber Type: Corning® SMF-28™ Fiber

Fiber Attenuation: dB/km

Fiber Quantity: km

Other: (Requested ship date, etc.)

Corning Incorporated
www.corning.com/opticalfiber

One Riverfront Plaza
Corning, NY 14831
U.S.A.

Phone: 800-525-2524 (U.S. and Canada)
607-786-8125 (International)

Fax: 800-539-3632 (U.S. and Canada)
607-786-8344 (International)

Email: cofic@corning.com

Europe

Phone: 00 800 6620 6621 (U.K.*, Ireland, Italy, France, Germany, The Netherlands, Spain and Sweden)

+1 607 786 8125 (All other countries)

Fax: +1 607 786 8344

Asia Pacific

Australia
Phone: 1-800-148-690
Fax: 1-800-148-568

Indonesia
Phone: 001-803-015-721-1261
Fax: 001-803-015-721-1262

Malaysia
Phone: 1-800-80-3156
Fax: 1-800-80-3155

Philippines
Phone: 1-800-1-116-0338
Fax: 1-800-1-116-0339

Singapore
Phone: 800-1300-955
Fax: 800-1300-956

Thailand
Phone: 001-800-1-3-721-1263
Fax: 001-800-1-3-721-1264

Latin America

Brazil
Phone: 000817-762-4732
Fax: 000817-762-4996

Mexico
Phone: 001-800-235-1719
Fax: 001-800-339-1472

Venezuela
Phone: 800-1-4418
Fax: 800-1-4419

Greater China

Beijing
Phone: (86) 10-6505-5066
Fax: (86) 10-6505-5077

Hong Kong
Phone: (852) 2807-2723
Fax: (852) 2807-2152

Shanghai
Phone: (86) 21-3222-4668
Fax: (86) 21-6288-1575

Taiwan
Phone: (886) 2-2716-0338
Fax: (886) 2-2716-0339

E-mail: GCCofic@corning.com

APPENDIX (B)

COVEGA

COVEGA Corporation
Super Luminescent Diode (SLED)
Part Description: 14 Pin Butterfly Packaged SLED
Package Description:1005SXL-0-0-T-S-A

Serial Number: SLD-6709-11742.6.A02
Test Date: 15-Oct-09

Summary of Test Data			
CW; T (Chip) =25.0 °C, T (Case) =25.0 °C			
Parameter			
Operating Current	I_{op}	600	mA
Center Wavelength	λ_c	1549.0	nm
ASE Power @ I_{op}	P_{ASE}	31.2	mW
Optical Bandwidth @ I_{op}	BW	55.3	nm
Max Gain Ripple (rms) @ I_{op}, Res. BW = 0.01 nm	ΔG	0.17	dB
Forward Voltage @ I_{op}	V_f	1.43	V
TEC Operation			
- TEC Current	I_{TEC}	0.29	A
- TEC Voltage	V_{TEC}	0.37	V
- Thermistor Resistance	R_{TH}	10K	Ω
Steinhart Constants : a=1.129241E-3; b=2.341077E-4; c=8.775468E-8			

Model: SLD1005 Rev: E
QA: Pass
Test Operator: Baron

COVEGA Corporation
Super Luminescent Diode (SLED)
Part Description: 14 Pin Butterfly Packaged SLED
Package Description:1005SXL-0-0-T-S-A

Serial Number: SLD-6709-11742.6.A02
Test Date: 15-Oct-09

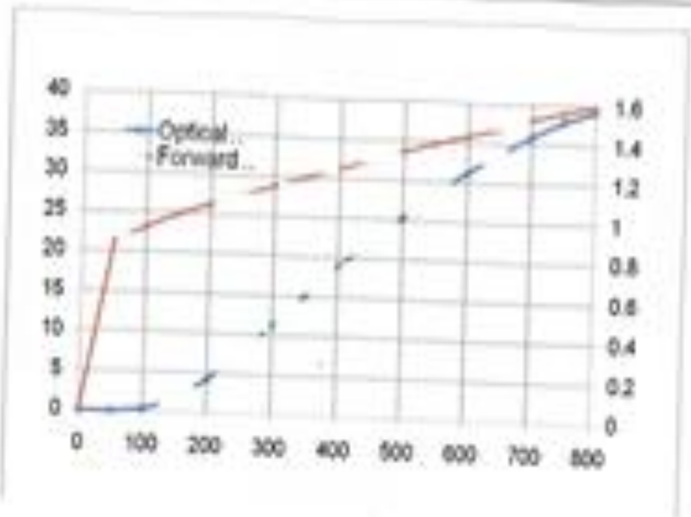

Figure 1: SLED LIV Plot

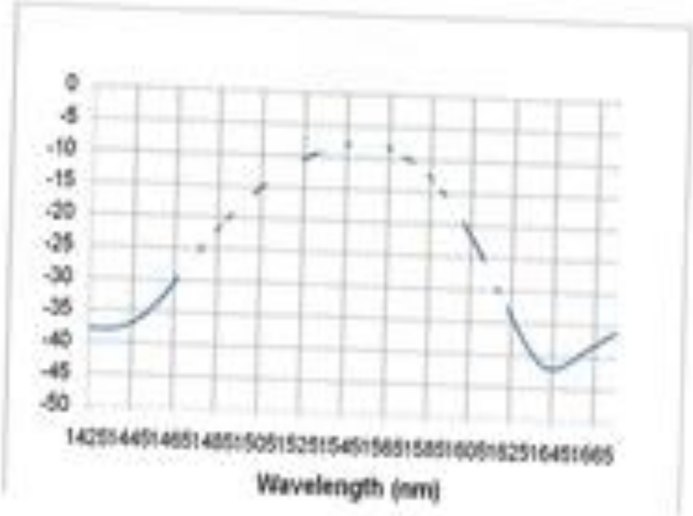

Figure 2: SLED Spectrum

COVEGA

COVEGA Corporation
Super Luminescent Diode (SLED)
Part Description: 14 Pin Butterfly Packaged SLED
Package Description: 1005SXL-0-0-T-S-A

Serial Number: SLD-6709-11742.6.A02
Test Date: 15-Oct-09

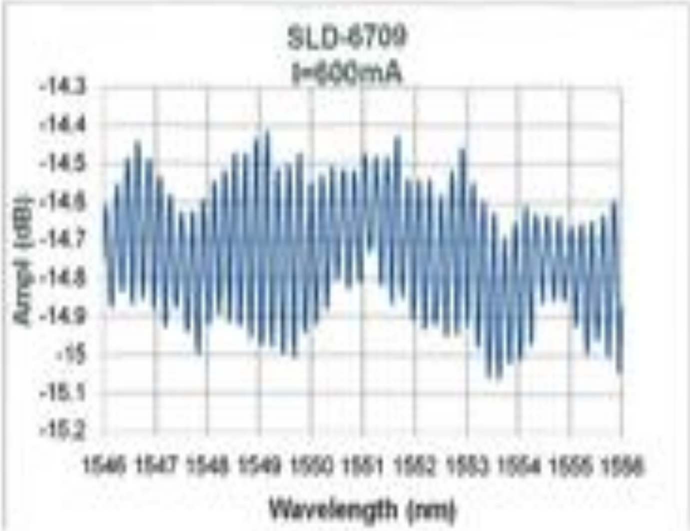

Figure 3: SLED Fine Spectrum

Packaging

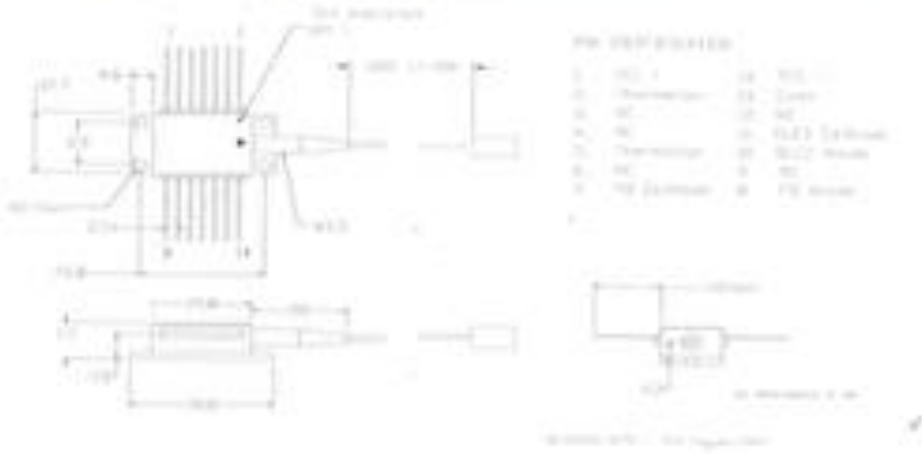

Attention:

Please observe the following precautions when mounting the butterfly package to a heatsink:

- The heatsink should be as flat as possible.
- Thermal grease or an alternative thin but compliant material is recommended to be used between package and heatsink.
- Screws should be tightened in a suitable sequence so that package mates to the heatsink without screw heads being forced up and into package snout.
- Maximum torque of 10~20oz·in (0.07~0.14N·m) is recommended for screw tightening.

Failure to comply to the above may cause damage to the internal thermo-electric cooler.

Covega Corporation
10335 Guilford Road, Jessup, MD 20794, USA
Phone: +1 877.226.8342 Fax: +1 240.456.7200 Email: [illegible] Web: [illegible]

APPENDIX (C)

For current pricing, please see our website.

Universal Butterfly Mount

LM14S2

The LM14S2 Butterfly Mount is designed to operate all lasers and two-port electro-optic devices in a 14-pin butterfly package. The top surface includes heat sink fins and a recessed region to mount the laser diode, resulting in a very low-profile package. The LM14S2 includes a laser diode TEC lockout feature, which disables the laser when the TEC controller is not active.† This mount is designed to allow up to 5 A of laser current and 5 A of TEC current. It also provides a Zero Insertion Force (ZIF) Socket, a remote interlock connection, and an LED to indicate when the laser diode is enabled.

This package comes with two adapter cards, each plugging into the connector at the bottom of the mount (see section below for details). A Bias-T Adapter is also included with the product, allowing for RF modulation of butterfly lasers specifically designed with this capability. The LM14S2 is pin-for-pin compatible with all Thorlabs' Benchtop Laser Diode Controllers (see pages 1436 - 1439), eliminating the need for custom-made interface cables.

† TEC lockout, which is easily bypassed if not required, only functions with Thorlabs' lasers and TEC controllers (see pages 1436 - 1480). The TEC controller requires that the laser package has an integrated TEC and thermal sensor.

Features

- Compatible with all Commercially Available Laser Modules and Two-Port Electro-Optic Devices in 14-Pin Butterfly Packages
- Zero Insertion Force (ZIF) Sockets
- Compatible with Thorlabs' Laser Diode and TEC Controllers (See Pages 1436 - 1480)
- Compact, Low-Profile Design
- TEC Lockout Protection Circuit

PARAMETER	VALUE
Maximum Laser Current	5 A
Polarity of Laser Diode	AG
Polarity of Monitor Diode	Floating
Maximum TEC Current	5 A
Temperature Sensor	Thermistor
Temperature Range*	0 to 70 °C
Temperature Coefficient of Heat Sink	3 °C/W
Dimensions	3.5" x 3.5" x 1.25" 88.7 mm x 88.9 mm x 31.8 mm

*At 25 °C with 2 A TEC current, integrated into laser package. Laser Diode dependent.

Mechanical Drawings Available on the WEB

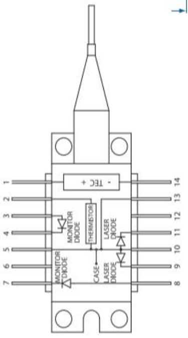

Type 1
Pump Laser Diode*

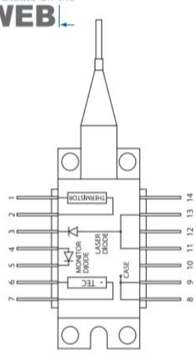

Type 2
Telecom Laser Diode*

*View shows alternate locations for monitor and laser diodes

LM14S2
Shown with a Two Port Electro-Optic Device

Adapter Cards for Custom PIN Configuration


LM14S2
Universal Adapter Card

The LM14S2 eliminates the restriction of fixed pin configurations by using swappable configuration cards that plug into a connector located on the bottom of the mount. Two cards are included with the LM14S2. One card is pre-configured for both Type 1 and Type 2 lasers. The second card is a user-configurable card (LM14S2-UA) designed to allow custom wiring of the mount.

PIN #	CONNECTOR (TYPE 1)	CONNECTOR (TYPE 2)
1	TEC Anode	Thermistor Ground
2	Thermistor	Thermistor
3	PD Anode	LD Cathode (DC)
4	PD Cathode	PD Anode
5	Thermistor Ground	PD Cathode
6	N.C.	TEC Anode
7	PD Cathhode	TEC Cathode
8	PD Anode	LD Anode, Ground
9	LD Cathode	LD Anode, Ground
10	LD Anode, Ground	N.C.
11	LD Cathode	LD Anode, Ground
12	N.C.	LD Cathode (RF)
13	LD Anode, Ground	LD Anode, Ground
14	TEC Cathode	N.C.

ITEM #	$	£	€	RMB	DESCRIPTION
LM14S2	$ 324.00	£ 233.28	€ 281,88	¥ 2,582.28	Universal 14-Pin Butterfly Laser Diode Mount
LM14S2-UA	$ 29.00	£ 20.88	€ 25,23	¥ 231.13	LM14S2 Universal Adapter Card for Custom Pin Configuration

APPENDIX (D)

THORLABS

Laser Diode Controller

LDC200C Series
Operation Manual

General Information

The Thorlabs LDC200C Series Laser Diode Controllers are high accuracy precise injection current controllers for laser diodes and LEDs. Together with a Thorlabs Temperature Controller a stable operation of the connected laser diode can be achieved. The LDC200C Series includes the following types:

- LDC200CV - designed for safe operation of VCSEL laser diodes.
- LDC201CU - ultra low noise current (<0.2µA RMS).
- LDC202C, LDC205C and LDC210C - enhanced compliance voltage (>10V) for use with blue laser diodes.
- LDC240C - higher current (4A).

The LDC200C Series controllers are easy to operate via the operating elements on the front panel. Operating parameters are shown on a 5-digit LED display. UP-DOWN keys allow to select the parameter to be displayed.

After switching on a LDC200C Series laser diode controller, it remains in LASER OFF mode. The laser current can be switched on/off using the appropriate key at the front panel.

Additionally the laser current can be switched by applying a TTL signal to the LD remote input at the rear of the unit.

The laser and the photodiode are connected via a 9-pin D-SUB jack at the rear of the unit. The output for the laser diode and the input for the photodiode are bipolar, thus all polarities of commercial available laser diodes can be connected.

The injection current or the optical output power of the laser diode can be modulated applying a modulation signal to the input at the rear of the unit.

A voltage proportional to the laser diode current is provided for monitoring purposes at an analog control output at the rear.

If an error occurs or the limit for the laser current is reached, the corresponding LED lights up and a short beep gives a warning.

For a low ripple and noise of the output current a mains filter is installed and the transformer is shielded carefully.

The LDC200C Series controller are cooled by an internal fan, which protects the unit against overheating in case of high environmental temperatures. With free air circulation a safe operation of the unit is guaranteed up to 40 °C ambient temperature.

Warning

Do not obstruct the air ventilation slots in the housing!

Note

In order to prevent damages to the laser diode, it is recommended to mount the laser into a suitable Thorlabs laser diode mount and connect it to the LDC200C Series using the supplied Thorlabs CAB400 cable. This ensures the utmost protection of the laser diode from damage by wrong connection.

APPENDIX (E)

THORLABS

Thermoelectric Temperature Controller

TED200C
Operation Manual

General Information

The thermoelectric Temperature Controller TED200C by Thorlabs is an extremely precise temperature controller for laser diodes and detectors.

The TED200C is excellently suited for:

- **wavelength stabilization of laser diodes**
- **noise reduction of detectors**
- **wavelength tuning by regulating the temperature**
- **modulation of wavelength by tuning the temperature**

The unit is easy to use due to the clearly arranged operating elements on the front panel. The operating parameters are shown by a 5-digit LED display, the measurement value shown is selected via keys.

The gain (P-share), the integral share and the derivative share of the PID temperature control loop can be set independent of each other.

Different temperature sensors can be used with the temperature controller TED200C, thermistors, or temperature IC sensors: AD590, AD592, LM135, LM 335. With a thermistor the temperature display is shown as resistance value in kΩ, if the TED200C is operated with a temperature sensor IC the temperature is shown in °C.

The output for the TEC current can be switched on or off via key from the front panel.

The temperature sensor and the TEC element are connected by a 15-pin D-sub jack at the rear of the unit.

At the output jack a control signal is available to drive an external LED to indicate TEC ON mode when the TEC current loop is activated.

The set value of the temperature can be changed with a knob at the front panel or via an analog input at the rear of the unit.

An analog voltage proportional to the actual value of the temperature is available at the rear of the unit for monitoring purposes.

The unit has been designed for safe operation with environmental temperatures of more than 40 °C provided that a free air circulation through the ventilation slots at the rear and at both sides of the unit is maintained.

Attention

Do not obstruct the air-ventilation slots in the housing!

In case of overheating caused by too high environmental temperatures or closed ventilation slots the unit automatically switches the output off to avoid damages.

The LED "OTP" (over-temperature-protection) indicates the over-temperature.

After temperature drop of about 10 °C the LED "OTP" extinguishes and the output current can be switched on again by pressing the key "ON".

If an error occurs (OTP or OPEN) the corresponding LED lights up and a beeper gives a short warning signal.

APPENDIX (F)

OSA (YOKOKAWA, Ando AQ6370) is a check device designed to measure and display the distribution of power of an optical signal over a specified wavelength span. An OSA trace displays power in the wavelength domain Figure below shows the image of OSA that used in the two experiments. The specification of this device are:

- High wavelength accuracy: $\pm$0.01 nm
- High wavelength resolution: 0.02 nm.
- Wide level range: +20 dBm to -90 dBm.
- Fast measurement: 0.2 sec.(100 nm span).
- Wavelength range: 600 nm to 1700 nm.

APPENDIX (G)

Dual window, SM Wind band Tree /Stare Coupler

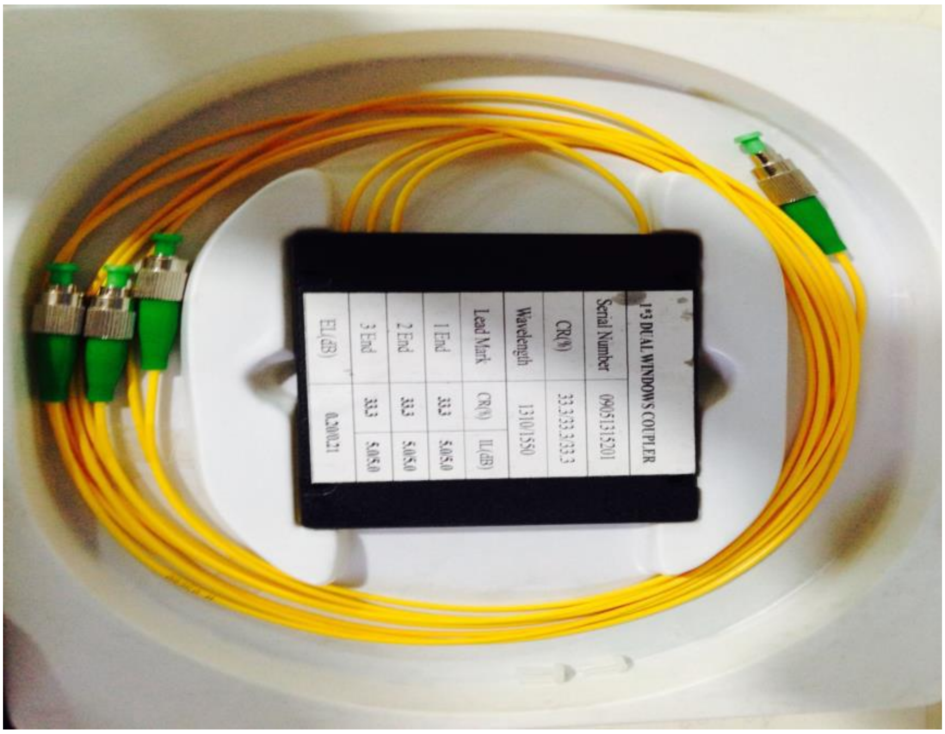

Product Description

Oplink's Dual window, single mode wideband tree and star couplers are high port count bi-directional products with excellent performance over two wide wavelength bands. They have very good uniformity, low excess loss and very low polarization sensitivity. All devices are tested according to industry standard test procedures and are supplied with all pertinent measurement data.

Oplink can provide customized designs to meet specialized feature applications. Also, Oplink offers modular assemblies that integrate other components to form a full functionmodule or subsystem.

Features

- Best Uniformity
- Ultra Low Insertion Loss
- High Directivity
- HIghly Stable & Reliable

Applications

- Telecommunications
- CATV Fiberoptic Links
- Fiber Amplifier System
- Fiberoptic Instruments

OPENSKY

Single Mode Dual Window Coupler Test Data

P/N: WBC-1 x 3-1315

S/N: 09091315049

Operating Wavelength: 1280~1620nm

Package Dimensions: 100 x 80 x 10.35mm

Fiber Length: 1m

Operating Temperature: -40~85℃

Connector: FC/APC

Data tested:

Items	Outpu t					
	1310nm			1550nm		
	1End	2End	3End	1End	2End	3End
Coupling Ratio(%)	33.26	33.28	33.46	33.32	33.35	33.33
Insertion Loss(dB)	5.0	5.0	5.0	5.0	5.0	5.0
PDL(dB)	0.02	0.04	0.03	0.03	0.05	0.03
WDL(dB)	<0.2	<0.3	<0.1	<0.1	<0.3	<0.2
Excess Loss(dB)	0.20			0.21		
Directivity(dB)	63			64		

APPENDIX
(H)

Fiber Bragg Grating

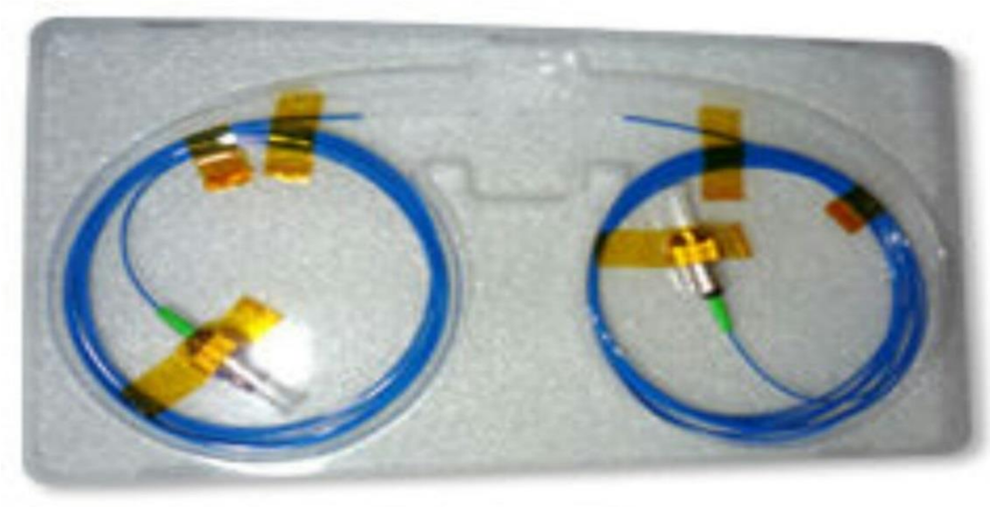

Reflectivity = 94.37%

Band width =0.206 nm

Bragg Wavelength =1545.559 nm

Grating length =10 mm

APPENDIX (I)

S1FC1550 - Fabry-Perot Bench top Laser Source, 1550 nm, 1.5 mW, FC/PC

APPENDIX (J)

Fusion Splicer

Clever

Striper

الخلاصة

المرشح الضوئي هو عنصر مهم جدا في النظام البصري يستخدم للسيطرة على مقدار وطور الاشارة القادمه. العديد من المرشحات الضوئيه صممت بأستخدام انواع مختلفة من متداخلات من نوع ماخزيندر اولهما هو الليف البصري المتعدد الانماط المحصور بين ليفين بصريين متماثلين احاديين النمط والاخر هو ليف براغ المحزز المحصور بين ليفين بصريين متماثلين احاديين النمط كذلك .حيث صممت هذه الانواع بطريقتين الاولى بمسار واحد والثانيه بمسارين.وقد تم تحقيق هذه التصاميم نظريا بأستخدام برنامج optisystem ومن ثم عمليا.

صممت هذه المتداخلات التي استخدمت كمرشحات ضوئيه للأشارات القادمه عن طريق السيطرة على ابعادها من خلال تسليط قوى او شد على مساحة المقطع العرضي لليف الضوئي .

عند تسليط قيم مختلفة من القوى على هذه الانواع من المتداخلات حصلنا على قابلية تنغيم وفرق بالطور معينين بكل نوع من انواع المرشحات الضوئيه وكانت افضل قابلية تنغيم حصلنا عليها للطور هي عند المتداخل من نوع الليف المتعدد الانماط المحصور بين ليفين بصريين متماثلين احاديين النمط ذو مسارين وكانت قيمة التنغيم تساوي(2.131) نانو متروحصلنا على فرق بالطور قيمته تساوي(16.9).

وزارة التعليم العالي والبحث العلمي

جامعة بغداد

معهد الليزر للدراسات العليا

التحقق من التأثيرات الميكانيكية على اداء مرشح متداخل ماخ-زيندر

رسالة مقدمة الى

معهد الليزر للدراسات العليا /جامعة بغداد /لاستكمال متطلبات نيل شهادة ماجستير علوم في الليزر/ الهندسة الالكترونية والاتصالات

من قبل

اية ثابت يحيى

بكالوريوس الهندسة الالكترونية والاتصالات, - 2012

بإشراف

الأستاذ المساعد الدكتورة تحرير صفاء منصور

1439 هـ **2018 م**